学位論文

Evaluation of a compact ground-based observation system using solar absorption spectroscopy and analysis of atmospheric CO₂ and CH₄ concentration dynamics

（太陽光の吸収分光法を用いたコンパクトな地上観測システ
ムの評価と大気中の CO_2 および CH_4 濃度動態の解析）

Xiuchun Qin

秦　秀春

Division of Particle and Astrophysical Science

Graduate School of Science

Nagoya University

Contents

4　XCH_4 and XCO_2 observations in Sichuan using OSA system

5　XCO_2 observations in Tokyo using OSA system

6 Summary of the thesis

Acknowledgments

Abstract

Atmospheric carbon dioxide (CO_2) and methane (CH_4) are the most important anthropogenic greenhouse gases and have been proved having a great influence on the changing of global temperature. It is critical for the understandings of source and sink of CO_2 and CH_4 to measure temporal variations of their concentrations in many places. In situ measurement near surface that a traditional method often heavily influenced by local sources. With global coverage and high measurement density, satellite observation of CO_2 and CH_4 has become an important approach to obtain CO_2 and CH_4 concentrations. However, there are still a lot of uncertainties in the main ground-based data source for validating satellite retrieval, as well as weakness in the instrument settings and inversion methods. As the main ground-based data source for validating satellite retrievals, the Total Carbon Column Observing Network (TCCON) sites are sparsely distributed globally with fixed positions, moreover, most sites are located in areas far from human activities. The TCCON uses a large FTS (Bruker 125HR wave number resolution ~ 0.01 cm^{-1}). Some groups use a small FTS (Bruker EM 27 resolution 0.5 cm^{-1}). Both of them are high in cost. To increase the density of observations, low-cost and easy-operating remote-sensing instruments are used as a promising complement to the current techniques. Column measurement by solar spectrometry is suitable for detecting effect of anthropogenic activities in urban area without strong influence from local sources around the observation site, because it can be used for smaller scales than that of the satellite sensors.

In this research, we used OSA (Optical Spectrum Analyzer, wavelength swept type spectrometer, resolution 0.2 cm^{-1}) to obtain the XCO_2 (CO_2 column-averaged volume

iv

mixing ratio) and XCH_4 (CH_4 column-averaged volume mixing ratio) with lower cost in Tokyo, Japan and Sichuan, China.

We used GOSAT-XCH_4 data from January 2010 to December 2013 to study the spatio-temporal variation of XCH_4 in Sichuan Basin where it presents consistent higher XCH_4 values than other parts of China. Our results show that the spatial distribution of GOSAT-XCH_4 is generally consistent with that of CH_4 emission, and abnormal high XCH_4 values can be seen in the Sichuan Basin, which is consistent with previous other research results. The regional variations of XCH_4 observed by GOSAT in Sichuan Basin are determined by not only the CH_4 emissions from ground sources but also very likely the regional topography and the related regional air transport. And then, we have utilized the OSA instrument at the Yanting station in the Sichuan Basin of China for September-November of 2013 because no ground-based column concentration data are available in this remote area. By analyzing the near-infrared solar spectra measured we obtain the XCH_4 and XCO_2. We compare the OSA results with those of GOSAT satellite. Both data sets are in good agreement. The results are also compared with the TCCON observation at the Lamont station that is located in the latitude zone same to the Yanting station. The OSA, GOSAT and TCCON values of the concentration ratios, XCH_4/XCO_2, are in good agreement except in the middle of September. Also, we measured the XCO_2 at the central area of the Tokyo metropolitan area for two years using the portable OSA instrument. To perform comparison, the data from a TCCON site in Tsukuba, which was located at the northeast edge of the metropolitan, were used. The seasonal trend coincided with the observations of the ground in situ instruments in central Tokyo. The diurnal variation in XCO_2 was correlated with the wind direction. The high XCO_2 values in central Tokyo were attributed to the large emission sources in

Tokyo. The high XCO_2 concentration during July 2015 may be caused by the local air retention.

The OSA instrument can be easily operated at any place and can provide useful information on source and sink of CO_2 and CH_4, because of its compact design, low power requirement and appreciable accuracy. This OSA system will help future construction of a ground-based greenhouse gas observation network.

The results in this thesis show that the small ground-based observation system we have developed not only can provide the time-varying data and provides verification data for satellites, but also greatly reduces the cost of greenhouse gas observations. The OSA instrument was portable and not expensive, and it can be easily operated at any place to measure the XCO_2 and XCH_4 values and to estimate the local CO_2 and CH_4 emissions and absorption processes, and using this as a reference, small-scale ground-based observing systems for CO_2, CH_4 and other greenhouse gases will be developed to provide more convenient global greenhouse gas observations.

Chapter 1

General Introduction

Earth's climate system is driven primarily by heat energy arriving from the Sun. When sunlight reaches the surface of the Earth, some of it is absorbed which warms the ground and some bounces back to space as heat. Because some gases in the Earth's atmosphere such as carbon dioxide (CO_2) and methane (CH_4) can absorb long-wave infrared radiation emitted by the Earth and return part of the energy back to the surface, increases the temperature of the Earth. This is called the greenhouse effect and the gases involved are called greenhouse gases (GHG_S).

The greenhouse effect under normal conditions maintains the average surface temperature at about 15°C, but since humans entered the industrial revolution, with the intensification of activities such as fossil burning and deforestation, excessive GHGs are emitted into the atmosphere, it has led to an ever-increasing greenhouse effect, and the global surface temperature has continued to rise. Global warming will redistribute global precipitation, melt glaciers and frozen soil, and increase sea levels. It will not only harm the balance of natural ecosystems, but also threaten human survival.

The CO_2 and CH_4 are potent GHGs that contribute to human-induced climate change. In 2011 the atmospheric concentrations of CO_2 and CH_4 have exceeded the pre-industrial levels 391 ppm and 1803 ppb by about 40% and 150%, respectively. Limiting climate change will require substantial and sustained reductions of greenhouse gas emissions, quantifying anthropogenic greenhouse gas emission is essential toward reduction (Duren

and Miller, 2012). The amount of anthropogenic GHGs emission is estimated by either the bottom-up or top-down methods. The bottom-up method uses diverse inventory data. The top-down method contrast requires measurement, reporting and verification of atmospheric composition data. It is already true that GHGs are increasing, and it is important to accurately determine the total emissions of GHGs. The amount of GHGs emitted in the atmosphere, which is determined by background concentration and atmospheric transport. Therefore, in order to know the GHGs emissions, it is necessary to accurately measure the time variation of GHGs in various places. In-situ measurements at the ground can provide diurnal change data of atmospheric CO_2, but suffers from the fact that they are heavily influenced by local contributions. Satellite observations are useful to improve the capability to monitor anthropogenic CO_2 emissions. The observations provide the uniform large-scale observation results. However, because they have a sun-synchronous orbit over a target is limited, result is that since cannot provide the detailed diurnal variation data. In addition, satellite data need ground-based observations to be validated by a globally distributed observation network such as Total Carbon Column Observing Network (TCCON; Wunch et al., 2011). Using high-resolution Fourier-transform infrared (FTIR) spectrometers, it provides a column-averaged CO2 mixing ratio (XCO_2) data with high precision and accuracy, but the number of these sites is limited because it is large and expensive. To increase density of observations, low-cost and easy-handling remote-sensing instruments are a promising complement to those current techniques. The column measurements by using solar absorption spectrometry can probe larger sample volumes than the in-situ measurements and smaller spectrum scales than the satellite sensors (Kobayashi et al. 2010, Frey et al. 2015. Hase et al. (2015)).

This thesis focuses on the greenhouse gas data analysis related to a low-cost, compact ground-based CO_2 solar spectrum observation system. In this chapter, the importance of the greenhouse gases CO_2 and CH_4 is described. Then, the current major measurement techniques is described in detail. Finally the aim of this thesis is presented.

1.1 Global warming and Greenhouse effects of atmospheric CO_2 and CH_4

Global warming has become one of the most important global environmental issues nowadays. After the pre-industrial era, due to human activities, the emissions of anthropogenic GHG such CO_2 and CH_4 have increased significantly.

The continuous increase in atmospheric concentrations of greenhouse gases is considered to be the main cause of rising global average temperatures. The global warming effect caused by greenhouse gases contributes about 78% (IPCC, 2014). Moreover, it is considered to induce the frequent occurrence of extreme climate events, such as extreme droughts in dry regions and floodis in rainier regions. These extreme climate events have caused tremendous damage to human life. CO_2 is the most important greenhouse gas causing global warming. The CO_2 concentration emitted by humans has exceeded the absorptive capacity of terrestrial ecosystems and oceans, disturbing the balance of the global carbon cycle and thus affecting the climate system (Falkowski et al. 2000; Schindler et al. 1999). Factors that directly contribute to the increase in atmospheric CO_2 concentration include anthropogenic emissions (fossil fuel combustion, anthropogenic combustion), natural emissions (ecosystem respiration, forest fires, volcanic eruptions, etc.), and CO_2 produced by the circulation of atmospheric transport

substances. Many researches proven that the anthropogenic emissions are the main contributor to regional atmospheric CO_2. And the CO_2 emitted by fossil fuel combustion caused by human factors is the main reason for the increase of global CO_2 concentration in the atmosphere (Falkowski et al. 2000). At present, the reduction of greenhouse gas emissions, especially the reduction of CO_2 emissions, is a global consensus. Therefore, accurate monitoring of CO_2 emissions information, study of the temporal and spatial distribution of CO_2 concentration and its spatio-temporal dynamic changes, including their sources and sinks, will help countries around the world develop reasonable and effective greenhouse gas emission reduction programs.

CH_4 is also one of the most important greenhouse gases, and is the major component of natural gas. The greenhouse effect generated by unit molecule of CH_4 is about 23 times higher than that of atmospheric CO_2. Therefore, it will be more effective to reduce the CH_4 emissions to mitigate the potential global warming than reducing the CO_2 emissions (Hogan et al. 1991).

The World Meteorological Organization (WMO) indicated in the "Greenhouse Gas Bulletin" published on September 9, 2014 that from the year 1990 to 2013, greenhouse effect had increased by 34% due to increasing CH_4 concentrations. Therefore, analyses of the CH_4 concentration variation and studies on its driving factors have drawn increasing attention. However, due to limited observation capabilities and understanding of CH_4 sources and sinks, the underlying driving factors for the regional CH_4 spatio-temporal variation are still unclear (He et al. 2012). The increase of global atmospheric CH_4 concentration is mainly due to significant emissions occurring as a result of animal husbandry and agriculture, in which irrigated rice paddy is one of the most important sources (Sshen et al. 1995).

In 1997, the United Nations Framework Convention on Climate Change (UNFCCC) countries have signed the "Kyoto Protocol" aimed at stabilizing atmospheric concentrations of greenhouse gases, especially CO_2, and placing the global carbon cycle under direct human control. It is required to monitor the source of CO_2 released into the atmosphere, but due to the limited understanding of CO_2 emission, absorption process and location, we cannot explain the current atmospheric CO_2 concentration change law, nor can we make accurate predictions of future atmospheric CO_2 concentration changes (Rayner et al., 2001; Michalak et al., 2011). At the same time, assessing the implementation of the treaty at various national scales and evaluating the response of the global carbon cycle to the implementation of the agreement are still challenging issues (Houweling et al. 2004). Therefore, responding to future climate and formulating policies and strategies for mitigating and adapting to climate change need to make accurate estimates of surface carbon sources and sinks, quantify atmospheric CO_2 concentrations, and need to manage the global carbon cycle effectively.

1.2   Observation of CO_2 and CH_4 concentrations in the atmosphere

It is critical for the understanding their sources and sinks using the continuously CO_2 and CH_4 distribution and its global variation. Atmospheric CH_4 and CO_2 observation methods mainly include in-situ measurement and remote sensing observation.   Ground-based observations have high accuracy, but they are mainly based on scattered single-point observations, and do not have the ability to provide uniform, global-wide observations (WMO, 2012). The satellite remote-sensing observations can be used for real-time

detection and unified detection in areas and large areas (Liu et al., 2012; NIES GOSAT Project, 2012).

1.2.1 In-situ measurement techniques

In-situ measurement can provide long-term, high-precision, systematic atmospheric CO_2 and CH_4 concentration observations at a fixed location. It is of great significance for the temporal and spatial variation of CO_2 and CH_4 concentration in the atmosphere, the source and sink information of the continental scale, and the prediction of atmospheric CO_2 and CH_4 concentration in the future.

Since the 1950s, relevant organizations in various countries have established greenhouse gas concentration background observation stations in different regions of the world. Most of these observatories are located in islands and coastal areas far from the sources of man-made emissions, and have obtained background concentrations of greenhouse gases that are not affected by regional human factors, and eventually formed observation networks (Figure 1.1). At present, the world's largest and well known international integrated atmospheric observation network is the Global Atmospheric Observation Network (GAW) established by the International Meteorological Organization (WMO) in 1990. As of June 2018, there were more than 200 stations in more than 60 countries around the world. Atmospheric CO_2 concentration data was reported to the World Data Center for Greenhouse Gases (WDCGG) in Japan. Observation points covered all latitudes in the world.

According to the scope and nature of the observing station representatives, GAW ground observing stations can be divided into global observatories, regional observatories

and cooperative observatories. Observing platforms can be divided into fixed platforms (surface fixed observatories, high towers), mobile platforms (aircraft, air balloons, ships, satellite remote sensing) and ice core measurements (GAW, 2009). In addition to observations of greenhouse gas concentrations, individual greenhouse gas profiles are also observed at some sites to obtain vertical distribution of atmospheric greenhouse gases. GAW atmospheric greenhouse gas concentration observations have also established a series of specifications in measurement methods, quality assessment, data management, analysis and forecasting, etc. to ensure that data from different countries and laboratories are comparable across the globe(WMO, 1978; WMO, 1971). In addition to WMO/GAW, the US National Oceanic and Atmospheric Administration-The Earth System Research Laboratory (NOAA/ESRL) established its own atmospheric greenhouse gas concentration observation network using most of the same observation stations as GAW and using different data analysis methods and developed the GLOBALVIEW-CO_2/CH_4 global greenhouse gas assimilation dataset. In addition, the CSIRO/CMAR, the Canadian Meteorological Agency (MSC), the National Institutes of Environmental Research (NIES) and other agencies also conducted a large number of greenhouse gas observations and research work respectively.

GAW Atmospheric greenhouse gas background observations provide reliable observational data to assess the long-term trends of GHGs concentrations in different latitude regions and global average conditions (Bell et al., 1999). The use of surface CO_2 observation data combined with atmospheric transport models can be used for inversion of surface carbon fluxes, and many scientists have conducted research on this. Enting et al., through the observation of atmospheric CO_2 and isotope $^{13}CO_2$, combined with the atmospheric trace gas transport model GISS, pointed out that at the global scale, marine

7

and terrestrial carbon sinks can be obtained from surface CO_2 concentration observations (Enting et al., 1995). Fan et al. calculated the temporal and spatial distribution of carbon uptake in terrestrial ecosystems using surface CO_2 observation data, by global chemical transport model (GCTM) and SKYHI models and ocean-atmosphere carbon flux data and fossil combustion CO_2 emissions data (Fan et al., 1998). From this we can see that based on the CO_2 observation data of surface atmospheric carbon, we first need to obtain the spatial and temporal distribution of atmospheric CO_2 concentration through the atmospheric transport model, and then obtain the distribution of surface carbon sources and carbon sinks. In addition to the uncertainty of the atmospheric transport model, due to the scarcity of ground observation stations, their uneven distribution, and their high cost, they have become the main factors restricting the accurate retrieval of carbon sources and carbon sinks. For example, Enting also pointed out that although surface observation data can provide constraints on the inversion of regional carbon sources and carbon sinks, it cannot reduce the uncertainty in the calculation of global carbon revenue and expenditure. Fan's research also showed that the existing data and model constraints can detect the carbon absorption of the terrestrial ecosystem in North America, but its magnitude cannot be determined. Due to the lack of observational data, the carbon flux in the tropics still has great uncertainty.

In summary, the concentration measurement of atmospheric GHGs based on surface observations has advantages such as high accuracy away from man-made pollution sources, and it plays an important role in revealing the dynamic law of atmospheric CO_2 concentration and in the early research on carbon source and carbon sink inversion. However, due to the high cost and low spatial resolution, different scholars still have great disagreement on the spatial and temporal distribution and size of carbon sources and

carbon sinks. Therefore, quantification of global carbon budget research urgently requires more observational data of GHGs, especially CO_2, that can be used in global atmospheric transport models.

1.2.2 Remote sensing techniques

Observed by remote sensing technology is the result of atmospheric CO_2 column concentration (XCO_2). XCO_2 refers to the ratio of atmospheric CO_2 molecules to total air molecules in the air column from the surface to the top of the atmosphere, reflecting the overall level of CO_2 from the near surface to the upper atmosphere. Movement of the atmosphere in the vertical direction does not affect column concentration values. Atmospheric CO_2 column concentration values will not change during the vertical interaction process between near-surface ecosystems and atmospheric CO_2, and can intuitively and accurately reflect the change of atmospheric CO_2 total concentration in the horizontal direction. When describing changes in carbon sources and sink fluxes, column concentrations are more accurate than near-surface atmospheric CO_2 concentrations (Wunch, 2010).

The XCO_2 and XCH_4 remote sensing platforms mainly include Space-based observing systems and ground-based observing systems.

1.2.2.1 Space based

Space-based observations are mainly satellite observations. Satellite remote sensing has the characteristics of rapidity, low cost, and large-scale continuous observation. It provides new ideas for solving the problem of ground station atmospheric GHGs

measurement. The GHGs in the atmosphere selectively absorb light at specific wavelengths. After the light passes through the atmosphere and returns to space, it has atmospheric GHGs content and other information. Based on this, atmospheric GHGs concentrations and profiles can be obtained.

Taking CO_2 as an example, it can be seen from the solar spectrum absorption diagram that CO_2 in the atmosphere mainly has 1.58 μm, 1.61 μm, 2.06 μm, 2.7 μm, 4.3 μm, and 15 μm, and 6 characteristic absorption bands. However, the band used for inversion of atmospheric CO_2 concentration should also satisfy conditions that are insensitive to temperature changes, less affected by other gas absorption, and less likely to be saturated by CO_2 absorption. Many scientists discussed the feasibility of using satellites to invert atmospheric CO_2 concentrations: analysis of the CO_2 absorption characteristics of 1.6μm, Tolton pointed out that the filter radiometer based on satellite sensor design has the potential to measure atmospheric CO_2 concentration from space (Tolton et al., 2001). Mao Jianping pointed out through spectral sensitivity experiments that under conditions of high signal-to-noise ratio and spectral resolution of the instrument, 1% CO_2 concentration on the surface can be detected using absorption features near 1.58 μm (Mao et al., 2004). Kuang et al. used simulated satellite measurements to show that the CO_2 concentration in the 1.58 μm and 2.06 μm absorption bands combined with the 0.76 μm absorption band can be used to invert high-precision atmospheric CO_2 concentrations (Kuang et al., 2002). The requirements for the accuracy of satellite observations of atmospheric CO_2 vary with the spatio-temporal distribution of data and the inversion of carbon flux at different regional scales. However, it is clear that the higher the accuracy (above 1 ppmv), the less the uncertainty in the estimation of surface carbon fluxes (Miller et al., 2007). The presence of clouds and aerosols in the atmosphere changes the optical path of CO_2

absorption, making the calculation of the CO_2 absorption spectrum more complicated. Surface factors, such as surface albedo and topographic changes, affect the ability of satellites to determine surface carbon flux at relatively small temporal and spatial scales. In addition to the low CO_2 content in the atmosphere, the current observation accuracy also imposes higher requirements on satellite signal-to-noise ratio, spectral resolution, and radiation resolution.

At present, satellites observing atmospheric CO_2 concentrations have reached the consensus that, including uncertainties such as instrument calibration, noise, and atmospheric conditions, the total uncertainty should be less than 1% (3.6 ppmv) to increase surface carbon fluxes inversion accuracy (Houweling et al., 2004). Based on the above research, the current special carbon satellites for atmospheric greenhouse gas observations are GOSAT, OCO-2, and TANSAT.

(1) GOSAT

On January 23, 2009, the Global Greenhouse Gases Observing Satellite (GOSAT), the world's first dedicated greenhouse gas detection satellite, was co-developed and launched by Japan Aerospace Development Agency (JAXA), the National Institute of Environmental Research (NIES), and the Ministry of the Environment (MOE). Its mission goal is to observe the global atmospheric CO_2 and CH_4 distribution. The scientific goal is to obtain global and regional distributions of anthropogenic emissions of atmospheric CO_2 sources and sinks through observations (Bousque et al. 1980, Fan et al. 1998). The GOSAT is a medium-sized satellite with a weight of 1650 kg and operates in a sun-synchronous orbit at an altitude of 666 km. Its spatial resolution is 500m below the sub-satellite point, its operating cycle is 98min, and it can cover the world every 3 days, collecting the latest data of about 56,000 observation points worldwide (Aumann et al.

2003). The GOSAT satellite carries two sensors: the Fourier Transform Spectrometer (FTS) and the Cloud and Aerosol Imager (CAI). FTS is used for greenhouse gas detection and CAI is used to collect cloud and aerosol information (Enting et al. 2003). The inversion accuracy of the atmospheric CO_2 mixture ratio needs to reach 1 to 4 ppmv. This accuracy can meet our research requirements, that is, the source and sink of CO_2 generated by human activities can be discriminated from the background of the temporal and spatial changes of natural sources and sinks. The above-mentioned observation targets place very high requirements on the spectral resolution and channel wavelength range of instruments for detecting CO_2. Therefore, the GOSAT satellite uses a Fourier transform spectroscopic interferometer for observation of greenhouse gases. The Thermal And Near infrared Sensor for carbon Observation (TANSO) sensor for CO_2 observation on the GOSAT satellite has high luminous flux and high spectral resolution. The first band of the TANSO (central wavelength 0.76 μm) is used to detect the O2 concentration and convert the atmospheric CO_2 content to a mixture ratio. Its second channel (1.56-1.72 μm) contains the absorption band of atmospheric CH_4, which increases the ability to detect atmospheric CH_4. Its third channel serves as an auxiliary detection channel for atmospheric CO_2 content. In addition, the TANSO-specific medium and long-wave infrared channel (5.5 to 14.3 μm) information can be used for nighttime observations of atmospheric CO_2 (Enting et al. 1995). The GOSAT satellite uses the cloud and aerosol imager CAI (Cloud Aerosol Imager) mounted on the same star to correct cloud and aerosol effects. The first channel of CAI is used for the observation of absorptive aerosols. Channel 2 and Channel 3 are the most commonly used visible light aerosol observation channels. Channel 4 can increase the detection of cirrus clouds (Table 1.1). In order to simulate the analysis of the scope and accuracy of GOSAT greenhouse gas satellite

12

observations, the National Institute of Environmental Studies (NIES) of Japan developed a forward (radiation transfer) and reverse (greenhouse gas inversion) simulation calculation model to estimate different scenarios (The inversion accuracy of clouds, clouds, aerosols, etc.)

(2) OCO-2

Orbiting Carbon Observatory-2 (OCO-2) is an American environmental science satellite which launched on 2 July 2014. A NASA mission aiming at quantifying the sources and sinks of CO_2 at regional scales and it is a replacement for the Orbiting Carbon Observatory which was lost in a launch failure in 2009 (Crisp, 2015). It is the second successful high-precision (better than 0.3%) CO_2 observing satellite, after GOSAT.

The Orbiting Carbon Observatory-2 (OCO-2) is NASA's first Earth-orbiting satellite dedicated to observing atmospheric CO_2 to better and clearly understand the carbon cycle. The mission's main goal is to measure CO_2 with enough precision and accuracy. The nadir resolution of OCO-2 is less than $1.3 \times 2.3 km^2$, much finer than GOSAT/TANSOFTS (diameter of 10.5 km) (Boland et al., 2009; Crisp et al., 2008; Crisp, 2015).

The OCO-2 grating spectrometers measure near-infrared spectra of sunlight reflected off the Earth's surface in three spectral regions around 765 nm (O_2 A band, or O_2A herein), 1.61 μm (weak CO_2 band, WCO_2), and 2.06 μm (strong CO_2 band, SCO_2), The O_2A band absorption directly constrains the dry-air column abundance and the atmospheric optical path length. The WCO_2 and SCO_2 bands provide information about both the CO_2 column abundance and aerosol properties (Table 1.2). By fitting those absorption features using an optimal estimation retrieval algorithm described in detail by Connor et al. (2008) and O'Dell et al. (2012), atmospheric abundances of surface pressure and CO_2 are retrieved along with other atmospheric and surface properties (e.g., water vapor, temperature, and

surface reflectance, aerosol and cloud optical depth and distribution).

Schwandner et al.(2017) pointed out that the observation data of the OCO-2 satellite reveals the different structures of CO_2 in the atmosphere caused by anthropogenic and natural point source emissions over several kilometers. Chatterjee et al. (2017) used OCO-2 observations to characterize the response of CO_2 concentrations in the tropical atmosphere to the strong El Niño events of 2015-2016. OCO-2 observations indicate that the tropical Pacific plays an important role in regulating the changes in atmospheric CO_2 concentrations in the early El Niño phase in 2015-2016. Sun et al. (2017) used the chlorophyll fluorescence imaging spectrometer (CFIS) for aerial observation of SIF and verified ground and space observations. The results show that OCO-2 clearly depicts the landscape gradient of the SIF and corresponds to different vegetation types. This is a capability that previous satellite missions did not possess.

(3) TanSat

China launched its first minisatellite dedicated to the carbon dioxide detection and monitoring at 15:22 UTC on December 22, 2016.TanSat is in a Sun-synchronous orbit with a local time of the descending node of ~13 : 30 min, an orbital altitude of ~700 km, and an angle of inclination of 98.2°.

The Chinese Carbon Dioxide Observation Satellite (TANSAT) was designed to focus on the global observation of CO_2. For retrieving carbon dioxide from TANSAT observations, cloud detection is an essential preprocessing step. The main payload aboard TanSat is the atmospheric carbon dioxide grating spectrometer (ACGS),The ACGS has a spatial resolution of 2×3 km, a swath of 20 km, a mass of 204 kg, and a peak power of 255. This spectrometer is a suite of three grating spectrometers that make coincident measurements of reflected sunlight in the near-infrared CO_2 band near 1.61 and 2.06 μm

and in the molecular oxygen A-band (O_2A) at 0.76 μm. The main payload of the TanSat satellite - a hyperspectral CO_2 detector with 3 channels, in which the spectral resolution of the O_2-A channel at 760 nm can be up to 0.04 nm, capable of capturing vegetation sunlight induced chlorophyll fluorescence to Fe (758 nm) And KI (771 nm) fill effects of two solar Fraunhofer dark lines, which can not only dynamically monitor the CO_2 concentration in the global atmosphere, but also accurately invert vegetation chlorophyll fluorescence (Zhongdong Yang et al) .

1.2.2.2 Ground based

1.2.2.2.1 TCCON

The resolution spectrum has higher sensitivity to changes in atmospheric CO_2 concentration. However, the space-based platform has strict restrictions on the weight, volume, and stability of the instrument, while the terrestrial telemetering spectrum instrument does not have such a problem. Therefore, OCO, GOSAT, and SCIAMACHY R&D teams have jointly established the Total Carbon Column Observing Network (TCCON), which uses ground-based FTS to obtain high-precision detection results and provides verification services for SCIA MACHYGOSAT and OCO space-based observations.

TCCON is an atmospheric CO_2 observation network created by the National Center for Atmospheric Research in the United States in 2004. It aims to increase people's awareness of the carbon cycle and provide verification data with sufficient accuracy for satellite observations of CO_2 column concentrations. TCCON uses a ground-based Fourier transform spectrometer to record spectral data in the range of 4000-9000 cm^{-1} in direct solar radiation by observing the near-infrared spectrum of the sun, and adopts a

nonlinear least squares spectral matching algorithm to perform inversion to obtain atmospheric CO_2. Concentrations of CH_4, N_2O, HF, CO, H_2O, and HDO. Because the instrument is directly aligned with the sunlight for observation, the TCCON data can avoid the influence of aerosols, cirrus clouds, etc. on the observation optical path and obtain high-precision CO_2 column concentration data. In order to maintain the consistency of data between different stations, all TCCON stations use the same observation instruments and software for data processing, including converting the instrument's interference pattern into spectral data and inverting gas concentration profiles using spectral data, and then using the average kernel function is weighted to obtain the CO_2 column concentration and other processes. The TCCON site uses the continuous observation mode to acquire spectral data, and the data obtained after the standardization process has good stability. Wunch compared the inversion CO_2 profile of the TCCON with observation data from the aircraft and calibrated the TCCON CO_2 column concentration inversion results. In sunny conditions, the TCCON CO_2 column concentration measurement accuracy can reach 0.25% (Wunch et al. 2011), which can be used to validate CO_2 column concentration data from GOSAT satellites. The TCCON observation site is sited according to a unified standard. There is no significant impact of human activities within 100 km, and there will be no significant change in the land use status in the site area within several decades. After nearly a decade of development, the TCCON observation sites are widely distributed in the global continents and ocean regions at various latitudes in the tropical to polar regions. The total number of TCCON observation sites has reached 26, of which 21 observation sites are available online (http://tccon.edu.cn).The site distribution as shown in Fig.1.2.

TCCON observation sites are located far away from the direct impact of human

activities and can represent the average distribution of atmospheric groups in the area where the observatory is located. These data are widely used in the verification of satellite remote sensing inversion (Kobayashi et al. 2010). However, due to the high cost of observation equipment at the TCCON ground site, high construction costs, and high labor costs for maintenance, the total number of ground-based atmospheric CO_2 sites at the current stage is limited and not evenly distributed. Insufficient ground observation data limit the accuracy of global carbon source and carbon sink inversion.

1.2.2.2.2 Small observation system

TCCON instruments are rather expensive and need large infrastructure to be set up and expert maintenance. Therefore TCCON stations have sparse global coverage, especially in Africa, South America and large parts of Asia (Wunch et al., 2015). Therefore, small, portable ground-based observation equipment is needed as a supplement.

Some researchers use the EM27™ spectrometer from Bruker to detect CO_2 absorption spectrum (Gisi et al., 2011; Frey et al., 2015; Hedelius et al.,2016). The interferometer of this spectrometer is the RockSolid™ pendulum style, with a CaF_2 beamsplitter and 2 cube corner mirrors. The spectrometer weighs 25 kg and measures 35×40×27 cm in size including the home-built trackersize. The resolution of spectrometer is 0.5 cm^{-1}. The spectrometer is only capable of recording single-sided interferograms. Although the differences of temporally coinciding measurements for the XCO_2 were small (0.12±0.08)% when compared to TCCON spectra (Gisi et al., 2012), but the instrument cost is relatively expensive.

1.3 The aim of this thesis

At present, the remote sensing observation methods of greenhouse gases are mainly satellite observations. Although satellite observations have the advantages of large scale and global coverage, they need corresponding ground verification data and cannot provide detailed daily variation results.

TCCON, the main observing network for terrestrial-verified satellite data, although providing high accuracy can provide detailed daily variation results, but currently there are few global sites and most of them are far from anthropogenic emissions areas, small-scale ground observation systems are needed to provide supplementary data. Therefore we use OSA to develop a small ground-based greenhouse gas observation system. We hope that the small ground-based observation system we have developed not only can provide the time-varying data and provides verification data for satellites, but also greatly reduces the cost of greenhouse gas observations.

In order to give full play to the advantages of the observing system and to continuously improve the observing system in the observation we use this system to perform solar spectrum observations in many places(City, farmland, ocean, desert), and then calculate XCO_2 concentration and XCH_4 concentration and analyze the reasons. Sichuan, China has been considered to be a region with high CH_4 emissions, but there has been no locally observed XCH_4 concentration results. In addition, the emission of CO_2 in large cities has a big influence on world CO_2 emissions. There are examples of measurements in big cities of the world, but there are few measurements in Tokyo.

In order to scientifically investigate the concentration of XCH_4 and XCO_2 in Sichuan and the anthropogenic emissions of CO_2 in Tokyo in metropolitan areas, we measured the

column-averaged concentrations XCO_2 and XCH_4, in Sichuan and Tokyo metropolitan city using a portable OSA instrument and hope obtain new knowledge from CO_2 and CH_4 observations in Sichuan and Tokyo measurements.
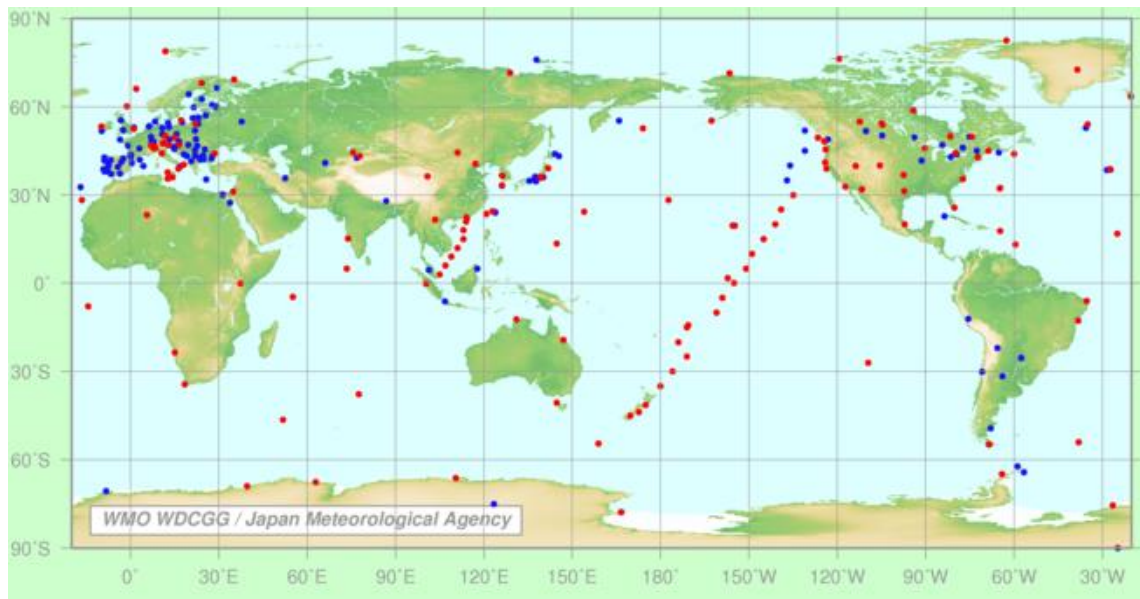
Figure 1.1 The distribution of the fixed stations that contribute data to the WDCGG.

Figure 1.2 Global TCCON site distributions

Table 1.1 GOSAT/TANSO-FTS 4 bands

Band	wavelength (μm)	object
Band 1	0.758−0.775	Detect O_2 concentration and obtain surface pressure
Band 2	1.56−1.72	Detecting gas concentrations using CO_2, CH_4 absorption bands
Band 3	1.92−2.08	CO_2, H_2O absorption bands, auxiliary channels for the determination of CO_2
Band 4	5.56−14.3	Detecting CO_2 channels

Table 1.2 The spectral information of OCO-2

Band	wavelength (μm)	object
Band 1	0.758−0.772	O_2 A band, Detect O_2 concentration and defining the total dry air column abundance
Band 2	1.594−1.619	weak CO_2 band, WCO_2, Detecting gas concentrations
Band 3	2.042−2.082	strong CO_2 band, SCO_2, auxiliary channels for the determination of CO_2

References

[1] C. B. Field, V. R. Barros, D. J. Dokken, K. J. Mach, M. D. Mastrandrea, T. E. Bilir, M. Chatterjee, K. L. Ebi, Y. O. Estrada, R. C. Genova, B. Girma, E. S. Kissel, A. N. Levy, S. MacCracken, P. R. Mastrandrea and L. L. White, IPCC, 2014: Climate Change 2014 Impacts, Adaptation, and Vulnerability. Part A: Global and Sectoral Aspects. Contribution of Working Group II to the Fifth Assessment Report of the Intergovernmental Panel on Climate Change, Cambridge University Press, 2014

[2] Duren RM, Miller CE (2012) Measuring the carbon emissions of megacities. Nat Clim Chang 2(8):560–562

[3] Wunch, D. et al., 2011. A method for evaluating bias in global measurements of CO_2 total columns from space, Atmos. Chem. Phys., 11, 12317–12337. https://www.atmos-chem-phys.net/11/12317/2011/acp-11-12317-2011.html.

[4] Kobayashi, N., Inoue, G., Kawasaki, M., Yoshioka, H., Minomura, M., Murata, I., Nagahama, T., Matsumi, Y., Tanaka, T., Morino, I., and Ibuki, T., 2010. Remotely operable compact instruments for measuring atmospheric CO_2 and CH_4 column densities at surface monitoring sites. Atmos. Meas. Tech., 3, 1103– 1112. https://www.atmos-meas-tech.net/3/1103/2010/amt-3-1103-2010.html.

[5] Hase, F., Frey, M., Blumenstock, T., Groß, J., Kiel, M., Kohlhepp, R., Mengistu Tsidu, G., Schäfer, K., Sha, M. K., and Orphal, J., 2015. Application of portable FTIR spectrometers for detecting greenhouse gas emissions of the major city Berlin. Atmos. Meas. Tech., 8, 3059-3068. https://www.atmos-meas-tech.net/8/3059/2015/.

[6] Hase, F., Frey, M., Blumenstock, T., Groß, J., Kiel, M., Kohlhepp, R., Mengistu Tsidu, G., Schäfer, K., Sha, M. K., and Orphal, J., 2015. Application of portable FTIR spectrometers for detecting greenhouse gas emissions of the major city Berlin. Atmos. Meas. Tech., 8, 3059-3068. https://www.atmos-meas-tech.net/8/3059/2015/.

[7] P. Falkowski, "The Global Carbon Cycle: A Test of Our Knowledge of Earth as a System," Science, 290(5490), pp. 291-296, 2000.

[8] D. W. Schindler, "Carbon cycling – the mysterious missing sink," Nature, 398(6723), pp. 105-107, 1999.

[9] K. B. Hogan, A. M. Thompson, and J. S. Hoffman, "Methane on the greenhouse agenda", *Nature*, vol.354, pp.181 - 182, 1991.

[10] Q. He, T. Yu, X. F. Gu, T. H. Cheng, Y. Zhang, D. H. Xie, "Global atmospheric methane variation and temporal-saptial distribution analysis based on ground-based and satellite data", *Remote Sensing Informations*,Vol.27,No.4,pp.35,2012.

[11] R. X. Shen, X. J. Shangguan, M. Wang, et al., "Methane emission from rice fields

in Guangzhou region and the spatial variance of methane emission in China", *Advance In Earth Science*, Vol.10,No.4,pp.2701,1995.

[12] Rayner P J, O'Brien D M. The utility of remotely sensed CO_2 concentration data in surface source inversions, Geophysical Research Letters, 2001, 28: 175-178

[13] Michalak A M, Jackson R B, Marland G, et al. A us carbon cycle science plan, 2011

[14] Houweling S, Breon F M, Aben I, et al. (2004) Inverse Modeling of CO_2 sources and sinks using satellite data: A synthetic inter-comparison of measurement techniques and their performance as a function of space and time. Atmospheric Chemistry and Physics, 4(2): 523-538.

[15] Y. Liu, X. Wang, M. Guo and H. Tani, "Mapping the FTS SWIR L2 product of XCO_2 and XCH_4 data from the GOSAT by the Kriging method – a case study in East Asia," International Journal of Remote Sensing, 33, pp. 3004-3025, 2012.

[16] NIES GOSAT Project, Global greenhouse gas observation by satellite, GOSAT Project, 2012

[17] GAW Report No. 184 Technical Report of Global Analysis Method for Major Greenhouse Gases by the World Data Centre Greenhouse Gases, 2009

[18] WMO International Operations Handbook for Measurement of Background Atmospheric Pollution Geneva: World Meteorological Organization, 1978, 491: 1-10

[19] WMO Operations Manual for Sampling and Analysis Techniques for Chemical Constituents in Air and Precipitation. Geneva: World Meteorological Organization, 1971, 299: 1-23

[20] Bell G D, Halpert M S, Ropelewski C F, et al. Climate assessment for 1998. Bull Amer Meteor Soc, 1999, 80(5): S1-S48

[21] Enting I G, T rudinger C M. A synthet ic in version of the concent ration an dD13 C of atmospheric CO_2[J]. Tellus, 1995, 47B: 318- 325

[22] Enting I G, Trudinger C M, Francey R J. A synthesis inversion of the concentration and δ13 C of atmospheric CO_2, Tellus B, 1995, 47, 35-52

[23] Fan S, Gloor M, Mahlman J, et al. A large terrestrial carbon sink in north America implied by atmospheric and oceanic carbon dioxide data and models, Science, 1998, 282: 442-446

[24] Tolton B T, Plouffe D. Sensitivity of radiometric measurements of the atmospheric CO_2, Applied Optics, 2001, 40(9): 1305-1313

[25] Mao J P, Kawa S R. Sensitivity studies for space-based measurement of atmospheric total column carbon dioxide using reflected sunlight, Applied Optics, 2004, 43(4): 914-927

[26] Kuang Z M, Margolis J, Toon G, et al. Spaceborne measurements of atmospheric CO_2 by high-resolution NIR spectrometry of reflected sunlight: An introductory study. Geophysical research letters, 2002 29(15): 1716, 10. 1029/2001GL014298

[27] Miller C E, Crisp D, DeCola PL, et al. Precision requirements for space-based XCO_2 data, Journal of geophysical research, 112, D10314, 19 PP., doi: 10. 1029/2006JD007659, 2007

[28] Houweling S, Breon F M, Aben I, et al. (2004) Inverse Modeling of CO_2 sources and sinks using satellite data: A synthetic inter-comparison of measurement techniques and their performance as a function of space and time. Atmospheric Chemistry and Physics, 4(2): 523-538.

[29] Bousquet, P., et al.. Regional changes in carbon dioxide fluxes of land and oceans since 1980 [J]. science, 2000, 290(5495): p. 1342-1346.

[30] Fan, S., et al.. A large terrestrial carbon sink in North America implied by atmospheric and oceanic carbon dioxide data and models [J]. science, 1998, 282(5388): p. 442-446.

[31] Aumann, H.H., et al.. AIRS/AMSU/HSB on the Aqua mission: Design, science objectives, data products, and processing systems [J]. Geoscience and Remote Sensing, IEEE Transactions on, 2003, 41(2): p. 253-264.

[32] Enting I G, T rudinger C M. A synthet ic in version of the concent ration an dD13 C of atmospheric CO_2[J]. Tellus, 1995, 47B: 318- 325

[33] Enting I G, Trudinger C M, Francey R J. A synthesis inversion of the concentration and δ13 C of atmospheric CO_2, Tellus B, 1995, 47, 35-52

[34] Crisp, D., Miller, C. E., and DeCola, P. L.: NASA Orbiting Carbon Observatory: measuring the column averaged carbon dioxide mole fraction from space, J. Appl. Remote Sens., 2, 23508, https://doi.org/10.1117/1.2898457, 2008.

[35] Boland, S., Brown, L. R., Burrows, J. P., Ciais, P., Connor, B. J., Crisp, D., Denning, A. S., Doney, S. C., Engelen, R., Fung, I. Y., Griffith, P., Jacob, D. J., Johnson, B., Martin-Torres, J., Michalak, A. M., Miller, C. E., Polonsky, I., Potter, C., Randerson, J. T., Rayner, P. J., Salawitch, R. J., Santee, M., Tans, P. P., Wennberg, P. O., Wunch, D., Wofsy, S. C., and Yung, Y. L.: The Need for Atmospheric Carbon Dioxide Measurements from Space: Contributions from a Rapid Reflight of the Orbiting Carbon Observatory, Tech. rep., available at: https://www.nasa.gov/pdf/363474main_OCO_Reflight.pdf (last access: 5 November 2011), 2009.

[36] Crisp, D.: Measuring atmospheric carbon dioxide from space with the Orbiting Carbon Observatory-2 (OCO-2), SPIE, 9607, 960702-1,

https://doi.org/10.1117/12.2187291, 2015.

[37] O'Dell, C. W., Connor, B., Bösch, H., O'Brien, D., Frankenberg, C., Castano, R., Christi, M., Eldering, D., Fisher, B., Gunson, M., McDuffie, J., Miller, C. E., Natraj, V., Oyafuso, F., Polonsky, I., Smyth, M., Taylor, T., Toon, G. C.,Wennberg, P. O., and Wunch, D.: The ACOS CO_2 retrieval algorithm – Part 1: Description and validation against synthetic observations, Atmos. Meas. Tech., 5, 99–121, https://doi.org/10.5194/amt-5-99-2012, 2012.

[38] Connor, B. J., Boesch, H., Toon, G. C., Sen, B., Miller, C. E., and Crisp, D.: Orbiting Carbon Observatory: Inverse method and prospective error analysis, J. Geophys. Res., 113, 1–14, https://doi.org/10.1029/2006JD008336, 2008.

[39] F. M. Schwandner et al., Spaceborne detection of localized carbon dioxide sources. Science 358, eaam5782 (2017).

[40] A. Chatterjee et al., Influence of El Niño on atmospheric CO_2 over the tropical Pacific Ocean: Findings from NASA's OCO-2 mission. Science 358, eaam5776 (2017).

[41] Y. Sun et al., OCO-2 advances photosynthesis observation from space via solar-induced chlorophyll fluorescence. Science 358, eaam5747 (2017).

[42] Zhongdong Yang et al.:Prelaunch Radiometric Calibration of the TanSat Atmospheric Carbon Dioxide Grating Spectromete .IEEE TRANSACTIONS ON GEOSCIENCE AND REMOTE SENSING, VOL. 56, NO. 7, JULY 2018

[43] D.Wunch, P. O. Wennberg, G. C. Toon.A method for evaluating bias in global measurements of CO_2 total columns from space [J]. Atmos. Chem. Phys., 11, 12317–12337, 2011 doi:10.5194/acp-11-12317-2011.

[44] Gisi, M., Hase, F., Dohe, S., Blumenstock, T., Simon, A., and Keens, A.: XCO_2-measurements with a tabletop FTS using solar absorption spectroscopy, Atmos. Meas. Tech., 5, 2969–2980, doi:10.5194/amt-5-2969-2012, 2012.

[45] Hedelius, J. K., Viatte, C., Wunch, D., Roehl, C. M., Toon, G. C., Chen, J., Jones, T., Wofsy, S. C., Franklin, J. E., Parker, H., Dubey, M. K., and Wennberg, P. O.: Assessment of errors and biases in retrievals of XCO_2, XCH_4, XCO, and XN_2O from a 0.5 cm^{-1} resolution solar-viewing spectrometer, Atmospheric Measurement Techniques, 9, 3527–3546, https://doi.org/10.5194/amt-9-3527-2016, https://www.atmos-meas-tech.net/9/3527/2016/, 2016.

[46] Kawasaki, M., Yoshioka, H., Jones, N. B., Macatangay, R., Griffith, D. W. T., Kawakami, S., Ohyama, H., Tanaka, T., Morino, I., Uchino, O. and Ibuki, T., 2012. Usability of optical spectrum analyzer in measuring atmospheric CO2 and CH4 column densities: inspection with FTS and aircraft profiles in situ. Atmos. Meas.

27

Tech. 5, 2593-2600. http://dx.doi.org/10.5194/amt-5-2593-2012.

Chapter 2

Ground based OSA observation system

2.1 Importance of small ground observation systems

It is critical for the understanding the sources and sinks of CO_2 and CH_4 using the continuously CO_2 and CH_4 distribution and its global variation. However, traditional measurement methods, in situ measurement suffers from the fact that it is heavily influenced by local contributions. With global coverage and high measurement density, satellite observation of CO_2 has become an important approach to obtain CO_2 concentrations. Many satellites for observing greenhouse gases that have been successfully launched, such as the American Carbon satellite OCO-2, Chinese TanSat, and Japanese GOSAT-2, and more satellites will be launched in the future, such as the European CarbonSat and Japanese GOSAT-3. However, as the main ground-based data source for validating satellite retrievals, the Total Carbon Column Observing Network (TCCON) sites are sparsely distributed globally with fixed positions, moreover, most sites are located in areas far from human activities. To increase the density of observations, low-cost and easy-operating remote-sensing instruments are used as a promising complement to the current techniques. Measurement of column amount with solar spectrometry is suitable for localized sources because it can be used for probing larger sample volumes than that can be probed using the in-situ measurements and

29

because it can be used for smaller scales than that of the satellite sensors.

Therefore, we use the ground-based observing system developed by the small-spectrum spectrometer to perform solar spectrum observation in different regions, and calculate XCO_2 and XCH_4, evaluate the performance of the system and analyze the causes of the concentration change, and then improve the system. This handy OSA measurement can provide the time-varying data that will help future construction of a ground-based greenhouse gas observation network. We hope to make some contributions to global greenhouse gas observations in the future.

2.2 Introduction of the OSA observing system

To measure the atmospheric CO_2 column density, our portable instrument consists of outdoor devices such as a solar telescope (30 cm long, 10 mm dia.), a portable sun tracker (Prede, ASTX-2, resolution 0.00225º) and a Global Positioning System (GPS) device (CanMore Electronics, GMS6-CR6), and indoor ones such as a tabletop OSA (Yokogawa, AQ6370-custom), an NIR intensity monitor (THORLABS, PAD10CS) and a laptop computer (Kobayashi et al., 2010, Kawasaki et al., 2012). A schematic diagram of the data acquisition system is shown in Fig. 2.1. The solar telescope is installed on the sun tracker. A long-pass filter (HOYA, RM100, $\lambda > 1000$ nm) with anti-reflection coating is placed in front of an object lens of the telescope. The solar signal is guided to the OSA and the intensity monitor via an optical fiber cable (Mitsubishi Cable Industry, seven quartz optical fibers in one cable). The quartz optical fibers (fiber diameter 60μm, design wavelength 1550 nm) has uniform transmittance around 1500-1700 nm. The center optical fiber is connected to the signal inlet of the OSA while the others to that of the intensity monitor. Reference solar intensity is monitored in 800–1800 nm

simultaneously with the OSA signal to compensate the OSA signal for solar intensity fluctuation caused by thin cloud blocking of the solar light. The absolute wavelength of the OSA is ± 0.02 nm at 1520-1580 nm with a grating optics, which is automatically calibrated by with a built-in wavelength reference system with an acetylene line absorption cell. The peak wavelengths in the spectrum are additionally calibrated by fitting of Fraunhofer lines. Our analysis minimizes the fitting residual by shifting the wavelength with an increment of 0.01 nm. The measurable signal level of the OSA is > -90 dB and typical solar spectral intensity is -50 dB. The spectral resolution is typically 0.049 nm (0.020 cm^{-1}). In our previous papers (Refs. 7 and 8) the OSA was used with a non-coated color filter equipped on the front side of the solar telescope which produced interference pattern noise due to an etalon effect in the spectra. In the present work, the interference noise is removed by using the anti-reflection coated filter. The OSA consists of a wavelength scanning monochromator.

The spectral scan time was 2-3 min in the previous work, while it is 12 s in this work. The OSA instrument is improved for the fast wavelength scan, which can avoid distortion of the spectra due to the sunlight intensity fluctuations. Geographical data and coordinated universal time are obtained from the GPS device. The clock of the computer is calibrated by the GPS signal at midnight every day. Specific parameters are described in our previous papers (Yokota et al., 2009, Frankenberg et al., 2015).

2.3 Observations using OSA

2.3.1 Selection of observation sites

CH_4 and CO_2 are potent GHGs that contribute to human-induced climate change.

Understanding the budget of the CH_4 and CO_2 has implications for future climate change scenarios and mitigation options to avert further global warming. Previous studies by (Hayashida et al., 2013, Xiong et al., 2009, Zhang et al., 2011) showed that a consistently high CH_4 concentration is observed in the Sichuan Basin, including Chongqing and Sichuan regions in south-western China. Although various studies have shown that the concentration of CH_4 in Sichuan is high, and satellites have a small number of observations, there are no local detailed observations to verify. So we used the OSA observation system to perform actual XCH_4 and XCO_2 observations in Sichuan.

We have not only observed in remote areas, but also in metropolitan areas for XCO_2. Schwandner et al. (2017) analyzed the OCO-2 satellite data and reported the high XCO_2 over the urban core but not over the suburban areas of Los Angeles, with the differences which vary seasonally from 4.4 to 6.1 ppm.

According to the GOSAT project report, the human-originated CO_2 in Tokyo's urban areas is about 0.5 ppm, which is much smaller than other metropolitan areas. The GOSAT transit data is very small. The nearest TCCON is nearly 60km from Tsukuba in the central area, where the population is small and cannot represent the change of CO_2 in urban areas. Therefore, we set up the OSA observation system in the center of Tokyo and actually observed the changes in CO_2 in the metropolitan area of Tokyo.

2.3.2 Parameter settings

The observing devices in Sichuan and Tokyo are roughly the same, but the details are slightly different. Among them, the spectral range of Sichuan is1672-1680 nm and 1568-1576 nm, and its purpose is to observe the absorption bands of CH_4 and CO_2. The

spectrum of Tokyo is set at 1568–1576 nm, only to observe the CO_2 absorption band. Moreover, the OSA used is slightly different. The specific parameter settings are shown in Table 2.1.

2.3.3 Introduction of Column-averaged dry-air molar mixing ratios

After the solar light passes through the atmospheric layer and interacts with the gas molecules, the rovibronic bands due to absorption by CH_4, CO_2 appear in the NIR spectra and Fraunhofer lines (Jenkins et al., 1981) also appear. The spectral range used for analyses of CH_4 is 1672−1680 nm while that of CO_2 concentrations is 1568−1576 nm. Here we briefly describe how the mixing ratios are obtained. We assume homogeneous vertical profiles of mixing ratios for CH_4 and CO_2 from 0 to 48 km altitudes to retrieve total column densities from observed spectra. As for spectral simulation, after we divide the air layer into 28 sublayers, for every 1 km at altitude up to 16 km, every 2 km at altitude 16-32 km, every 4 km at altitude 32-48 km, applying the Beer-Lambert law to CO_2 absorption in each layer for a certain CO_2 mixing ratio, summing up their absorbance with a line-by-line radiative transfer calculation method. We calculate the corresponding absorption spectra for the CO_2 column densities. The molecular absorption is taken into account through a Voigt line-shape and Boltzmann distribution model. The values of total column density for CH_4 or CO_2, absorption baseline level, water vapor column density and spectral wavelength shift are treated as fitting parameters between observed and simulated spectra with a non-linear least square fitting method. Examples of measured absorption spectra are shown in Fig. 2.2, in which spectral fitting is satisfactory with calculated ones with a spectral resolution of

33

0.049 nm.

To obtain the column-averaged molar mixing ratios, the total column densities of CO_2 are divided by total column densities of dry air estimated from weather data of pressure and humidity (Washenfelder et al., 2006). The total column density of dry air is obtained by subtracting the mass of water vapor based on the reanalysis weather data of the relative humidity of the ground and the upper atmosphere. Air masses of the layers are calculated from the solar zenith angles (SZA) obtained from the GPS time and geography data of the station. The XCO_2 data is slightly dependent on SZA. For this dependency we test a correction formula similar to that implemented by Wunch et al (2010). The correction influences only slightly our results for daily averaged values since the deviation are calculated to be less than 0.1%.

As for the spectral database, we tested both HITRAN2008 and HITRAN2012 (Rothman et al., 2009, Rothman et al., 2013). There are differences of 1.1 and 0.032 ppm in the retrieved mixing ratios of CO_2 and CH_4, respectively, between the results using the HITRAN2008 and 2012 databases. The differences are stable and considered to be small compared to the standard deviations (1σ) of XCO_2 and XCH_4. The HITRAN2008 database is used for both the measurements and calibrations because data processing time is shorter.

Since the molecular absorption lines in the NIR are optically thick as well as pressure and temperature dependent, the spectral retrieval in the NIR requires a detailed representation of the vertical profiles of meteorological parameters. Meteorological reanalysis data at four points surrounding the observation point are downloaded from MDISC Data subset (MERRA-2 inst3_3d_asm_Np) in Goddard Earth Sciences Data and Information Services Center (GES DISC), which consist of surface geopotential

heights, air temperature, specific humidity and surface pressure at 42 layers divided from 0.1 hPa to 1000 hPa (Fig. 2.3). The meteorological data at the observation point and time was interpolated by bilinear method from the four data sets and by linear method from the data of the interval for three hours.

Impacts of the weather parameters to the fitting calculations by shifting altitude distributions of pressure and temperature by 1% (10 hPa on the ground) and 1 K are estimated to be 0.020 and 0.012 ppm for XCH_4, and 4 and 1.6 ppm for XCO_2 respectively. We take the spectral wavelength shift as a parameter in the fitting process. Since the full data channels for wavelength scan are 4001, one channel corresponds to 0.002 nm. The spectral shift caused by one digit shift may have an impact of 0.2 ppm for XCO_2.

In case that the spectral fitting in the retrieval calculation is poor because the solar light intensity was not stable enough due to interruptions of cloud during the measurements, we eliminated the data that have a deviation over the averaged fitting deviation ($1\sigma_{av}$) 1.0×10^{-4} in units of absorbance, where σ_{av} is defined as the sum of squared deviations divided by total number of data points.

2.3.4 Evaluation of instrument performance Comparison of the instrument sensitivity

Because the instrument's own model has different performance, and the vibration during transportation may cause slight changes in the instrument structure, and the instrument related parameters may change due to the passage of time and instrument wear. To verify the performance of the instrument, we also observed with the OAS and TCCON instruments, simultaneously. TCCON has been carefully calibrated against tower and

aircraft measurements and provides a reference for remote-sensing measurements of GHGs observations. We put the OSA next to TCCON for observation, compare the observed data, and find the correction factor.

For the observation in Sichuan, we have obtained the scale factors of XCH_4 and XCO_2 for the present data processing program by analyzing the OSA spectral data at 10:00-14:00 daily measured at University of Wollongong, Australia (34.406°S, 150.879°E) in 2010-2011 where calibration study was conducted for the presently used OSA instrument, referring to the TCCON data. Unstable weather conditions or occasional thin-cloudy conditions reduce reliability of the OSA data since one spectral scan took about 3 min duration and compensation to solar intensity fluctuation is imperfect. We eliminated data points (the 10-min averaged values) if the data have a deviation over 0.14 ppm for XCH_4 and 10.2 ppm for XCO_2, which are averaged standard deviations (2σ) calculated for one day periods. Thus selected data points of 66 days are plotted in Fig. 2.4. The scale factor for the OSA XCH_4 and XCO_2 datas are determined to be 1.005 and 0.991:

$$XCH4(scaled）= XCH4 \ (retrieved) / 1.005 \qquad (2.1)$$
$$XCO_2(scaled）= XCO_2 \ (retrieved) / 0.991 \qquad (2.2)$$

The observed standard deviations (1σ) of the scale factors for 10-min average values are 0.032 for XCH_4 and 0.011 for XCO_2, which corresponds to 0.061 ppm for XCH_4 and 4.5 ppm for XCO_2. The standard deviations of 1-hour average values are 0.038 ppm for XCH_4 and 2.8 ppm for XCO_2.

For the observation in Tokyo, as for the TCCON FTS data, the scale factor and standard

error are 0.989 and 0.001, respectively (Wunch et al., 2010). The Tsukuba TCCON data available to us are reported to be scaled. The XCO_2 data of the OSA were compared with that of a co-located TCOON FTS instrument between April 22, to July 31, 2017 at the National Institute for Environmental Studies (NIES) at Tsukuba, Japan (36.05°N, 140.12°E). XCO_2 data are selected during a solar time of 10:00–14:00. When the solar light intensity is not stable enough due to occasional interruptions by clouds within a unit spectral scanning time of 1 min, spectral fittings in the retrieval calculations become poor. We eliminate the data over the averaged fitting deviation of 1.0×10^{-4} in units of absorbance. After selection, the number of days under measurable weather conditions is 67 days that range from April to July 2017. According to the comparison between OSA and FTS at Tsukuba under above conditions, the scale factor for the OSA XCO_2 data was determined to be 1.003:

$$XCO_2 \text{ (scaled)} = XCO_2 \text{ (retrieved)} /1.003 \qquad (2.3)$$

In the following descriptions, we use the OSA data that were corrected using this factor. The observed standard deviation (1σ) and error of the scale factor for 10-min average values were 0.011 and 0.0008 (0.3 ppm) for XCO_2, respectively (Fig 2.5).

The scale factors of Eqs. (2.1) and (2.2) are used in the observations of Sichuan in Chapter 4, and the scale factor of Eqs. (2.3) are used in the observations in Chapter 5 in Tokyo.
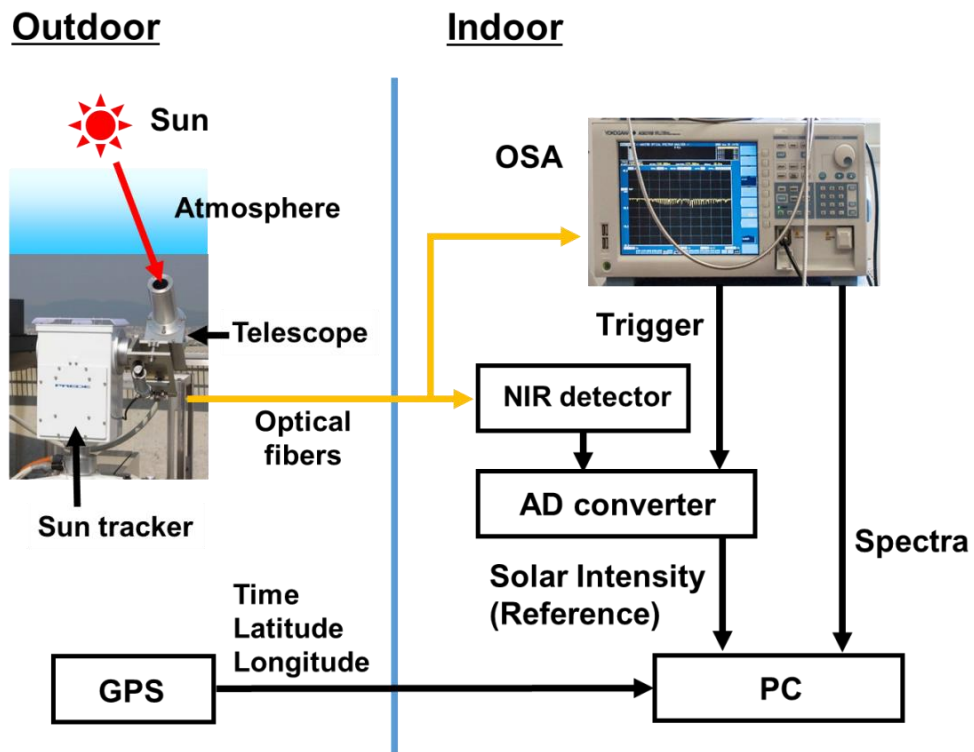
Fig 2.1 Schematic of the CO_2 column density measurement system. OSA: optical spectrum analyzer, AD converter: analog-digital signal converter, PC: personal computer, and GPS: global positioning system receiver.
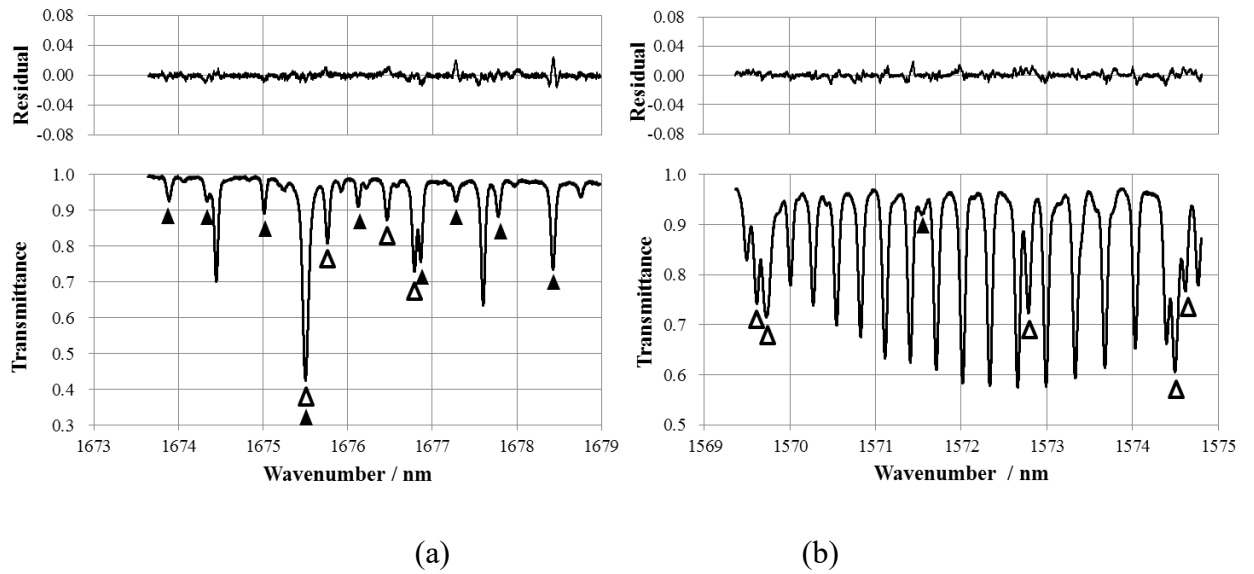
(a)   (b)

Fig 2.2 Examples of OSA spectra of Oct. 23th, 2013. Lower panel: Observed absorption spectra of (a) CH_4 and (b) CO_2. The fitting deviations between the observed and calculated spectra are shown in the upper panels of each spectrum. Open triangle: Fraunhofer lines, Solid triangle: H_2O peaks.

| (a) | (b) |
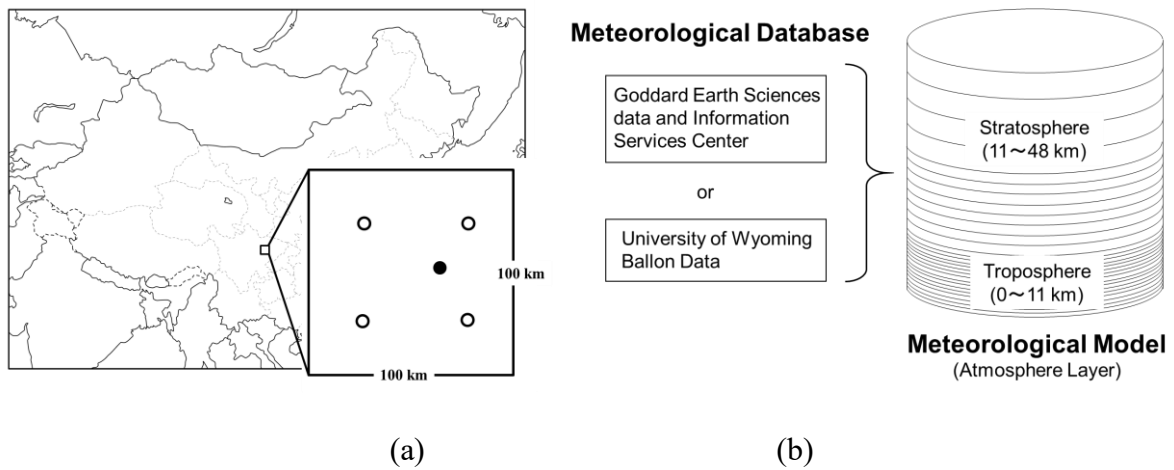
Fig 2.3   (a) open circle: location of meteorological data of GES DISC, filled circle: the Yanting observation station, (b) Sublayers up to 48 km altitude and incorporation of weather data.
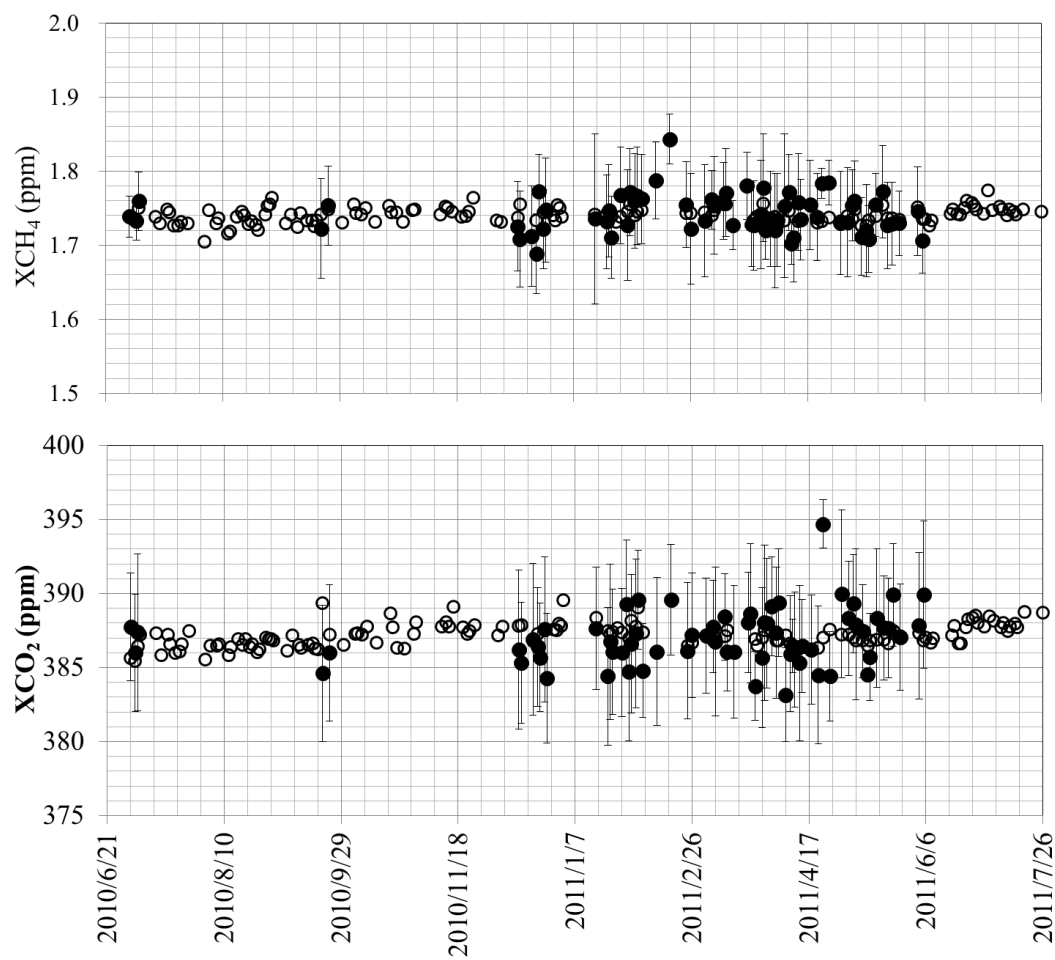
Fig 2.4 Comparison of the OSA data (filled circles, not scaled) and the TCCON data (open circles) at University of Wollongong, Australia, in May 2010-July 2011.
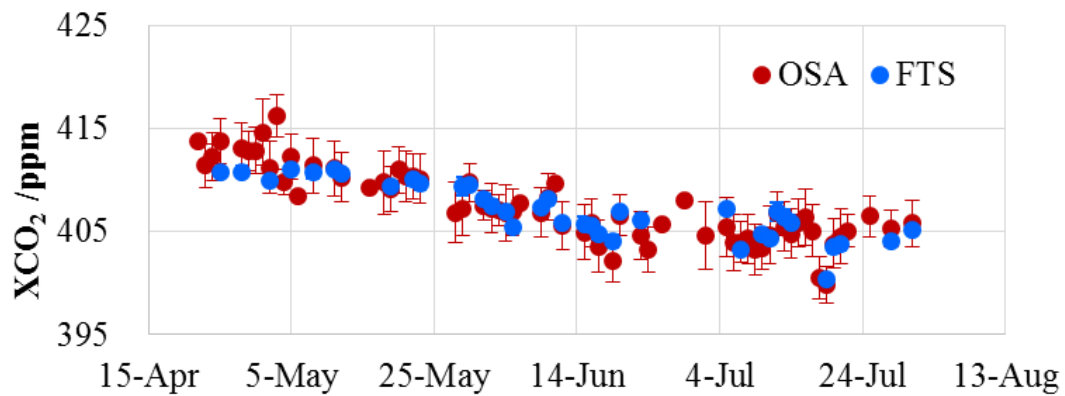
Fig 2.5 Comparison of the scaled OSA (red solid circle) and the FTS data (blue solid

circle) at NIES for a change in the daily average data during solar time 10:00–14:00

Table 2.1: The specific parameter settings of OSA

Station	OSA Type	Wavelength range	Scanning speed	Time period
Sichuan	AQ6370-custom	1672−1680 nm CH_4 1568−1576 nm. CO_2	12 seconds / scan	10:00-14:00
Tokyo	AQ6370B	1568–1576 nm CO_2	12 seconds / scan	9:00-15:00

References

[1] N. Kobayashi, G. Inoue, M. Kawasaki, et al., "Remotely operable compact instruments for measuring atmospheric CO_2 and CH4 column densities at surface monitoring sites," Atmos. Meas. Tech. 3, 1103–1112 (2010). [doi: 10.5194/amt-3-1103-2010]

[2] M. Kawasaki, H. Yoshioka, N. B. Jones, et al., "Usability of optical spectrum analyzer in measuring atmospheric CO_2 and CH4 column densities: Inspection with FTS and aircraft profiles in situ," Atmos. Meas. Tech. 5, 2593–2600 (2012). [doi:10.5194/amt-5-2593-2012].

[3] Yokota, T., Yoshida, Y., N. Eguchi, Ota, Y., Tanaka, T., Watanabe, H., Maksyutov, S., 2009. Global Concentrations of CO_2 and CH4 Retrieved from GOSAT: First Preliminary Results. Sola 5, 160–163. https://doi.org/10.2151/sola.2009-041.

[4] C. Frankenberg, R. Pollock, R. Lee, et al., "The Orbiting Carbon Observatory (OCO2): spectrometer performance evaluation using pre-launch direct sun measurements," Atmos. Meas. Tech. 8, 301–313 (2015). [doi:10.5194/amt-8-301-2015]

[5] S. Hayashida, A. Ono, S. Yoshizaki, et al., "Methane concentrations over Monsoon Asia as observed by SCIAMACHY: Signals of methane emission from rice cultivation," Remote Sens. Environ. 139, 246–256 (2013). [doi:10.1016/j.rse.2013.08.008].

[6] X. Xiong, S. Houweling, J. Wei, F. S. Maddy, and C. Barnet, "Methane plume over south Asia during the monsoon season: satellite observation and model simulation", *Atmos. Chem. Phys.*, vol. 9,pp.783-794, 2009.

[7] X. Y. Zhang, H. Jiang, Y. Q. Wang, Y. Han, M. Buchwitz, O. Schneising, and J.P. Burrows, "Spatial variations of atmospheric methane concentrations in China", *International Journal of Remote Sensing*,vol.32,pp.833 — 847, 2011.

[8] Schwandner, F. M. et al., 2017. Spaceborne detection of localized carbon dioxide sources. Science, 358, 3-4. http://science.sciencemag.org/content/358/6360/eaam5782.

[9] F. A. Jenkins and H. E. White, Fundamentals of Optics, 4th Ed, McGraw-Hill (1981) [ISBN 0072561912]

[10] R. A. Washenfelder, G. C. Toon, J. F. Blavier, et al., "Carbon dioxide column abundances at the Wisconsin Tall Tower site," J. Geophys. Res. Atmos. 111, 1–11 (2006). [doi:10.1029/2006JD007154]

[11] D. Wunch, G. C. Toon, P. O. Wennberg, et al.," Calibration of the Total Carbon

Column Observing Network using aircraft profile data," Atmos. Meas. Tech. 3, 1351–1362 (2010). [doi:10.5194/amt-3-1351-2010]

[12] Rothman, L. S., Gordon I. E., Barbe A. et al., "The HITRAN2008 molecular spectroscopic database," J. Quant. Spectrosc. Radiat. Transfer, 110, 533-572 (2009), [doi:10.1016/j.jqsrt.2009.02.013,2009]

[13] Rothman, L. S., Gordon I. E., Babikov Y. et al. "The HITRAN2012 molecular spectroscopic database," J. Quant. Spectrosc. Radiat. Transfer, 130, 4-50 (2013). [http://doi.org/10.1016/j.jqsrt.2013.07.002]

Chapter 3

Analysis of GOSAT XCH$_4$ and XCO$_2$ in Sichuan

Abstract

Since in the previous study, there were few studies using satellite data to analyze CH$_4$ emissions, so in this chapter, we analyzed the atmospheric column-averaged methane (XCH$_4$) observations from GOSAT, spanning from January 2010 to December 2013, to study the spatio-temporal variation of XCH$_4$ in China. In further, we investigate the driving mechanism of XCH$_4$ spatio-temporal variations, especially for high XCH$_4$ values shown over Sichuan Basin in south-west China, by analyzing both the emission mechanism of rice planting process, which is one of main CH$_4$ emission source in China, and the regional atmosphere dynamic transportation. The results indicate that spatially the Sichuan Basin presents a higher XCH$_4$ concentration than other regions in China, and is 17 ppb higher than the paddy area in the same latitude zone. Seasonally, XCH$_4$ in Sichuan Basin during rice harvest season (August and September) is generally higher than that in the early stage of the cultivation period (May), which is consistent with the general knowledge obtained from the ground measurements of CH$_4$ emissions process in rice paddy fields. However, comparing to paddy area in the same latitude zone, Sichuan Basin shows a relatively higher XCH$_4$ value during the winter of non-cultivation period when the emissions from rice paddies are weak and surface air temperature is low. To further investigate the high XCH$_4$ concentration during this low-emission period, we use the Hybrid Single-Particle Lagrangian Integrated Trajectory (HYSPLIT) model to simulate the atmosphere dynamic transport process, and the result suggests that the typical closed topography of Sichuan Basin, which may leads to CH$_4$ accumulation and keep it from diffusion, is one possible reason for the high XCH$_4$ value in winter. It is concluded that the spatial distribution and temporal variation of XCH$_4$ from GOSAT

observations are influenced by both emission sources, such as the regional rice paddies emissions, and the regional topography, such as Sichuan Basin which results in gas retention.

3.1 Introduction

Atmospheric CH_4 is one of the most important greenhouse gases, and the greenhouse effect generated by unit molecule of CH_4 is about 23 times higher than that of atmospheric CO_2. Therefore, it will be more effective to reduce the CH_4 emissions to mitigate the potential global warming than reducing CO_2 emissions (Hogan et al., 1991). The World Meteorological Organization (WMO) indicated in the "Greenhouse Gas Bulletin" published on September 9, 2014 that from the year 1990 to 2013, greenhouse effect had increased by 34% due to increasing concentrations of greenhouse gases such as CO_2 and CH_4. Global warming has become one of the most important global environmental issues nowadays. Therefore, analyses of the CH_4 concentration variation and studies on its driving factors have drawn increasing attention. However, due to limited observation capabilities and understanding of CH_4 sources and sinks, the underlying driving factors for the regional CH_4 spatio-temporal variation are still unclear (He et al., 2012). The increase of global atmospheric CH_4 concentration is mainly due to agricultural activities, in which irrigated rice paddy is one of the most important sources (Shen et al., 1995). China is the world's largest rice producer, accounting for about 22% of the rice planting area in the world and 37% of the global production. Therefore, studies of China's regional CH_4 emissions and its driving factors are of importance to understand the regional and global carbon cycle and the changing climate.

Since 1983, WMO has established a global greenhouse gases reference network for continuous observation of atmospheric greenhouse gases, including CH_4 concentration. However, due to the limited observation stations in many parts of the world, it is still difficult to comprehensively understand the global distribution and variation of CH_4 (Zhou et al., 1998, WMO 2001). Satellite remote sensing observation of atmospheric CH_4 concentration, which provides continuous observations at the global scale, plays an increasingly important role to improve our understanding of the distribution of sources and sinks of CH_4 and the carbon cycle (Kirschke et al., 2013, Deng et

al., 2014). To date, several satellites for observing CH_4 had been launched, including Atmospheric Infrared Sounder (AIRS) on the EOS/Aqua platform (Xiong et al., 2008), SCanning Imaging Absorption spectrometer for Atmospheric CHartographY (SCIAMACHY) (Frankenberg et al., 2004, Hayashida et al., 2013), and the Greenhouse gases Observing SATellite (GOSAT) (Yokota et al., 2009), and a lot of valuable observations have been obtained. Using AIRS data, Xiong et al. (2009) investigated a strong enhancement of CH_4 over South China region during the summer July, August and September in the middle to upper troposphere, and its relationship with transport and local surface CH_4 emission. Zhang et al. (2011) discovered that the vertical distribution of CH_4 concentration in the troposphere of China area decreases as the altitudinal increases. Moreover, seasonal CH_4 concentration in the eastern and northern parts of China presents a double-peak variation, with the highest concentration in summer and the second highest in winter. Hayashida et al. (2013) analyzed the relationship between rice paddy emission and XCH_4 concentration in Southeast Asia using satellite data obtained by SCIAMACHY, and found that there is a strong correlation between the two variables in Southeast Asia. Zhang et al. (2011) showed that paddy CH_4 emission is the major source of CH_4 in China and found that the air temperature, normalized difference vegetation index (NDVI) and soil total nitrogen explain more than 75% of the XCH_4 variation in China. Previous studies by (Hayashida et al., 2013, Xiong et al., 2009, Zhang et al., 2011) also showed that a consistently high CH_4 concentration is observed in the Sichuan Basin, including Chongqing and Sichuan regions in south-western China. These studies greatly improved the estimation of regional and national CH_4 emissions as well as our understanding of the CH_4 emission mechanism. However, most of previous studies focused on examining the correlation between the CH_4 variation and emissions from rice paddies, while potential driving factors for CH_4 variation, such as the atmospheric dynamic transport and influence from external sources, are not well analyzed, and therefore the underlying mechanism affecting the spatial and temporal distribution of CH_4 has not been comprehensively understood. Moreover, the used satellite observations of CH_4 concentration by most previous studies are primarily obtained from SCIAMACHY (Xiong et al., 2009, Zhang et al., 2011), which was launched on board ENVISAT and operational from March 2002 to April 2012. However, due to sensor problems happened in the end of the year 2005, the SCIAMACHY observing instrument became unstable since 2006 (He et

al., 2012). The GOSAT, launched on January 23, 2009, is the world's first spacecraft dedicated to observe greenhouse gases, including CO_2 and CH_4 (Hamazaki et al., 2004). GOSAT data has been widely used in many previous studies for studying CO_2 (Xiong et al., 2008, Xiong et al., 2008, Zeng et al., 2013, Lei et al., 2014., Zeng et al., 2014,), while studies on analyzing CH_4 from GOSAT observations are still rare.

In this study, XCH_4 observations from GOSAT, spanning from January 2010 to December 2013, are analyzed to study the spatio-temporal variation of XCH_4 in China and its relationship with regional surface emissions. In further, we investigate the driving mechanism of XCH_4 spatio-temporal variations, especially for high XCH_4 values shown over Sichuan Basin in south-west China, by combining the emission mechanism of rice planting process, the meteorology data, the surface emission data and the regional atmosphere dynamic transportation.

3.1.1 Station

Figure 3.1 shows the study area of China land region, the Sichuan Basin and the corresponding same latitude zone in the east for comparison of XCH_4 variation. Sichuan Basin is located in the upper reaches of the Yangtze River, encompassing the eastern part of Sichuan Province and most of Chongqing city, with an elevation of about 500 meters above the sea level. The Basin has a close topography, in which the eastern, southern and northern part of the basin is surrounded by mountains; and to the western is Qinghai-Tibet Plateau, which makes it difficult for air flow diffusion. The summer season of the basin lasts for 4 to 5 months with rich rain and temperatures as high as 25 ~ 29 °C during the hottest month, which is suitable for rice growing and make the basin one of China's five major rice-producing regions (Xia et al., 2004). The paddy region in Sichuan Basin with elevation less than 1000 meters is chosen to be the study area. In addition, Yanting county (105°27′E,31°16′N, ~420m in altitude), where we conducted ground-based observation of XCO_2 and XCH_4 (Qin et al., 2014, Kawasaki et al., 2012), and Yueyang city (116°42′E,43°38′N, ~40m in altitude), which is located between Hunan province and Hubei province in the same latitude paddy zone with Yanting, as shown in Figure 3.1, are chosen to be centers of the atmospheric molecule trajectory simulation.

3.1.2 Data

3.1.2.1 Satellite data

In this study, 3-year GOSAT XCH_4 Level 2 data (Version 02.XX) for General User (GU) from the year 2010 to 2012 are collected. XCH_4 data are retrieved using the spectra observed from Thermal And Near-infrared Sensor for carbon Observation Fourier Transform Spectrometer (TANSO-FTS) onboard the satellite with an orbiting period of 3 days. The nadir footprint of the instrument has a diameter of about 10.5 km at sea level. Compared to early versions, this 02.xx version XCH_4 data (https://data.gosat.nies.go.jp/gateway/gateway/MenuPage/open.do) were improved by identifying and correcting the error characteristics in retrieval, such as handling of aerosol scattering (Yoshida et al., 2013) which has a big impact on the GOSAT retrieval accuracy. The comparison result with data of the TCCON shows the bias and standard deviation of the GOSAT XCH_4 data are −5.9 and 12.6 ppb, respectively (Yoshida et al., 2013). Our ground measurement results implemented at Yanting Station using OSA (Qin et al., 2014, Kawasaki et al., 2012) for October- November of 2013 present 24 ppb lower deviation comparing with the GOSAT-XCH_4 data within 400 km distance from the station. Our XCH_4 data are the averaged values for the local mean solar time of 10-14 h, which show a decreasing tendency from the beginning of October to the end of November by 90 ppb, and have one standard deviation of 70 ppb. More detailed analysis is still in process.

3.1.2.2 Meteorological data

To study the relationship between air temperature and satellite-observed XCH_4 concentration, monthly mean temperature data in Sichuan Basin and the paddy area in the same latitude zone are collected from the China Meteorological Data Sharing System (http://cdc.cma.gov.cn/), which are based on the basic-reference surface weather observation station and automatic stations in China. We obtain the temperature data from the 19 stations in Sichuan Basin and 33 stations in the paddy areas in the same latitude zone from January 2010 to December 2013, and calculate the regional monthly-mean temperature of the two areas for the following analysis.

3.1.2.3 Emission dataset

CH_4 emissions from human activities and natural processes correspond to anthropogenic sources and natural sources respectively, in which anthropogenic emissions account for about 60% (WMO 2014). The anthropogenic emissions are mainly from rice cultivation, ruminants, waste disposal, biomass burning, and energy industries. The used dataset of CH_4 emissions is from the Emissions Database for Global Atmospheric Research (EDGAR) v4.2 data (http://edgar.jrc.ec.europa.eu/.) for the year 2010 on spatial grid of $0.1° \times 0.1°$. EDGAR is joint project of the European Commission JRC Joint Research Centre and the Netherlands Environmental Assessment Agency, and the data are mainly from point source emissions and global energy statistics database of the International Energy Agency (IEA). The EDGAR CH_4 emission data include emissions from agricultural soils, gases, industrial process and animal enteric fermentation (Yue et al., 2012). Figure 3.2 shows the spatial distribution of CH_4 emissions in China for the year 2010. The area of high emission sources around the Sichuan Basin are mainly located to the east and northeast, followed by the south, whereas the emissions to the west and north are almost negligible.

3.2 Data processing and analysis

In order to study the influence of nonlocal sources and atmospheric transport on CH_4 concentration, Hybrid Single-Particle Lagrangian Integrated Trajectory model (HYSPLIT) is used to simulate the atmospheric transport by successively setting Yanting and Yueyang as center point under the weather conditions of the year 2013. The HYSPLIT model is a complete system, developed jointly by NOAA and Australia's Bureau of Meteorology, for computing simple air parcel trajectories to complex dispersion and deposition simulations, allowing a variety of meteorological elements in the input file, varying physical processes and different types of emission sources. Past studies showed that 3-5 days trajectory simulation is an appropriate simulation period to study regional impact (Stohl et al., 1996, Rousseau et al., 2004). Therefore, three-day (72 hours) period is chosen in this study to implement the trajectory simulation using HYSPLIT. The simulations were started from the UTC time 00:00, 06:00, 12:00, and 18:00 respectively, with simulated height of 500 meters

above the ground. The simulated trajectories are aggregated using 0.5 ° × 0.5 ° grids to calculate the number of trajectory lines and the corresponding orientations within each grid under certain atmospheric conditions. CH$_4$ sources and sinks can then be further analyzed by combing the simulation data and the distribution of CH$_4$ emissions.

3.3 Results and discussion

Using the GOSAT XCH$_4$ Level 2 dataset collected from January 2010 to December 2013, we aggregated all the data into 2.5°×2.5° grids and calculated the averaged data within each grid to obtain the spatial distribution of XCH$_4$ in China, as shown in Figure 3.3. We found that the spatial variation of XCH$_4$ from GOSAT is generally consistent with XCH$_4$ bottom-up calculated emission data from EDGAR as shown in Figure 3.2. From Figure 3.3, it can be seen that west China shows a much lower value than south-east region. The lowest value exits in Qinghai-Tibet Plateau, where little CH$_4$ emission happens because the elevation is high (about 3000 meter on average) and there are much less human activities. However, the Sichuan Basin next to the Qinghai-Tibet Plateau presents the highest XCH$_4$ concentration in China. This overall distribution from GOSAT data shown in Figure 3.3 agrees with previous studies (Zhang et al., 2011).

A more detailed demonstration of the XCH$_4$ seasonal variations is shown in Figure3. 4, in which the seasonal variation of all the GOSAT XCH$_4$ data in China region with monthly mean data, the Sichuan Basin and the rice paddy fields in the same latitude zone are compared. The XCH$_4$ value in China land region varies from 1702 to 1917 ppb with mean value of 1794 ppb, and also presents an annual increase and a seasonal cycle with highest value in Autumn (July to September) and lowest value in Winter (November to January). This temporal variation is consistent with ground-based observation result from Waliguan, one of the World Data Centre for Greenhouse Gases (WDCGG) stations in China (Wei et al., 2000, Zhang et al., 2013). Moreover, XCH$_4$ in both of the Sichuan Basin and the rice paddy field area in the same latitude zone of the basin present general higher XCH$_4$ value than the averaged value in China land region, and XCH$_4$ value in previous region are on average 17 ppb higher than that in latter region. The difference of 17 ppb is

larger than the standard deviation (12.6 ppb) of the GOSAT XCH_4 data error, indicating a XCH_4 difference between the two regions with high confidence.

Two main factors that contribute to the XCH_4 concentration variability are the local surface CH_4 emission and the large scale atmosphere dynamic transport. Among the CH_4 emissions, more than 60% percent are from human activities, in which agriculture related emissions are the main component. According to statistics from EDGAR, as shown in Figure 3.2, in the Sichuan Basin the proportions of CH_4 emissions from agriculture related emission, fuel gas and waste water are 44%, 14% and 13%, respectively. On the other hand, the typical closed topography of Sichuan Basin, which results in low surface wind speed and CH_4 accumulation and keeps it from outward diffusion, together with high CH_4 emissions from large area of rice paddy fields in the Sichuan Basin are possibly the main reasons for the high XCH_4 value in region (Zhang et al., 2011). To further investigate the high XCH_4 value in this region, two factors, including the emission mechanism of rice paddy which is the main CH_4 emission source and the regional atmosphere dynamic transportation are analyzed to investigate the underlying processes leading to XCH_4 variability in the Sichuan Basin.

3.3.1 Relationship between seasonal variation of XCH_4 and emissions from rice paddies

Emissions of CH_4 from rice paddies become active through soil CH_4 production, re-oxidation and transmission and release from plant through the aeration organizations (Wei et al., 2000). The emission process of CH_4 is influenced by many factors including weather, water management, fertilization, soil respiration and rice growth (Wei et al., 2000, Chen et al., 1993, Wang et al., 2008). As shown by previous studies, the temperature is one of the most important factors influencing the CH_4 emissions from rice paddies (Shangguan et al., 1993, Yu et al., 1994) and the CH_4 emission will increase 3 times as the temperature increases by 10 ℃(Wang et al., 1995). The Sichuan Basin paddy region mainly includes winter rice paddy, which is characterized by irrigation in March, planting in May and rice harvesting in September. Afterwards the land keeps soil moisture and

remains arable until transplanting rice in the following May (Zhang et al., 2011, Wang et al., 2008). This kind of paddy field is flooded during all four seasons to keep the soil in a reduced state.

Figure 3.5 (a) and (b) show the relationship between the monthly averaged surface air temperature from weather stations and the XCH_4 values in the Sichuan Basin and the corresponding paddy fields in the same latitude zone, respectively. From Figure 3.5(a), in the Sichuan basin region the averaged XCH_4 value in September is generally higher than that in May, as expected according to the seasonal variation of CH_4 emissions due to rice paddy cultivation with planting in May and harvest in September. However, XCH_4 value during the non-cultivation season, especially from November to December and January to February, is unexpectedly higher than that in September which is the harvest month in cultivation. As shown in Figure 3.5(b), paddy rice regions in the same latitude zone show a different feature from the Sichuan Basin. From the available monthly mean XCH_4 data shown in Figure 3.5, we can see that both regions present an annual maximum of XCH_4 concentration in September. Moreover, we found the seasonal variation of XCH_4 of paddy regions in the latitude zone as shown in Figure 3.5(b) agrees well with the seasonal variation of surface air temperature, while the Sichuan Basin in Figure 3.5(a) presents a relatively higher XCH_4 value during low temperature period in winter. For the period during July and August, unfortunately, almost no GOSAT XCH_4 data are available during this rainy season because of the frequency clouds. As presented by Hayashida et al. (2013) using the SCIAMACHY data, this period, which is right before the paddy harvest time, presents the highest CH_4 concentration, corresponding to the highest surface air temperature.

It can be concluded that, in the Sichuan Basin region as in Figure 3.5(a), the seasonal variation of XCH_4 is generally consistent with CH_4 emissions from cultivation of rice paddy fields. However, higher XCH_4 is unexpectedly observed during the low temperature period in winter, which will be further investigated in the following sections in this paper. For the rice paddy fields located in the same latitude zone in Figure 3.5(b), the seasonal variation of XCH_4 generally agrees with CH_4 emissions from cultivation of rice paddy fields, and consistent with the surface air temperature variation.

3.3.2 Relationship between XCH$_4$ variation and atmospheric transport

HYSPLIT model is used to simulate atmospheric transport and trajectories to investigate the influence of transport on high XCH$_4$ concentration in January, February, November and December in the Sichuan Basin. Based on the source of gas molecules, a simulation can be categorized into backward trajectory simulation and forward trajectory simulation. A backward track simulation can be used to analyze the impact of external sources on local circumstances, and a forward trajectory simulation can be used to examine atmospheric dynamics and transport in a specific region. In this study, we chose Yanting and Yueyang in Sichuan Basin, as shown in Figure 3.1, as the target regions and implemented both the forward and backward simulation every three days beginning respectively from the two target regions at four UTC time (00:00, 06:00, 12:00, 18:00) each day for the year 2013. There are in total 4 trajectories for each target regions each day. Figure 3.6 shows gridded results from the backward simulation of the Sichuan Basin for each month in 2013. Figure 3.7 shows the results from forward trajectory simulation by setting Yanting and Yueyang City as the target regions in the year 2013.

Using all the trajectories from HYSPLIT forward simulation, as shown in Figure 3.7, we calculate the number of trajectories that remains in the target regions within different time ranges, to study the atmospheric transport and diffusion of CH_4 molecules from the study regions. Each trajectory line from the HYSPLIT output is a series of 73 hourly trajectory points, including the initial time (0 hour) and all hourly output of the 3 day simulation (3 day×24 hours). For each trajectory line, the time when the line intersects with the study region boundary is obtained and then used to calculate the staying time of the molecule inside the study area. The total number of daily trajectories inside the study region is grouped into 4 different time length (0, 12, 24 and 48 hours) and then further grouped into monthly statistics using the following equation (3.1).

$$L_m = \sum_{j=1}^{m_d} \sum_{i=1}^{4} n_{ij} \quad \begin{cases} n_{ij} = 1 \ (h_{ij} \geq H) \\ n_{ij} = 0 \ (h_{ij} < H) \end{cases} \ (H = 0, 12, 24, 48; \ h_{ij} \in (0,72])$$

(3.1)

where L_m is the number of trajectories staying inside the study area in month m. m_d is the number of day in the corresponding month. i is the daily number of trajectories. j is the *j-th* day in month m. h_{ij} is the time length from target point to the area boundary of the *i-th* trajectory in *j-th* day, which quantify the transport time by the molecules to be transported out of the study region. The value is from 0 to 72 hours. H stands for the 4 different time length. We define the Sichuan Basin region (Figure 3.7 (a)) and the circle region centering on Yueyang with 2.5° radius (Figure 3.7(b)) as two target regions. Figure 3.8 shows the number of CH_4 molecule trajectories staying inside these two target regions after 4 different transport running time in each month for the year 2013 calculated from equation (3.1) based on the forward simulations.

From Figure 3.8, in the Sichuan Basin region the number of staying trajectories is generally higher than Yueyang area, especially the result after 48 hours of transport, which indicates a strong gas retention phenomenon in the Sichuan Basin. For January, February, November and December in the basin region, the number of staying trajectories inside this area is obviously larger than other months, even after 48 hours of transport. However, the number of staying trajectories in Yueyang region is smaller in these months. Comparing with seasonal variation of XCH_4 in Figure 3.5, we found the seasonal variation of the number of staying trajectory inside the study region agrees well with the seasonal variation of XCH_4. Moreover, from Figure 3.7 we found in the Sichuan Basin area the air parcel trajectories are aggregating in a volute shape, indicating weak outward diffusion of the CH_4 molecules. However, the overall atmosphere transport in Yueyang as observed from the trajectories is distributed in obvious along the north-east and south-west direction, which is very different from the Sichuan Basin possibly mainly due to their different topography.

Compared with the backward simulation results in Figure 3.6, the Sichuan Basin is weakly influenced by emissions from a small part of the eastern China source region in February, and from north-eastern part in November, and is consistently and greatly influenced from north regions all the year, where, however, almost no CH_4 emission sources exist according to EDGAR emission data shown in Figure 3.2. Therefore, we conclude that in January, February, November and December, the CH_4 in Sichuan Basin is partly affected by the CH_4 emissions from the north-east and north regions, where the emissions are small, indicating the high XCH_4 values during these four months are not results of strong influence by external emission sources.

Regarding CH$_4$ emission from sources other than rice paddies, which might be impacting the spring/winter high in Sichuan Basin, we examined the GISS bottom-up emission inventory data (Matthews et al. 1991) as shown in Figure 8 (6-2, Sichuan Basin) in Hayashida et al. (2013). We found that during the cultivation season almost all the CH$_4$ emission is from rice cultivation, while during the winter non-cultivation season the rice emission is close to zero and the emissions from other sources are also very small that the GOSAT-observed high XCH$_4$ value during spring/winter are not likely from these sources.

From both the spatial and temporal variation of XCH$_4$ from GOSAT data as described and discussed above, it can be concluded that the typical closed topography of Sichuan Basin, which leads to CH$_4$ accumulation and keep it from diffusion, is one important reason for the high XCH$_4$ value observed in this region.

As the main sink of atmospheric CH$_4$, the reaction of CH$_4$ with hydroxyl radicals (OH) removes almost 90% of CH$_4$ (IPCC 2001). Because of a stronger chemical loss happened in summer, the CH$_4$ concentrations are generally lowest in summer and highest in winter, as reported by (WDCGG 2012) using the background observations from the monitoring network data. However, GOSAT XCH$_4$ data in this study shows a different seasonal variation in Sichuan Basin characterized by higher concentration during summer and autumn (rice cultivation season) and lower concentration during winter and spring (non-cultivation season), which are consistent with Hayashida et al. (2013) using the SCIAMACHY XCH$_4$ data. Unfortunately, few XCH$_4$ retrievals from GOSAT during summer are available for further investigation.

3.4 Conclusions

In this chapter, GOSAT-XCH$_4$ data from January 2010 to December 2013 are used to study the spatio-temporal variation of XCH$_4$ in China, especially for Sichuan Basin where it presents consistent higher XCH$_4$ values than other parts of China. We further investigate the driving factors, including the CH$_4$ emissions and regional atmosphere dynamic transport, to study the variations of CH$_4$ concentration in the basin, and evaluate the potential role of satellite-observed XCH$_4$ data in analyzing the regional variation of CH$_4$.

Our results show that the spatial distribution of GOSAT-XCH$_4$ is generally consistent with that of CH$_4$ emission, and abnormal high XCH$_4$ values can be seen in the Sichuan Basin, which is consistent with previous results from SCIAMACHY (Hayashida et al, 2012; Xiong et al, 2009). The seasonal variation of XCH$_4$ is highly related to the CH$_4$ emissions from rice paddy fields during rice growing period from April to October, and presents a difference feature from background CH$_4$ variation related to stronger CH$_4$ lose in summer due to chemical reaction. During the rice harvesting season of August to September, XCH$_4$ data are higher than that in early stage of rice growing about in April. However, the abnormal high XCH$_4$ data are shown in the winter when the CH$_4$ emissions from rice paddy fields are weak and the surface air temperature is low. By implementing the trajectory simulation using HYSPLIT in the basin, we found the typical closed topography of Sichuan Basin, which may leads to CH$_4$ accumulation and keep it from diffusion, is one possible reason for the extreme high XCH$_4$ value in winter. The influence of CH$_4$ emissions from sources other than rice paddies is also discussed and bottom-up emission inventory data show that they are not likely big causes of the observed winter high XCH$_4$ value in Sichuan Basin. It can be indicated that the regional variations of XCH$_4$ observed by GOSAT in Sichuan Basin are determined by not only

the CH_4 emissions from ground sources but also very likely the regional topography and the related regional air transport.

Our result from studying the CH_4 variations in Sichuan Basin, especially the abnormal higher value during winter, and their driving factors demonstrate a certain potential of using GOSAT-XCH_4 for investigating the regional CH_4 changes. This study presents preliminary results of CH_4 in China, and a further investigation of the CH_4 in the basin is still necessary as more satellite observations of CH_4 with improving accuracy are available in the coming future to further study the CH_4 variations and regional emissions (Parker et al., 2011).
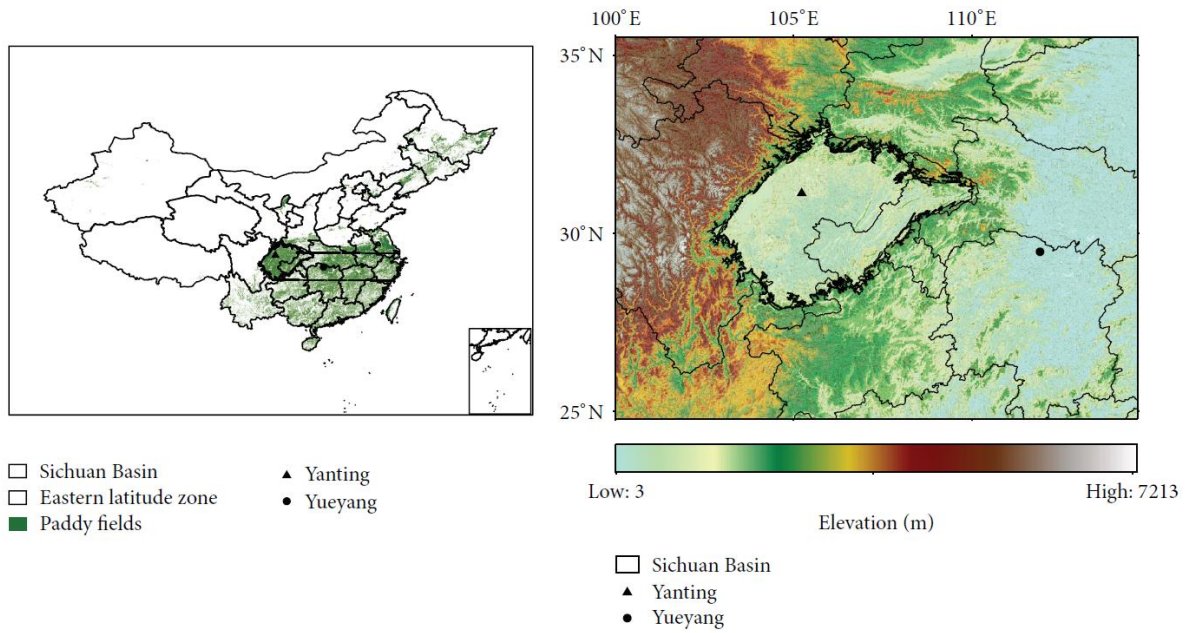
(a) Study Region and Paddy Fields   (b) Sichuan Basin

Fig 3.1 (a) Paddy fields distribution in China, the Sichuan Basin (black line polygon) and the comparative study regions (within two horizontal lines) at the same latitude zone to the east of the basin, and (b) the terrain elevation of the Sichuan Basin. Also showed in (a) and (b) are the localtions of Yanting (solid triangle) and Yueyang (solid circle).
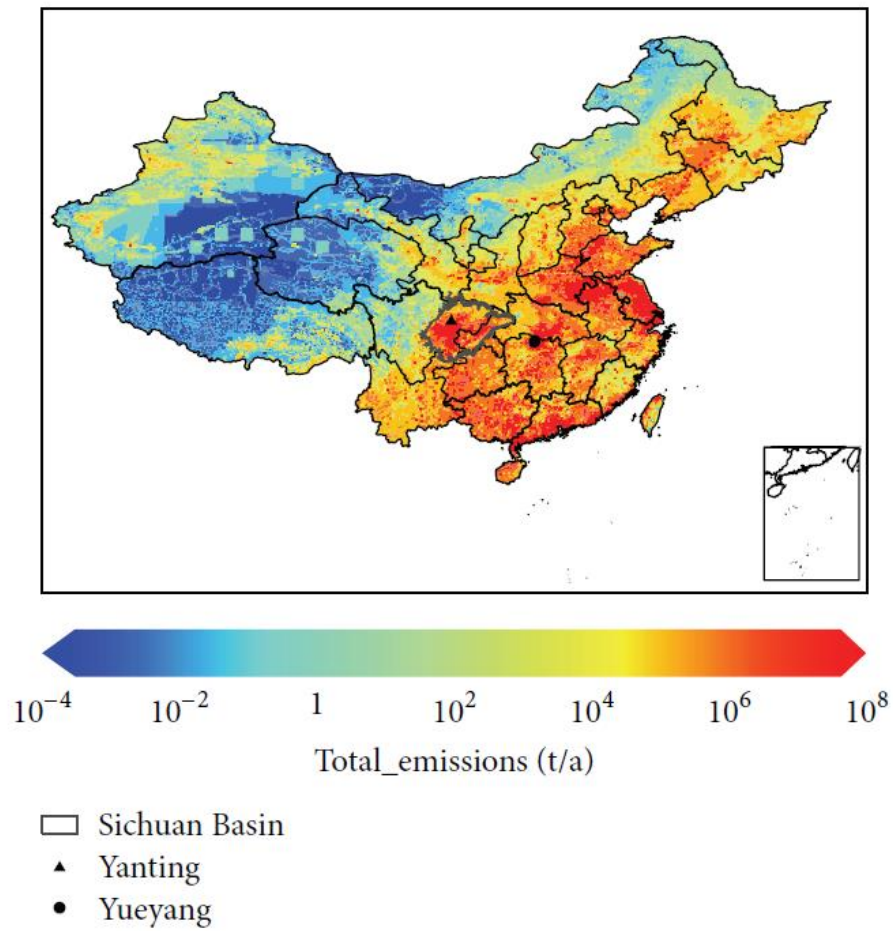
Fig 3.2 Amount of CH$_4$ emissions in China region in 2010 from EGDAR4.2 data (a colorbar of the emission value is shown by taking their base 10 logarithms).
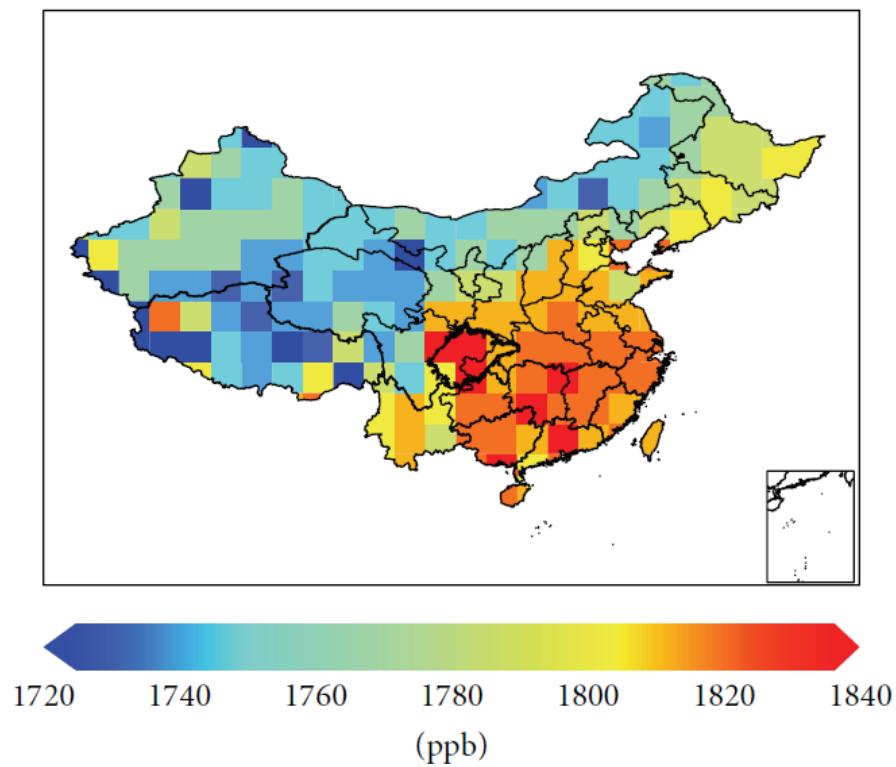
Fig 3.3 Spatial distribution of XCH$_4$ aggregated into 2.5°×2.5° from GOSAT observations spanning from January 2010 to December 2013.
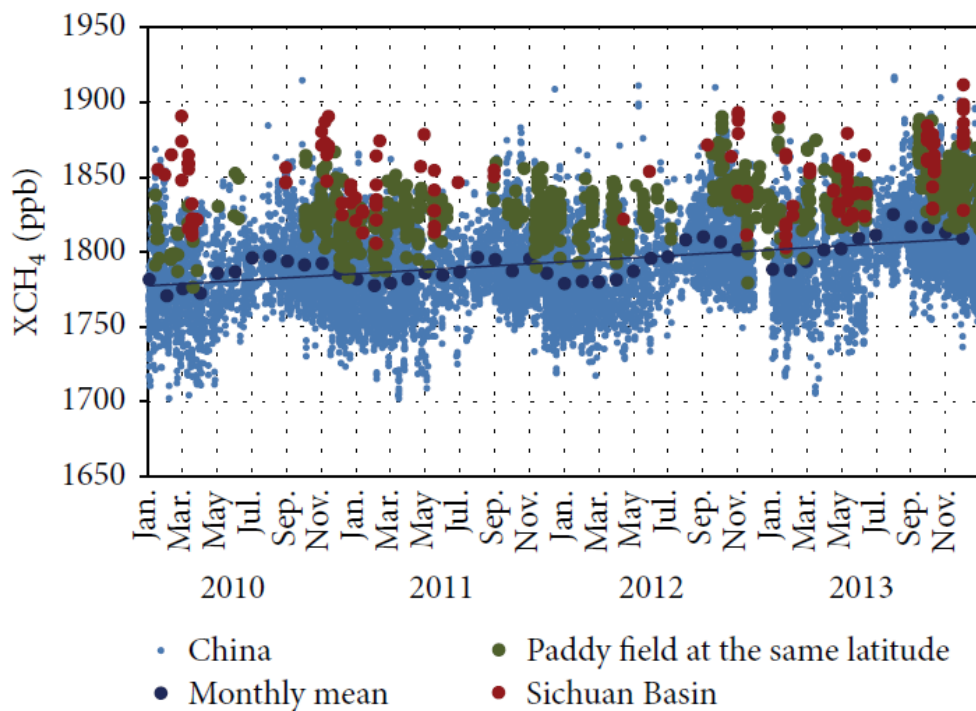
Fig 3.4 The seasonal variation of all the GOSAT XCH$_4$ data over China land region (light blue dots), the Sichuan Basin (red dots) and the rice paddy fields (dark green dots) in the same latitude zone from January 2010 to December 2013. The dark blue dots are the monthly mean for land region and the blue line shows the corresponding trend from linear fitting.
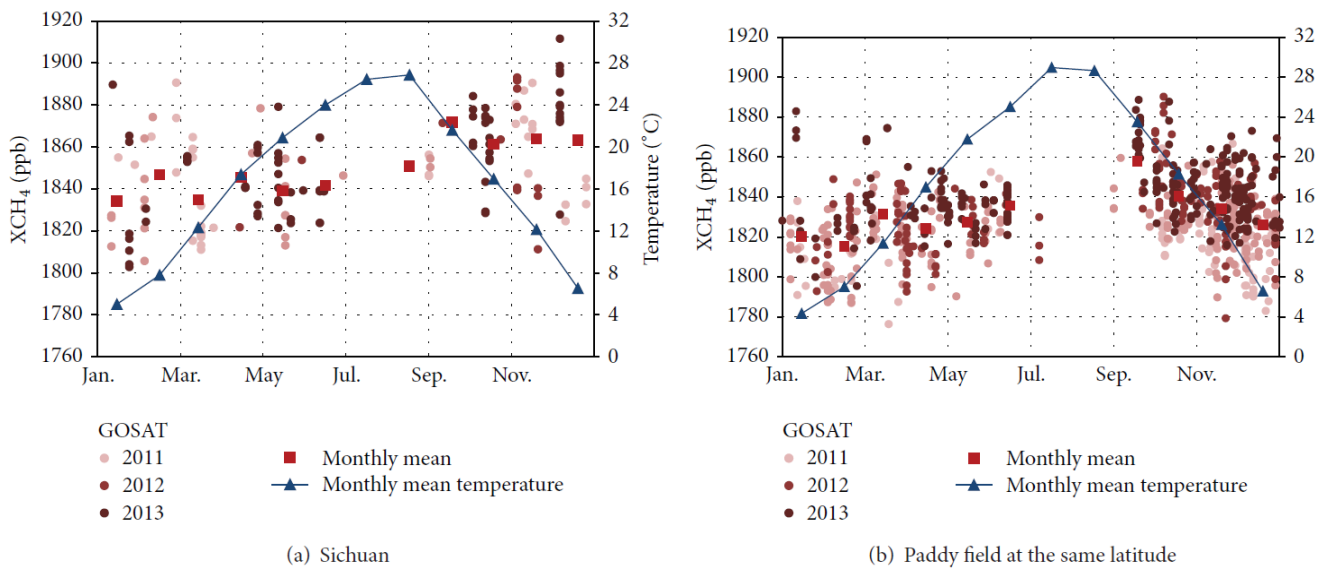
Fig 3.5 Comparison of XCH4 value from GOSAT and the corresponding surface air temperature values from weather stations in (a) the Sichuan Basin and (b) the rice paddy fields in the same latitude region. The time lable of months in x-axis indicates the beginning of each month.
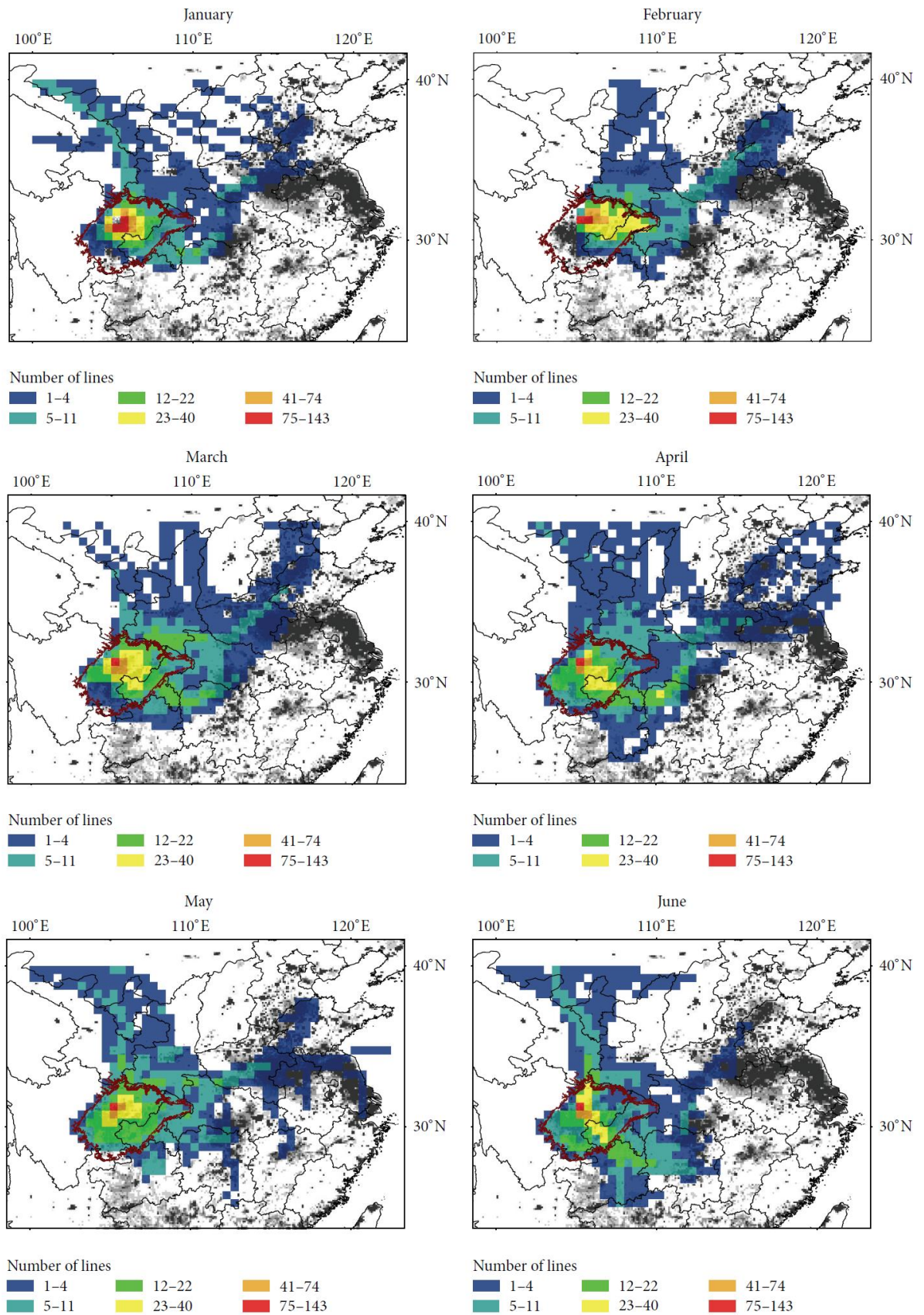
Fig 3.6: The density of the backward simulated trajectories, which are gridded into 0.5 by 0.5 degree grids, from Yanting in the Sichuan Basin for each month in 2013.
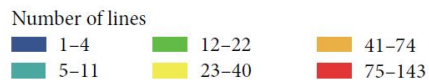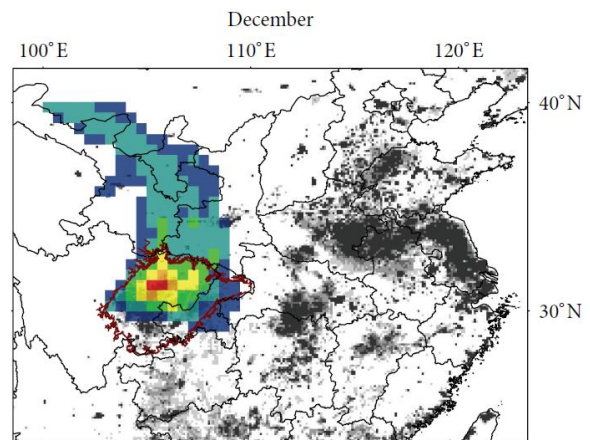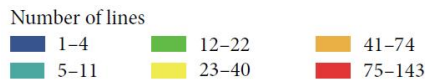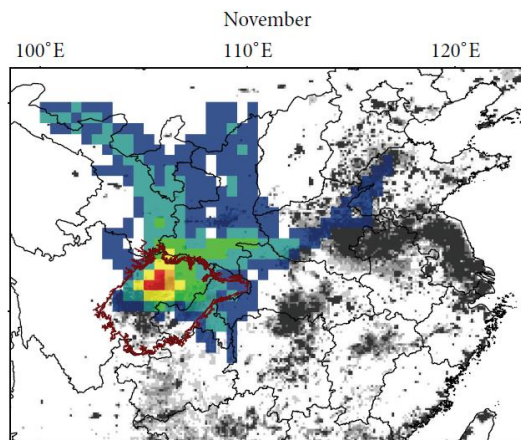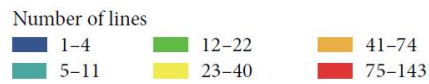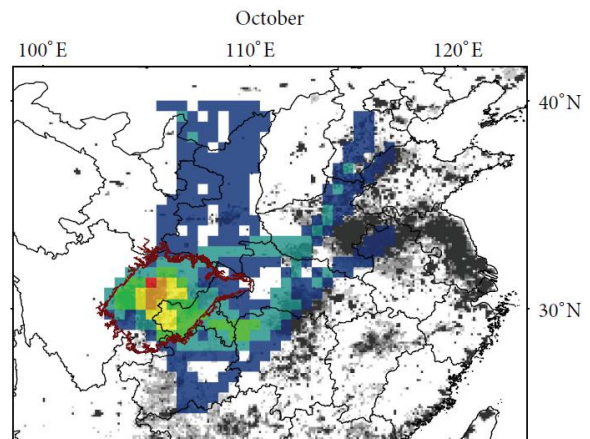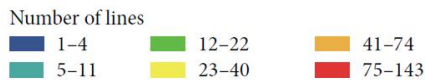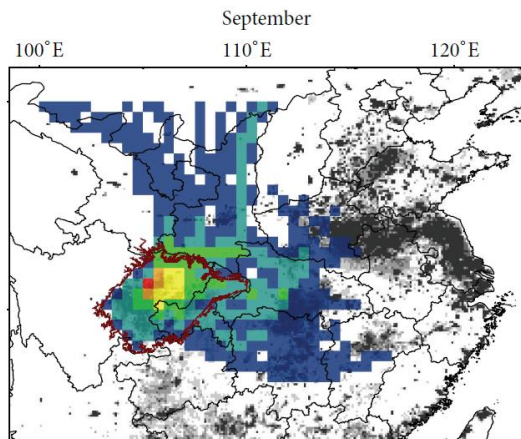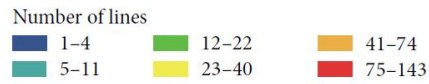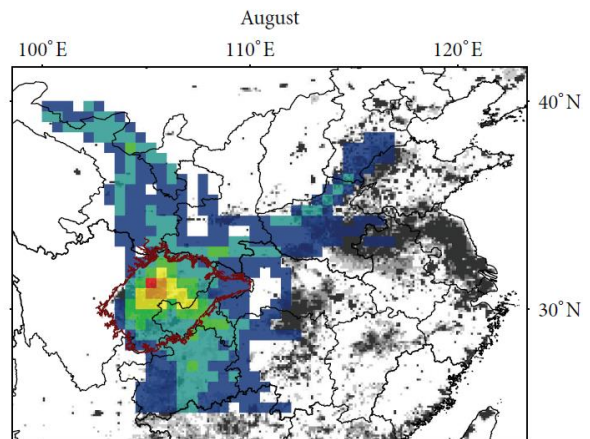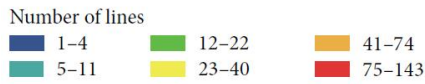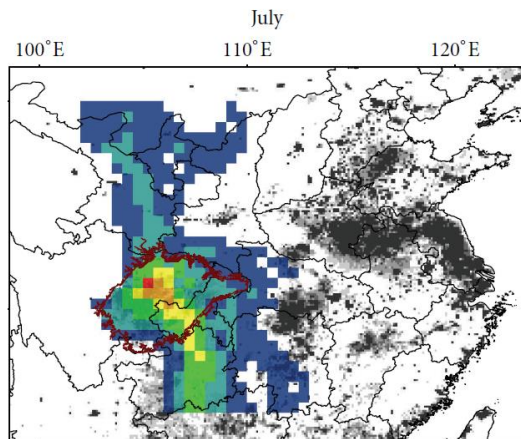
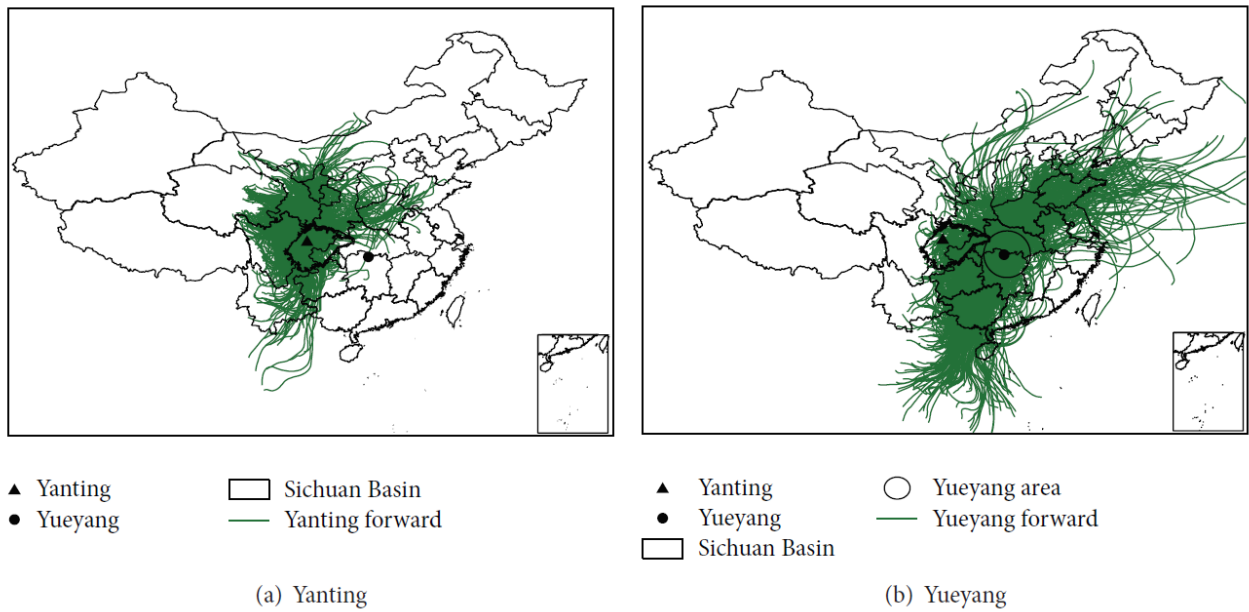Fig 3.6 Continued.

(a) Yanting

(b) Yueyang

Fig 3.7 The spatial distribution of forward trajectory simulation from (a) Yanting (solid triangle) in Sichuan Basin and (b) Yueyang area (solid circle).
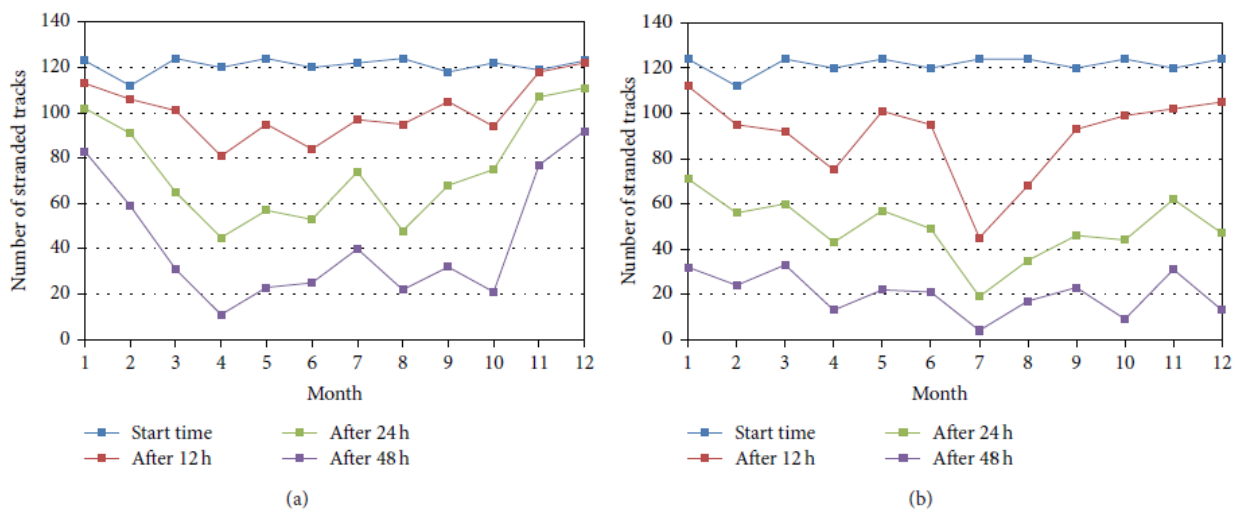
Fig 3.8 The number of trajectories that still stay inside the study area of (a) the Sichuan Basin, and (b) the circle region centering on Yueyang with 2.5° radius after 4 different transport time (0, 12, 24 and 48 hours).

References

[1] K. B. Hogan, A. M. Thompson, and J. S. Hoffman, "Methane on the greenhouse agenda", *Nature*, vol.354, pp.181 - 182, 1991.

[2] Q. He, T. Yu, X. F. Gu, T. H. Cheng, Y. Zhang, D. H. Xie, "Global atmospheric methane variation and temporal-saptial distribution analysis based on ground-based and satellite data", *Remote Sensing Informations*,Vol.27,No.4,pp.35,2012.

[3] R. X. Shen, X. J. Shangguan, M. Wang, et al., "Methane emission from rice fields in Guangzhou region and the spatial variance of methane emission in China", *Advance In Earth Science*, Vol.10,No.4,pp.2701,1995.

[4] L. X. Zhou, J. Tang, Y. P. Wen, et al., "Characteristics of atmospheric methane concentration variation at Mt. Waliguan", *Quarterly Journal of Applied Meteorology*, vol.9, pp.385–391, 1998.

[5] WMO. Strategy for the Implementation of the Global Atmosphere Watch Programme(2001–2007), a contribution to the implementation of the WMO longterm plan. GAW Report, pp.142: 1–21. 2001.

[6] Kirschke, Stefanie, Philippe Bousquet, Philippe Ciais, et al., "Three decades of global methane sources and sinks." *Nature Geoscience 6*, no. 10, pp.813-823, 2013.

[7] F. Deng, D. B. A. Jones, D. K. Henze, et al. ," Inferring regional sources and sinks of atmospheric CO_2 from GOSAT XCO_2 data", *Atmos. Chem. Phys.*, no. 14, pp. 3703-3727, doi:10.5194/acp-14-3703-2014, 2014.

[8] X. Xiong, C. D. Barnet, E. Maddy , C. Sweeney , X. Liu , L. Zhou, and M. Goldberg, " Characterization and Validation of Methane Products from the Atmospheric Infrared Sounder (AIRS)", *J. Geophys. Res.*, no. 113, G00A01, doi:10.1029/2007JG000500, 2008.

[9] C. Frankenberg, J. F. Meirink, P. Bergamaschi, et al., "Satellite cartography of atmospheric methane from SCIAMACHY on board ENVISAT: Analysis of the years 2003 and 2004", *Geophys. Res.*, vol.111, no.07303, doi:10.1029/2005JD006235,2006.

[10] S. Hayashida, A. Ono, S. Yoshizaki, C. Frankenberg , W. Takeuchi, X. Yan, "Methane concentrations over Monsoon Asia as observed by SCIAMACHY: Signals of methane emission from rice cultivation", *Remote Sensing of Environment*. Vol.8,no.8,2013. doi:10.1016/j.rse.2013.08.008

[11] T. Yokota, Y. Yoshida, N. O. Eguchi, et al., "Global concentrations of CO_2 and

CH$_4$ retrieved from GOSAT: First preliminary results", *Scientific online letters on the atmosphere: SOLA*, vol.5, pp.160-163,DOI: 10.2151/sola.2009-041, 2009.

[12] X. Xiong, S. Houweling, J. Wei, F. S. Maddy, and C. Barnet, "Methane plume over south Asia during the monsoon season: satellite observation and model simulation", *Atmos. Chem. Phys.*, vol. 9,pp.783-794, 2009.

[13] X. Y. Zhang, H. Jiang, Y. Q. Wang, Y. Han, M. Buchwitz, O. Schneising, and J.P. Burrows, "Spatial variations of atmospheric methane concentrations in China", *International Journal of Remote Sensing*,vol.32,pp.833 — 847, 2011.

[14] T. Hamazaki, A. Kuze, and K. Kondo, "Sensor system for greenhouse gas observing satellite (GOSAT)", in Optical Science and Technology, the SPIE 49th Annual Meeting. 2004. International Society for Optics and Photonics.

[15] Z. C. Zeng, L. P. Lei, L.J. Guo, L. Zhang. B. Zhang, "Incorporating temporal variability toimprove geostatistical analysis of satellite-observed CO$_2$ in China", *Chinese Science Bulletin*,Vol.58,No.16,pp.1948-1954,2013.

[16] L. P. Lei, X. H. Guan, Z. C. Zeng, B. Zhang, F. Ru, and R. Bu. "A comparison of atmospheric CO$_2$ concentration GOSAT-based observations and model simulations", *Science China Earth Sciences 57*, no. 6, PP. 1393-1402,2014.

[17] J. X. Xia, L. J. Deng, S. R. Zhang, "Effects of environmental factors on the Sichuan Basin rice quality", China to soil Society Tenth National Congress and the fifth member representative cross-strait academic exchanges and Fertilizer Symposium for agricultural and environmental soilscience topics articles.2004.

[18] X. C. Qin, L. P. Lei, M. Kawasaki, M. Ohashi, T. Kuroki, Z. C. Zeng. B. Zhang, "Retrieval and Analysis of Atmospheric XCO$_2$ Using Ground-Based Spectral Observation", *Spectroscopy and Spectral Analysis*, vol.34, no.7, pp.1729-1735,2014.

[19] M. Kawasaki, H. Yoshioka, H, N. Jones, et al., "Usability of optical spectrum analyzer in measuring atmospheric CO$_2$ and CH$_4$ column densities: inspection with FTS and aircraft profiles in situ", *Atmospheric Measurement Techniques*.vol.5, pp.2593-2600, 2012.

[20] https://data.gosat.nies.go.jp/gateway/gateway/MenuPage/open.do.

[21] Y. Yoshida, N. Kikuchi, I. Morino, O. Uchino, S. Oshchepkov, et al., "Improvement of the retrieval algorithm for GOSAT SWIR XCO$_2$ and XCH$_4$ and their validation using TCCON data", *Atmospheric Measurement Techniques*, vol.6, pp.1533–1547, 2013.

[22] http://cdc.cma.gov.cn/index.jsp.

[23] WMO GREENHOUSE GAS BULLETIN , No. 10 ,9 September 2014.

[24] http://edgar.jrc.ec.europa.eu/.

[25] Q. Yue, G. J. Zhang, Z. Wang, "Preliminary estimation of methane emission and its distribution in china", *GEOGRAPHICAL RESEARCH*,vol.31,no.9,pp.1559-1568.2012.

[26] A. Stohl, "Trajectorystatisticsanew method to establishsource-receptor relationships of air pollutants and its application to the transport of particulate sulfate in Europe", *Atmos.Environ*, vol.30, pp.579-587,1996.

[27] D. D. Rousseau, D. Duzer, J. L. Etienne, et al., "Pollen record of rapidly changing air trajectories to the North Pole". *Geophys. Res*,Vol.109, no.6,DOI: 10.1029/2003JD003985,2004.

[28] G. J. Zhang, "Temporal and spatial distribution of column vertical density and emission of methane in China", *East China Normal University*,2011.

[29] C. F. Wei, M. Gao, Q. Huang, F. C. Che, J.-H. Yang, D. T. Xie, Z. C. Cai, H. Xu, "Effects of tillage-cropping systems on methane emission from year-round flooded paddy field in Southwest China", *Acta pedologica sinica*,vol.37,no. 2,pp.157-165,2000.

[30] F. Zhang, L. X. Zhou, X. Lin, "Temporal variation of atmospheric CH_4 and the potential source regions at Waliguan, China", *Science China Earth Sciences 56*, no. 5, pp.727-736. 2013

[31] D. Z. Chen, M.-X. Wang, X.-J. Shangguan, J. Huang, "methane emission from rice fields in the south-east China", *Advance In Earth Science*, vol.8,no. 5,pp.47,1993.

[32] Y. Y. Wang, W. W. Chen, Z. C. Zhao, J.-X. Gu, "Characteristics and emission from cold paddy field in the Sanjiang Plain", *Transactions of the CSAE*, vol.24,no.10,pp.170-176,2008.

[33] X. J. Shangguan, M. X. Wang and R. X. Shen, "regularity of methane emission from rice paddy fields", *Advance In Earth Science*,vol.8,no. 5,pp. 23,1993.

[34] X. K. Yu, N. Li, C. Y. Li, B. Shao, W. D. Wang, X. L. Xie, "Effect of temperature on methane emissions from rice paddies", *Advance In Earth Science*., vol.9,no. 5,pp.54- 56,1994.

[35] W. D. Wang, X. L. Xie, x. j. Shangguan, D. Z. Chen, M. X.Wang, "Laws of methane production in paddy soil in red earth hilly area of South China", *Rural Eco-Environment*, vol.11,no.3,pp. 11- 14,1995.

[36] R. Parker, H. Boesch, A. Cogan, et al., "the observations from the Greenhouse Gases Observing SATellite: Comparison to ground-based TCCON data and model calculations", *Geophysical Research Letters*,Vol.38,no.15,pp.5-6,DOI: 10.1029/2011GL047871,2011.

[37] Z. Zeng, L. Lei, S. Hou, F. Ru, X. Guan and B. Zhang, "A Regional Gap-Filling Method Based on Spatio-temporal Variogram Model of CO_2 Columns," IEEE Transactions on Geoscience and Remote Sensing, Vol. 52, No. 5, DOI: 10.1109/TGRS.2013.2273807, 2014.

[38] E. Matthews, I. Fung and J. Lerner, "Methane emission from rice cultivation: Geographic and seasonal distribution of cultivated areas and emissions," Global Biogeochemical Cycles, 5, 3–24, 1991.

[39] Intergovernmental Panel on Climate Change (IPCC), "Climate Change 2001: The Scientific Basis," 881 pp., Cambridge Univ. Press, New York, 2001.

[40] World Meteorological Organization, WDCGG Data Report No. 36, 2012.

Chapter 4

XCH$_4$ and XCO$_2$ observations in Sichuan using OSA system

Abstract

The CH$_4$ and CO$_2$ in the atmosphere are mainly from anthropogenic and biological sources. Among them, the CH$_4$ of the biological emission source is mainly the final product of the decomposition of organic matter in anaerobic environments, such as rice paddies, water-saturated soils etc. Many results indicate that spatially the paddy field area presents higher CH$_4$ concentrations than other regions. The geographical distribution of the emissions from one of anthropogenic sources, rice cultivation, is assessed by global and regional inventories or by land surface models. Most emission is from the area around 30°N, including China and India. The geographical distribution of high XCH$_4$ corresponds to strong emissions from regions where rice is cultivated. In China, the concentrations of CH$_4$ is the Sichuan Basin because rice cultivation emits CH$_4$ and the Basin topography slows down air spread according to analysis of the GOSAT data and the hybrid single-particle Lagrangian integrated trajectory (HYSPLIT) model calculations (Qin et al, 2015). The station density of TCCON is sparse especially in the areas remote from human settlements. Satellite observations can provide the GHG data globally but only for brief time every few days at each target. To provide detailed time-varying data of XCH$_4$ and XCO$_2$ in the Sichuan Basin in China, we here report measurements by using the OSA and a portable sun tracker in the fall of 2013. The OSA measures solar absorption spectra in the near-infrared (NIR) region. Our results are compared with the GOSAT satellite data targeted near Yanting in the Sichuan Basin during the same observation period as well as the ground-based TCCON observation data at the latitude zone same as our observation

station.

4.1 Introduction

CH_4 and CO_2 are potent GHGs that contribute to human-induced climate change. Understanding the evolution of the CH_4 budget as well as CO_2 has implications for future climate change scenarios and mitigation options to avert further global warming. The GHG budget includes emissions from anthropogenic sources (*e.g.* rice paddy, fossil fuel) and natural sources (*e.g.* wetland), which are estimated using top-down method that combines global measurements of atmospheric GHGs concentrations at ground-based stations and by satellites with an atmospheric inversion framework. Examples are the surface station network like TCCON network equipped with high-precision and high-accuracy Fourier transform infrared spectrometers (Wunch et al., 2011; Wunch et al., 2015; Wunch et al., 2005), satellite-borne instruments like SCIAMACHY (Frankenberg et al., 2005), GOSAT (Yokota et al., 2009) or OCO-2 sensors (Frankenberg et al., 2015). Reducing uncertainties in individual GHG sources, the atmospheric observation sites density has improved with the measurements of column-averaged molar mixing ratios, XCH_4 and XCO_2. Along with those established atmospheric observing networks, the development of a portable column spectrometer can partition regional emission sources to cover sparse world-wide observation points. There have been attempts with use of a desktop optical spectrum analyzer (Kobayashi et al., 2010; Kawasaki et a., 2012) for the back-ground measurement of column-averaged dry air abundances of CO_2 and CH_4, and a portable FTIR spectrometer for the quantification of localized sources(Hase et al., 2015; Butz et a., 2017). An alternative approach to remote sensing is the boundary layer abundance measurement, the downside of which is the high sensitivity to vertical exchange of air masses and local sources near vicinity.

The CH_4 and CO_2 in the atmosphere are mainly from anthropogenic and biological sources. Among them, the CH_4 of the biological emission source is mainly the final

product of the decomposition of organic matter in anaerobic environments, such as rice paddies, water-saturated soils etc. Many results indicate that spatially the paddy field area presents higher CH_4 concentrations than other regions. The geographical distribution of the emissions from one of anthropogenic sources, rice cultivation, is assessed by global and regional inventories or by land surface models. Most emission is from the area around 30°N, including China and India (Hayashida et al., 2013; Chen et al., 2013; Zhang et al., 2013; Yan et al., 2003). The geographical distribution of high XCH_4 corresponds to strong emissions from regions where rice is cultivated, as indicated in the inventory maps. In China the concentrations of CH_4 is the Sichuan Basin because rice cultivation emits CH_4 and the Basin topography slows down air spread according to analysis of the GOSAT data and the HYbrid Single-Particle Lagrangian Integrated Trajectory (HYSPLIT) model calculations (Hayashida et al., 2013; Qin et al., 2015).

The station density of TCCON is sparse especially in the areas remote from human settlements. Satellite observations can provide the GHG data globally but only for brief time every few days at each target. To provide detailed time-varying data of XCH_4 and XCO_2 in the Sichuan Basin in China, we here report measurements by using a desktop OSA and a portable sun tracker in the fall of 2013. The OSA measures solar absorption spectra in the near-infrared (NIR) region. Our results are compared with the GOSAT satellite data targeted near Yanting in the Sichuan Basin during the same observation period as well as the ground-based TCCON observation data at the latitude zone same as our observation station. The present instrument, used for greenhouse gases observations, is suited for operation at remote places because of its compact design, low power requirement and appreciable accuracy.

4.2 Introduction of observation station

Our observation station is located at the Yanting Agro-ecological Experimental Station of Purple Soil (105.45°E, 31.27°N, 483 m a.s.l.) surrounded by mountains about 150 km

north-east away from the capital of the Sichuan province in the Sichuan Basin as shown in Fig. 4.1. The station belongs to Institute of Mountain Hazards and Environment, Chinese Academy of Sciences. The Sichuan Basin is in the upper reaches of the Yangtze River and the southwest part of China. It is one of the five major rice producing areas in China because of its high rainfall and hot temperatures.

4.3 Calibrations

As described in the chapter 2, we obtain the scale factors as shown in Eqs. *(2.1) and (2.2)* by analyzing the OSA spectral data previously measured at University of Wollongong, Australia, where a calibration study was conducted for the OSA instrument using a co-located TCCON Fourier transform spectrometer

In the following descriptions we use the OSA data corrected by these factors. The observed standard deviations (1σ) of the scale factors for 10-min average values are 0.032 for XCH_4 and 0.011 for XCO_2, which corresponds to 0.061 ppm for XCH_4 and 4.5 ppm for XCO_2. The standard deviations of 1-hour average values are 0.038 ppm for XCH_4 and 2.8 ppm for XCO_2.

As for TCCON raw data, the scale factors are 0.978 (standard error 0.002) for XCH_4 and 0.989 (0.001) for XCO_2 (Rothman et al., 2013). The standard errors of TCCON data correspond to 0.004 ppm for CH_4 and 0.4 ppm for XCO_2. The TCCON data available to us are reported to be scaled. As for the GOSAT satellite data (version 02) available to us, the retrieval algorithm shows biases and standard deviations, -0.0059 and 0.0126 ppm for XCH_4 and -1.48 and 2.09 ppm for XCO_2, respectively (Yoshida et al., 2013). In the following descriptions we use the GOSAT data corrected for these biases.

4.4 Results and discussion

4.4.1 Diurnal and Temporal Variations of CH_4 and CO_2

The OSA observation can provide daytime diurnal variations. During the period of September-November of 2013, the number of days under measurable weather conditions was fifteen days in a three-month campaign. The diurnal variations in XCH_4 and XCO_2 for solar time of 10:00-14:00 of a sunny day, October 12th, 2013, are shown in Fig. 4.2. To see the averaged diurnal variations, the lower panel of Fig. 4.3 presents the XCO_2 averaged deviations data over all observation period. In this figure, firstly the deviation in XCO_2 from the daily mean value, $XCO_2(d,t) - <XCO_2(d,t)>_d$, is calculated for a certain solar time, t, of a certain day, d. Secondly the deviations at that time t are averaged over all available days, $<XCO_2(d,t) - <XCO_2(d,t)>_d>_t$. When examining Fig. 4.3, the diurnal variation is not conspicuous within the standard deviation of 2.6 ppm because the reduction of atmospheric CO_2 due to the photosynthesis by plants was possibly small during the observation time of 10:00-14:00 around the Yanting station. Although *Sichuan's* most important *industry is* agriculture, it has strong presence in a variety of heavy and light industries. Yanting is located at 150 km northeast of Chengdu (population 14 billion), the capital of the province, and 80 km east-southeast of Mianyang (5 billion), a large industrial city. When examining the diurnal variation of the averaged deviations of XCO_2, we estimate that polluted air masses of those megacities did not come to the Yanting area during the campaign period since the wind directions are mostly southeast according to the NOAA HYSPLIT model back-trajectory calculations except Oct. 23rd. The diurnal variation of the XCH_4 averaged deviations in Fig. 4.3 (upper panel) is also not conspicuous within the standard deviation of 0.042 ppm, suggesting that the emission and dissipation processes of CH_4 do not have strong diurnal variations in 10:00-14:00. Satellite cannot provide diurnal variations because measurements are performed at the limited overpass time (~13:00 solar time) every three days at each observation target (TCCON site).

Figure 4.4 shows the time series of the daily mean values. The $<XCH_4>$ values are high during the observation period of September-November, 2013. The Sichuan Basin paddy region is characterized by irrigation in March, planting in May, and rice harvesting

in September. Saga and Tsukuba TCCON stations in Japan are located in the latitude zone same to the Yanting station. A large anomaly of XCH_4 was seen there in August-September, 2013 according to Ishizawa et al. (2016), which was attributed to the anomalous atmospheric pressure pattern over East Asia during the summer of 2013. The CH_4-rich air was effectively transported to Japan from the strong CH_4 source areas in southeast China. Saga and Tsukuba stations are located along the substantially CH_4-rich air flow from east China. The CH_4 emissions from the Sichuan Basin during the August-September period may also have contributed to the CH_4-rich air.

The upward variation of $<XCO_2>$ in Fig. 4.4 is consistent with the mid latitude seasonal variation of XCO_2, that is, low in summer and high in winter in the boundary layer due to vegetation activity change, however, its amplitude is large. A satellite-derived carbon dioxide variation over China from 2003 to 2011 shows that XCO_2 has the lowest value in September and then rises in the southwestern part of China (Yuyue et al., 2017). Qin et al. (2015) studied the seasonal XCH_4 variations in the Sichuan Basin, simulating atmospheric transport and diffusion by setting Yanting as the center point. They estimated the number of trajectories that remain in the target region within certain time ranges in each month for the year 2013. For January, February, November and December in the basin region, the number of staying trajectories inside this area is larger than for other months. This calculation suggests that the closed topography of the basin leads to CH_4 accumulation and keeps it from diffusion from the region. The CO_2 accumulation can also take place in the Sichuan Basin in November and result in the high CO_2 concentrations in November.

4.4.2 Comparison of OSA Data with GOSAT and TCCON Data

The GOSAT (ver.02.21) XCH_4 and XCO_2 observation points available during this campaign period are plotted in the right hand side of Fig. 4.1, which are targeted within 300 km away area centered at the Yanting station. The altitudes of those GOSAT

observation targets are roughly 1000 m, almost equal to the average height of the Sichuan Basin. Under these restrictions, the GOSAT data are available for five days (34 points) during September-December, 2013. When the observation targets are within the ranges of 50 km, the data were available for one day (3 points) for the entire period, and within 200 km for four days (20 points). To compare the OSA and GOSAT data, the temporal series of XCH_4 and XCO_2 are plotted in Fig. 4.4. XCH_4 are slightly decreasing because of lowering in biogenic activity in fall, while XCO_2 are increasing. The small differences between the OSA and GOSAT data may be due to the fact that the GOSAT observation regions are much geographically wider than the OSA observation area at Yanting.

The $XCH4/XCO_2$ ratios of OSA and GOSAT are plotted in Fig.4.5. The comparisons of the ratio values $XCH4/XCO_2$ can reduce the influences of observational biases due to light scattering on aerosols and other optical parameters. This method is efficient due to the small spectral distance of ~0.1 μm between the CH4 and CO_2 solar light absorption bands. The decreasing time-series trends of OSA and GOSAT are consistent to each other since XCO_2 increases in winter.

The TCCON network has no station near the Sichuan Basin. The Lamont TCCON station in Oklahoma, USA (97.49°W, 36.60°N, 320 m a.s.l.) is located in an inland region of the latitude zone same as the Yanting station. The average annual temperature of Lamont is 15.5°C and the main planting is wheat and sorghum while those of Yanting are 16.7°C and rice, respectively. Both the Lamont and Yanting stations belong to a grassland ecosystem. The XCH_4/XCO_2 ratios at Lamont in Fig. 4.5 is constant around 0.046 and flat for the time-series trend while the values of OSA and GOAST at Yanting are higher than those of Lamont in September, and in other months these three data sets are consistent. The methane concentration in September is high, which is in good agreement with the time when much methane from the rice cultivation of this rural field comes out.

4.5 Conclusions

We have utilized a portable column concentration observing instrument at the Yanting station in the Sichuan Basin of China for September-November of 2013 because no ground-based column concentration data are available in this remote area. By analyzing the near-infrared solar spectra measured with the optical spectrum analyzer (OSA), we obtain the column-averaged dry-air molar mixing ratios of atmospheric methane, XCH_4, and carbon dioxide, XCO_2. The diurnal variations of both species are not conspicuous for local time of 10:00-14:00 during the campaign period. Furthermore, we compare the OSA results with those of GOSAT satellite, which targeted the spots within 300 km range region from the Yanting station in the same observation period. Both data sets are in good agreement. The results are also compared with the TCCON observation at the Lamont station that is located in the latitude zone same to the Yanting station. The OSA, GOSAT and TCCON values of the concentration ratios, XCH_4/XCO_2, are in good agreement except in the middle of September. There is an appreciable difference between the OSA observation in the Sichuan Basin and the TCCON observation at the Lamont station in September. This handy OSA measurement can provide the time-varying data and will be useful for future constructions of a ground-based greenhouse gas observation network.
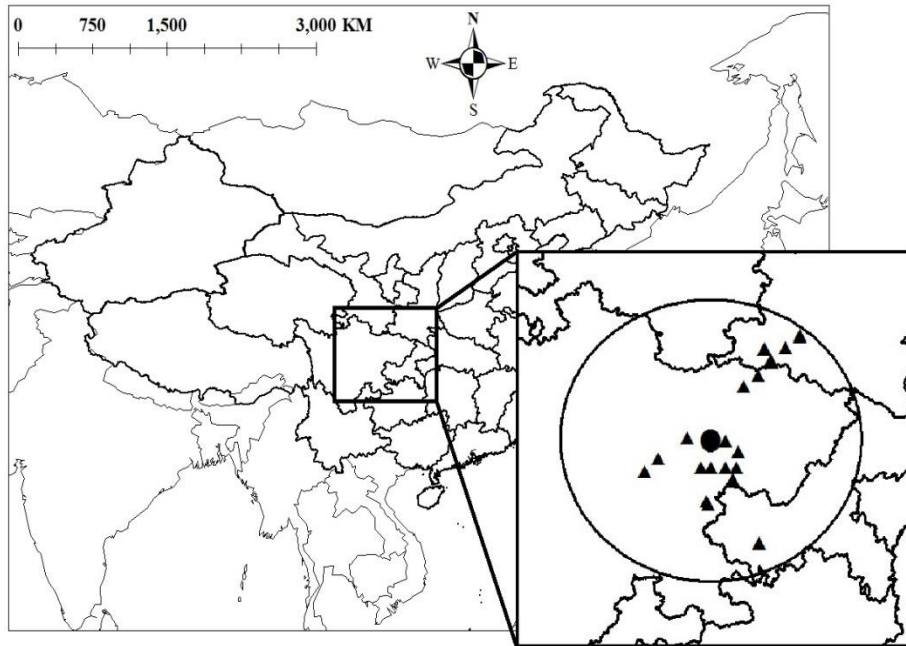
Fig 4.1   Maps of the Sichuan Basin of China. Inset filled circle: location of the Yanting station, filled triangles: GOSAT sattelite observation targets available within 300 km range region centered at the Yanting station and with the altitude lower than 1000 m.
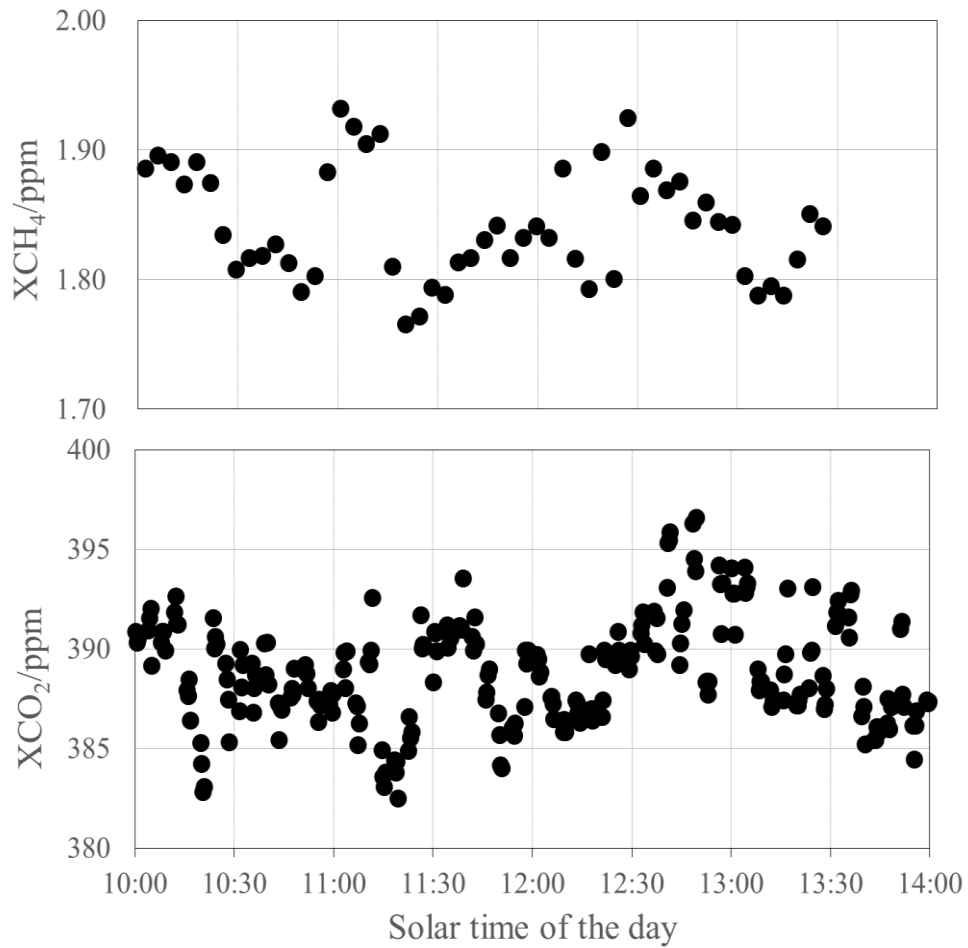
Fig 4.2 Diurnal variations of XCH_4 (upper) and XCO_2 (lower) obtained by the OSA measurements on October 12th, 2013. The OSA data are scaled by the scale factors given in the text.
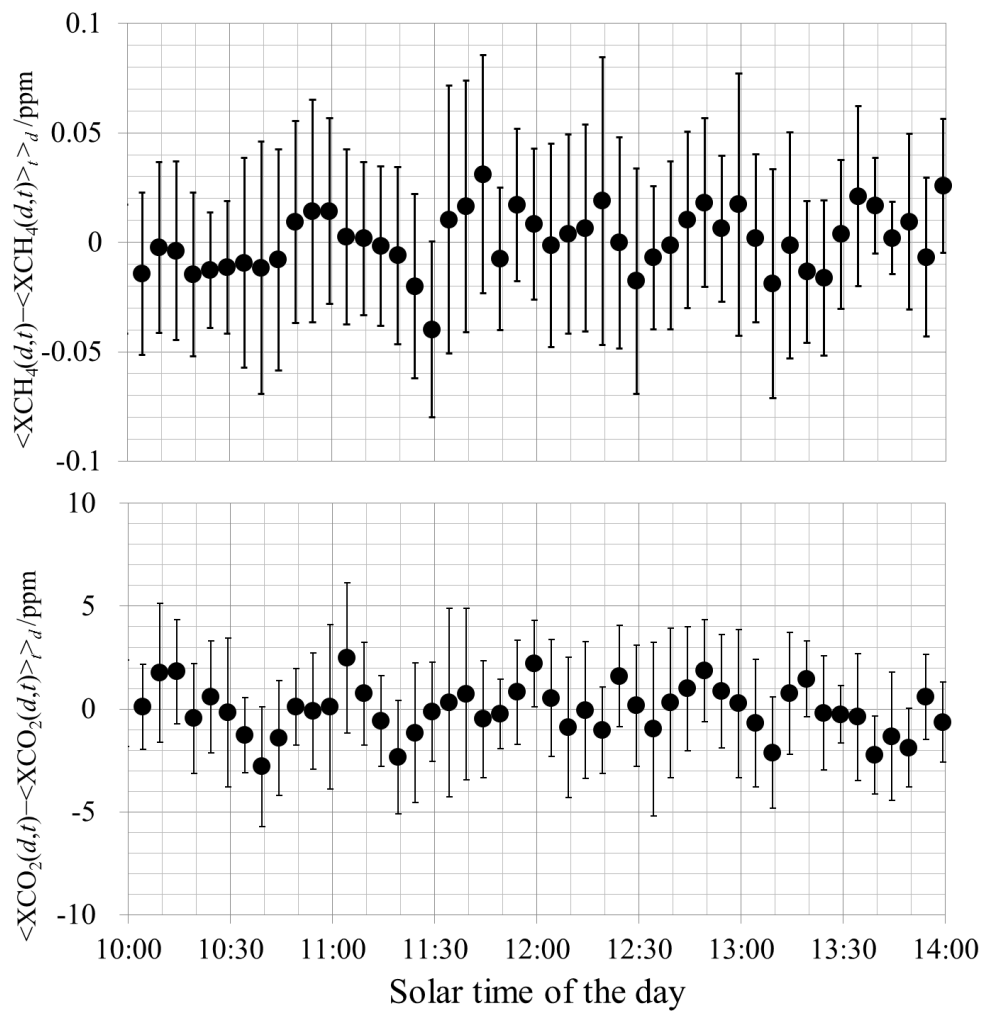
Fig 4.3　The averaged deviations in diurnal variations of XCH_4 (upper) and XCO_2 (lower). The vertical bars stand for one standard deviations for the fifteen-day average. OSA data are scaled by the scale factors given in the text.
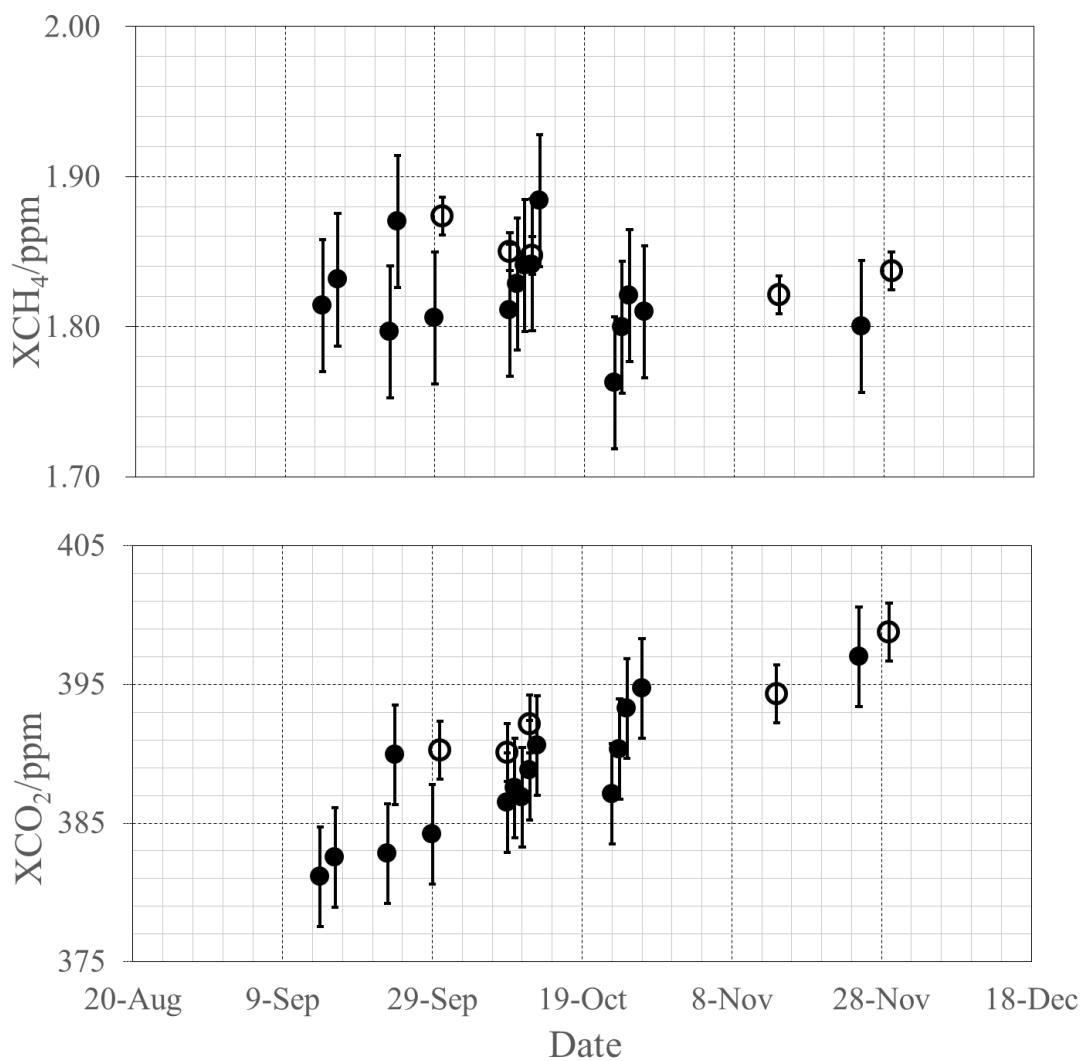
Fig 4.4　Time series of daily mean XCH_4 (upper) and XCO_2 (lower) averaged over 10:00-14:00 solar time obtained by the OSA (filled circle) with those of simultaneous observations by the GOSAT satellite (open circle) in the Sichuan Basin area from September to December. The OSA data are scaled by the scale factors given in the text. The GOSAT data are bise-corrected as described in the text.
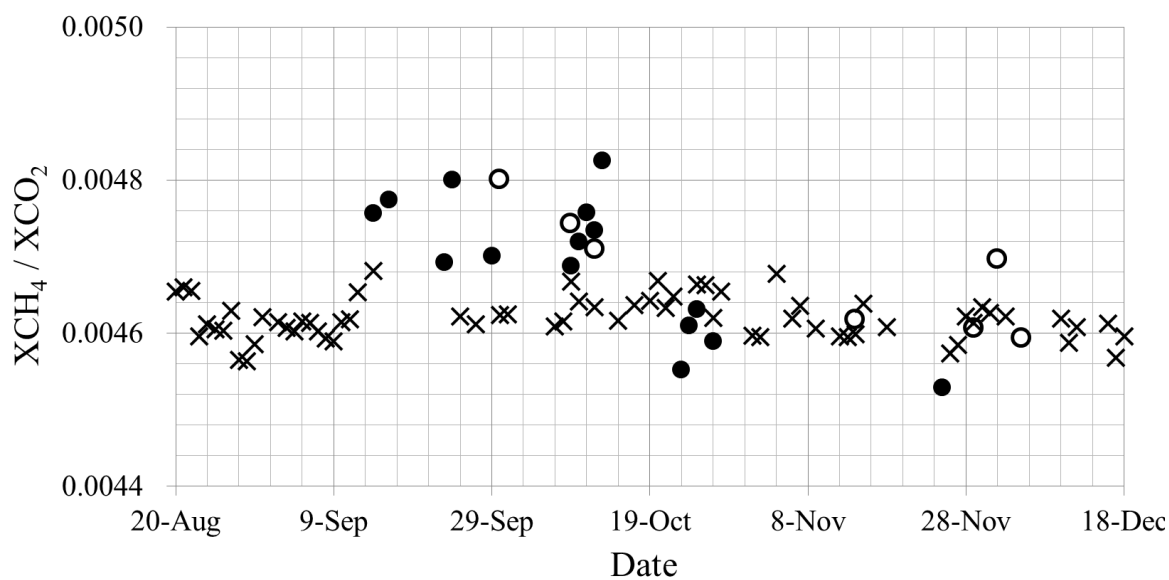
Fig 4.5 Comparisons of daily XCH_4/XCO_2 (ppm/ppm) ratios obtained by the OSA (filled circle) the Yanting station with those of simultaneous observations by the GOSAT satellite (open circle) in the Sichuan Basin area. The TCCON observations (cross) at Lamont station in Oklahoma, USA, which is located at the latitude zone same as the Yanting station. The OSA data are scaled by the scale factors and the GOSAT data are biase-corrected as described in the text. The TCCON data available to us are reported to be scaled.

References

[1] D. Wunch, G. C. Toon, J.-F. L. Blavier et al., "The Total Carbon Column Observing Network," Phil. Trans. Roy. Soc. A, 369, 2087–2112 (2011). [doi:10.1098/rsta.2010.0240]

[2] D. Wunch , G. C. Toon, V. Sherlock, N. M. Deutscheret al., "The Total Carbon Column Observing Network's GGG2014 Data Version," [doi:10.14291/tccon.ggg2014.documentation.R0/1221662, 2015]

[3] TCCON: A Global Total Carbon Column Observing Network, [http://www.tccon.caltech.edu]

[4] C. Frankenberg, J. F. Meirink, M. van Weele, et al., " Assessing Methane Emissions from Global Space-Borne Observations," Science, 308, 1010–1014 (2005). [doi:10.1126/science.1106644]

[5] T. Yokota, Y. Yoshida, N. Eguchi et al., " Global Concentrations of CO_2 and CH4 Retrieved from GOSAT: First Preliminary Results," Sola 5, 160–163 (2009). [doi:10.2151/sola.2009-041]

[6] C. Frankenberg, R. Pollock, R. Lee, et al., "The Orbiting Carbon Observatory (OCO_2): spectrometer performance evaluation using pre-launch direct sun measurements," Atmos. Meas. Tech. 8, 301–313 (2015). [doi:10.5194/amt-8-301-2015]

[7] N. Kobayashi, G. Inoue, M. Kawasaki, et al., "Remotely operable compact instruments for measuring atmospheric CO_2 and CH4 column densities at surface monitoring sites," Atmos. Meas. Tech. 3, 1103–1112 (2010). [doi: 10.5194/amt-3-1103-2010]

[8] M. Kawasaki, H. Yoshioka, N. B. Jones, et al., "Usability of optical spectrum analyzer in measuring atmospheric CO_2 and CH4 column densities: Inspection with FTS and aircraft profiles in situ," Atmos. Meas. Tech. 5, 2593–2600 (2012). [doi:10.5194/amt-5-2593-2012]

[9] 9 F. Hase, M. Frey, T. Blumenstock, et al., "Application of portable FTIR spectrometers for detecting greenhouse gas emissions of the major city Berlin," Atmos. Meas. Tech. 8, 3059-3068 (2015). [doi:10.5194/amt-8-3059-2015]

[10] A. Butz, A. S. Dinger, N. Bobrowski, et al., "Remote sensing of volcanic CO_2, HF, HCl, SO2, and BrO in the downwind plume of Mt. Etna," Atmos. Meas. Tech. 10, 1–14 (2017) [doi:10.5194/amt-10-1-2017]

[11] S. Hayashida, A. Ono, S. Yoshizaki, et al., "Methane concentrations over Monsoon Asia as observed by SCIAMACHY: Signals of methane emission from rice cultivation," Remote Sens. Environ. 139, 246–256 (2013). [doi:10.1016/j.rse.2013.08.008]

[12] H-A. Chen, Q-A. Zhu, C-G. Peng, et al., "Methane emissions from rice paddies natural wetlands, lakes in China: synthesis new estimate," Global Change Biol. 19, 19–32 (2013). [doi:10.1111/gcb.12034]

[13] B-W. Zhang, H-Q. Tian, W. Ren, et al., "Methane emissions from global rice fields:

Magnitude, spatiotemporal patterns, and environmental controls," Global Biogeochem. Cycles. 30, 1246–1263 (2016). [doi:10.1002/2016GB005381]

[14]   A. Bhatia, N. Jain and H. Pathak, "Methane and nitrous oxide emissions from Indian rice paddies, agricultural soils and crop residue burning," Greenhouse Gases Sci. Technol. 3, 196-211 (2013). [doi: 10.1002/ghg.1339]

[15]   X-Y. Yan, Z-C. Cai, T. Ohara, et al., "Methane emission from rice fields in mainland China: Amount and seasonal and spatial distribution," J. Geophys. Res. 108, (2003). [doi:10.1029/2002JD003182]

[16]   X-C. Qin, L-P. Lei, Z-C. He, et al., "Preliminary assessment of methane concentration variation observed by GOSAT in China," Adv. Meteorol. Article ID 125059 (2015). [doi:10.1155/2015/125059]

[17] F. A. Jenkins and H. E. White, Fundamentals of Optics, 4th Ed, McGraw-Hill (1981) [ISBN 0072561912]

[18]   Rothman, L. S., Gordon I. E., Barbe A. et al., "The HITRAN2008 molecular spectroscopic database," J. Quant. Spectrosc. Radiat. Transfer, 110, 533-572 (2009), [doi:10.1016/j.jqsrt.2009.02.013,2009]

[19] Rothman, L. S., Gordon I. E., Babikov Y. et al. "The HITRAN2012 molecular spectroscopic database," J. Quant. Spectrosc. Radiat. Transfer, 130, 4-50 (2013). [http://doi.org/10.1016/j.jqsrt.2013.07.002]

[20] R. A. Washenfelder, G. C. Toon, J. F. Blavier, et al., "Carbon dioxide column abundances at the Wisconsin Tall Tower site," J. Geophys. Res. Atmos. 111, 1–11 (2006). [doi:10.1029/2006JD007154]

[21]   D. Wunch, G. C. Toon, P. O. Wennberg, et al.," Calibration of the Total Carbon Column Observing Network using aircraft profile data," Atmos. Meas. Tech. 3, 1351–1362 (2010). [doi:10.5194/amt-3-1351-2010]

[22]   Y. Yoshida, N. Kikuchi, I. Morino, et al.," Improvement of the retrieval algorithm for GOSAT SWIR XCO_2 and XCH_4 and their validation using TCCON data," Atmos. Meas. Tech. 6, 1533–1547 (2013). [doi:10.5194/amt-6-1533-2013]

[23]   M. Ishizawa, O. Uchino, I. Morino, et al., "Large XCH_4 anomaly in summer 2013 over northeast Asia observed by GOSAT," Atmos. Chem. Phys. 16, 9149–9161 (2016). [doi:10.5194/acp-16-9149-2016]

[24]   Xu, Yuyue, et al. "Variations in satellite-derived carbon dioxide over different regions of China from 2003 to 2011," Atmos.Environ. 150, 379-388 (2017). [http://dx.doi.org/10.1016/j.atmosenv.2016.11.032]

Chapter 5

XCO$_2$ observations in Tokyo using OSA system

Abstract

The metropolitan area of Tokyo, which is the capital of Japan, emits a large amount of CO$_2$, which is an anthropogenic greenhouse gas. In this chapter, we measured the day-time column-averaged dry-air molar mixing ratios of atmospheric CO$_2$, XCO$_2$, in the central area of Tokyo during September 2014–August 2016 using a portable optical spectrometer. The observed seasonal cycle is compared with the seasonal cycle that is observed at the TCCON site in Tsukuba, which is located 60 km to the northeastern direction of Tokyo. The differences in XCO$_2$ between the two sites are high (~5 ppm) during December–February and low (~0.5 ppm) during June–September. The characteristic variations of XCO$_2$ in Tokyo are interpreted in terms of local emission sources and surface meteorological data, by referring to the variations in the concentrations of surface CO$_2$. The sharp peaks in XCO$_2$ at both the Tokyo and Tsukuba sites in July are interpreted in terms of local air retention in the areas, as indicated by the aircraft profiles and wind-flow forward trajectory calculations. Finally, we compare the ground-based column measurements with the top-down satellite column observations.

5.1 Introduction

Urban areas are significant sources of fossil fuel CO$_2$, further, urban areas host more than 50% of the world's population and produce more than 70% of the total CO$_2$ emissions (UN, 2006). Because the contribution of megacities to the world-wide emission of CO$_2$ is out of proportion with their small surface area (IEA, 2017; Oda et al.,

2018), quantifying the anthropogenic greenhouse gas emission is essential to ensure reduction of CO_2 (Duren et al., 2012). The high CO_2 concentrations in megacities have been reported to quantify sources and sinks. Satellite observations are useful for improving the capability to monitor anthropogenic CO_2 emissions. Kort et al. (2012) reported on monitoring the CO_2 emissions from megacities using the data obtained from the GOSAT. Hakkarainen et al. (2016) performed the OCO-2 satellite observations of anthropogenic CO_2 over the majorly polluted regions across various continents. Janardanan et al. (2016) reported that the CO_2 abundances that were obtained from the satellite measurements do not match with those obtained from the emission inventories. In situ ground-based measurements can also provide data for atmospheric CO_2. Measurements of ground CO_2 emissions have been analyzed in case of Paris, which is another megacity (Bréon et al., 2015; Xueref-Remy et al., 2018). Globally distributed observation networks, such as the TCCON, use high-resolution FTS (Wunch et al., 2011), to provide the XCO_2 data with high precision and high accuracy, however, the number of these non-mobile sites is limited. To increase the density of observations, low-cost and easy-to-handle remote-sensing instruments are used as a promising complement to the current techniques. Column measurement by solar spectrometry is suitable for localized sources because it can be used for probing larger sample volumes than that can be probed using the in situ measurements and because it can be used for smaller scales than that of the satellite sensors (Wilson et al., 2007; Kobayashi et al., 2010; Frey et al., 2015; Hase et al., 2015; Bréon et al., 2015).

  In this study, we investigate the seasonal cycle and diurnal variations of XCO_2 through measurements that were performed using a portable OSA at a site in the central area of metropolitan Tokyo. The observed XCO_2 data are compared with those at the TCCON site in Tsukuba, 60 km northeast of Tokyo. The high XCO_2 concentration in the winter season and the abrupt increase in July are interpreted by referring to the results of the aircraft profiles and the wind-flow forward-trajectory calculations.

5.2 Introduction of observation station

The Tokyo observation site, the Senior High School of Tokyo Gakugei University (35.63°N, 139.68°E), is located in the southern residential area of central Tokyo. Fig.5.1a depicts the spatial distribution of the Open-source Data Inventory for Anthropogenic CO_2 (ODIAC) fossil fuel emission dataset points (Oda et al., 2018; 1×1 km mesh; Available at http://db.cger.nies.go.jp/dataset/ODIAC; Data downloaded in Jul. 2017) for the Kanto Plain, which includes both the Tokyo and the Tsukuba observation sites. The locations of the observation sites and thermal power plants in Tokyo are illustrated in Fig. 5.1b. The power plants are distributed in the eastern and southern coastal areas.

5.3 Data preparation for analysis

5.3.1 Column averaged CO_2 concentration from OSA observation

Because the spectrometers and the analytical procedures that were employed were different at the Tokyo OSA and the Tsukuba FTS observation sites, a comparison was performed by moving the OSA instrument from the Tokyo site to the Tsukuba site and by measuring the XCO_2 values simultaneously using the OSA and FTS instruments for four months from a period of April to July 2017. The comparison study, which is described in the supplementary information, was conducted for the OSA instrument with a co-located TCCON FTS, furthermore, the scale factor for the OSA XCO_2 was derived.

5.3.2 CONTRAIL aircraft and GOSAT satellite data

To explain the high values of XCO_2 through the OSA observations in July 2015, we used the results that were obtained by performing in situ aircraft measurements of the Comprehensive Observation Network for TRace gases by AIrLiner (CONTRAIL)

91

project (Machida et al., 2008). The CONTRAIL Aircraft data at a height range of 3–10 km were used with the departure and arrival flights at the Tokyo Haneda Airport in July 2015.

The XCO_2 values that were measured using the GOSAT satellite around the Tokyo site were also compared with the values that were obtained using ground-based observations in this study. The GOSAT satellite measured the amount of XCO_2 by observing the ground surface reflection of solar light at approximately 13:00 (solar time) once every three days (Yokota et al., 2009). The GOSAT SWIR (Short Wavelength InfraRed) Level 2 XCO_2 data (version 02.72) used in this study had a bias of ~0.07 ppm as compared with that of the TCCON data and a standard deviation of ~2.36 ppm (NIES GOSAT Project, https://data2.gosat.nies.go.jp /doc/document.html). Only the GOSAT data for the area (a circle with 10 km radius) that was centered at the Tokyo site (Fig. 5.1b). For the comparison with the GOSAT data, the XCO_2 obtained by the OSA were averaged over 12:30-13:30 solar time. Under these condition, the GOSAT and OSA data considered 29 (39 points) and 271 days between September 2014 and August 2016, respectively.

5.3.3 Surface CO_2 concentration

The differences between the surface CO_2 concentrations of Tokyo and Tsukuba were analyzed to perform comparison with the column concentrations of XCO_2 that were obtained in this study. The surface CO_2 concentrations in Tokyo were measured at the Tokyo Metropolitan Research Institute for Environmental Protection (TMRIEP) (35.67°N, 139.82°E) using an NDIR (Non Dispersive Infrared) instrument (Shimadzu, URA-207, one-hour average). In Tsukuba, the CO_2 concentrations were measured at the National Institute of Advanced Industrial Science and Technology (AIST) (36.05°N, 140.12°E), which is located 200 m to the north of the Tsukuba site, using a mass spectrometer (Ishidoya and Murayama, 2014).

We analyzed the relation between the wind direction/speed, XCO_2, and the surface NO_2 concentrations to estimate the CO_2 emission sources around the Tokyo observation

site. The one-hour averaged surface meteorological and NO_2 data were obtained from the Atmospheric Environmental Regional Observation System (AEROS, http://soramame.taiki.go.jp) that was provided by the Ministry of the Environment, Government of Japan at the Setagaya observation site (35.65°N, 139.65°E), which is located 2.6 km northeast of the Tokyo site.

5.4 Results and discussion

5.4.1 Seasonal cycles of XCO_2

Figure 5.2 depicts the daily averaged XCO_2 at the Tokyo site and the Tsukuba TCCON site between September 2014 and August 2016. The seasonal variations of the daily-averaged XCO_2 values are fitted using the following formula with a linear trend and using 365-day and (365/2)-day periodicities:

$$XCO_2(t) = I_{intercept} + T_{rend} \times t + AMP_1 \times \cos\left(2\pi \frac{t-\Phi_1}{365.25}\right) + AMP_2 \times$$
$$\cos\left(4\pi \frac{t-\Phi_2}{365.25}\right) \quad (5.1),$$

where $I_{intercept}$ is the intercept on January 1, 2014; T_{rend} is the yearly trend; AMP_1 and AMP_2 are the amplitudes with a period of one and a half year, respectively; and Φ_1 and Φ_2 are the phase shifts for one and a half year cycles, respectively. The best-fitted curves are illustrated in Fig. 5.2. The parameters are presented in Table 1.

The seasonal variations of XCO_2 at the Tsukuba site are the maximum at around March–April and the minimum during August–September. This seasonal behavior is extensively observed in the rural areas of the northern mid latitude zone (Wunch et al., 2013; Inoue et al., 2016). However, the seasonal variations of XCO_2 at the Tokyo site depict the maximum value during December–January and the minimum value during July–August, and the amplitude is large, which are characteristic features that may be caused due to heating-related emissions in urban areas (Briber et al., 2013).

93

5.4.2 Difference between Tokyo and Tsukuba

The average value of $<XCO_2(Tokyo)>$ during the observation period is 403.4 ± 4.14 (1σ) ppm, whereas that of $<XCO_2(Tsukuba)>$ is 401.2 ± 3.0 (1σ) ppm, which is lower by 2.1 ppm than in Tokyo. The large variation in XCO_2 during winter is probably caused due to the large anthropogenic emissions of CO_2 that were caused by heating in the Tokyo area.

Schwandner et al. (2017) analyzed the OCO_2 satellite data and reported the high XCO_2 over the urban core but not over the suburban areas of Los Angeles, with the differences which vary seasonally from 4.4 to 6.1 ppm. They attributed these differences to some anthropogenic activity. The differences between the Tokyo and Tsukuba sites in this study are a little smaller than their reported values. Probably, the meteorological conditions in the Tokyo megacity were different from those in Los Angeles. The Tokyo metropolitan area is located in the Kanto Plain, which is open to the surrounding ocean (Fig. 5.1a), whereas the Los Angeles metropolitan area is inland basin and is surrounded by mountains; therefore, the air masses with high CO_2 concentration can be easily stagnated. The photochemical smog phenomena occurred frequently in Los Angeles in 1960–70 and have been partially attributed to these geographical and meteorological features (Parrish et al., 2011).

Figure 5.3 depicts the monthly average values of the surface CO_2 concentrations at Tokyo and Tsukuba (as described in Section 3.2) since 2014. The average difference between the surface CO_2 values of Tokyo and Tsukuba is 10.1 ppm. Because the contribution of the surface CO_2 concentration to the column-averaged XCO_2 is approximately 1/5 due to the contribution of the atmospheric boundary layer to the total column amount, a difference of 2 ppm between the XCO_2 values of Tokyo and Tsukuba can be explained by this difference.

5.4.3 Effect of weather condition

Effects of wind direction/speed on $<XCO_2(Tokyo)>$ in each season were examined.

Fig. 5.4 depicts that the southerly–southeasterly wind causes the high $<XCO_2(Tokyo)>$ values, regardless of the season and the wind speed. This may be caused due to the CO_2 emission from the power plants that were located in the southern area of Tokyo (Fig. 5.1b).

In July 2015 and July–August of 2016, the $<XCO_2>$ variations at both Tokyo and Tsukuba do not follow the simple seasonal cycle that is expressed in Eq. 5.1 with the 365-day and (365/2)-day periodicity terms. Figure 5.5 depicts an extremely high XCO_2 toward the end of July 2015. To analyze the sources of these high values, we compared the XCO_2 concentrations at the Tokyo site with the pressure-weighted average values of the CONTRAIL aircraft data of the departed and arrived flights at the Tokyo Haneda Airport in the 3–10 km height range and with the surface measurements in Tokyo during the same period. We observed that the trend in the XCO_2 values and the surface measurement of CO_2 were very consistent; however, the XCO_2 values in the free troposphere (3–10 km altitude) were approximately constant. This indicates that the high CO_2 concentration in the boundary layer (lower than 3 km altitude) contributes to the high XCO_2 concentration that is observed during this period.

To investigate the influence of atmospheric transport on the high XCO_2 concentrations in late July 2015, the Hybrid Single-Particle Lagrangian Integrated Trajectory (HYSPLIT) model calculations are applied (Stein et al., 2015). The data of trajectories are obtained at altitude of 500, 1000, and 1500 m at noon in July 2015. The corresponding 72-h forward trajectory trace lengths for the highest-XCO_2 day (July 27) and the lowest-XCO_2 day (July 14) are ~200 and ~4000 km, respectively, as depicted in Fig. 5.6 of the supplementary information. This indicates that the local air retention caused the high XCO_2 values.

5.4.4 Typical diurnal variations of XCO_2 at the Tokyo site

On November 14, 2014, the content of XCO_2 at the Tokyo site was higher than the monthly average XCO_2 of November (Fig. 5.7a). The of XCO_2 in the afternoon (local time) was much higher than that in the morning even though the rush hour humps in

XCO_2 and NOx were observed at around 9:00. The wind direction was observed to be northeast in the morning, whereas it altered to southwest in the afternoon. These results indicate that the high CO_2 pollution is caused due to the thermal power plants that are located in the west and southwest of the Tokyo observation site.

On October 8, 2015, the XCO_2 value was lower than the monthly average value, and the NO_X concentration was low (Fig. 5.7b). The wind direction was northern during the entire day, and the wind speed was high. There are forest areas in the northern direction, and air masses from the northern areas outside the Tokyo megacity are not affected by the impacts of residential, mobile, and power-plant emissions. These local weather conditions eliminate the local accumulation of the polluted air and cause the approximately low values of XCO_2 and NOx.

On December 16, 2015, the XCO_2 and NOx values were observed to be higher than the monthly mean value after 10:00 (Fig. 5.7c). Because the wind speed was low, the local CO_2 emissions from residential mobile sources were accumulated, which caused the observed high values of XCO_2 and NOx.

5.4.5 Comparison with the GOSAT satellite observations

One of the objectives of the CO_2 measurements using OSA in Tokyo was to validate the GOSAT data for which the standard products of XCO_2 that were measured over the surface, which was covered with asphalt or concrete, depicted some negative biases because of the underestimation of surface reflection during the retrieval processes (Gavrilov et al., 2013). Fig. 5.8 depicts the XCO_2 values of the GOSAT satellite that was obtained for the observation targets, which were available within the 10 km range of the region that was centered at the Tokyo site (Fig. 5.1b) during the same period. Although the XCO_2 values of OSA and GOSAT are observed to be in almost good agreement, the GOSAT winter data were sometimes significantly smaller than those observed by the OSA.

5.5 Conclusions

The column-averaged concentrations of CO_2, XCO_2, at the central area of the Tokyo metropolitan city were measured for two years using a portable OSA instrument. To perform comparison, the data from a TCCON site in Tsukuba, which was located at the northeast edge of the metropolitan, were used. The seasonal trend coincided with the observations of the ground in situ instruments in metropolitan urban areas. The diurnal variation in XCO_2 was correlated with the wind direction. The high XCO_2 values in central Tokyo were attributed to the large local emission sources, e.g., thermal power plants and automobile exhausts. The high XCO_2 concentration during July 2015 may be caused by the local air retention. The OSA instrument was portable and not expensive, and it can be easily operated at any place to measure the XCO_2 values and to estimate the local CO_2 emissions and absorption processes. While the satellite passes over a specific study area once every three days at approximately 13:00, the OSA instrument can provide continuous diurnal observations of XCO_2 during daytime. In future, the ground site network with several OSA instruments will provide systematic analyses of the carbon cycles.

<div align="center">(a)   (b)</div>
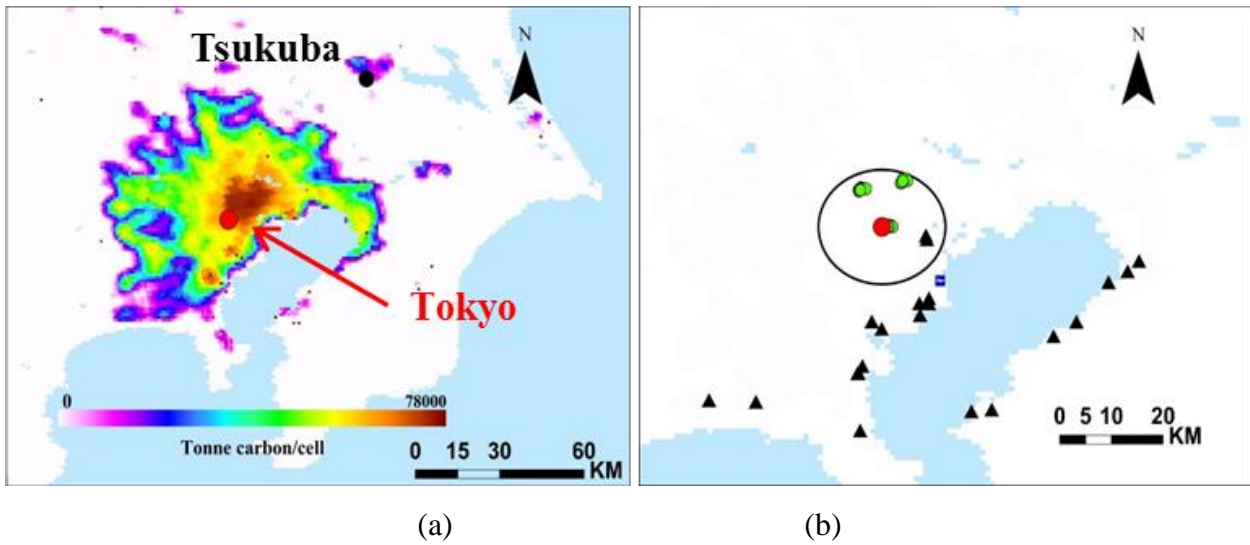
Fig 5.1 (a) CO_2 emissions in the Tokyo metropolitan region (Kanto Planes) in December 2015 based on the ODIAC Fossil fuel emission dataset (Oda et al., 2018). The locations of the observation sites at Tokyo and Tsukuba are indicated. (b) Red circle: OSA Tokyo observation site, green circle: GOSAT satellite observation target within the 10-km range of the region that was centered at the observation site, black triangle: thermal power plants, blue square: the Tokyo Haneda Airport.
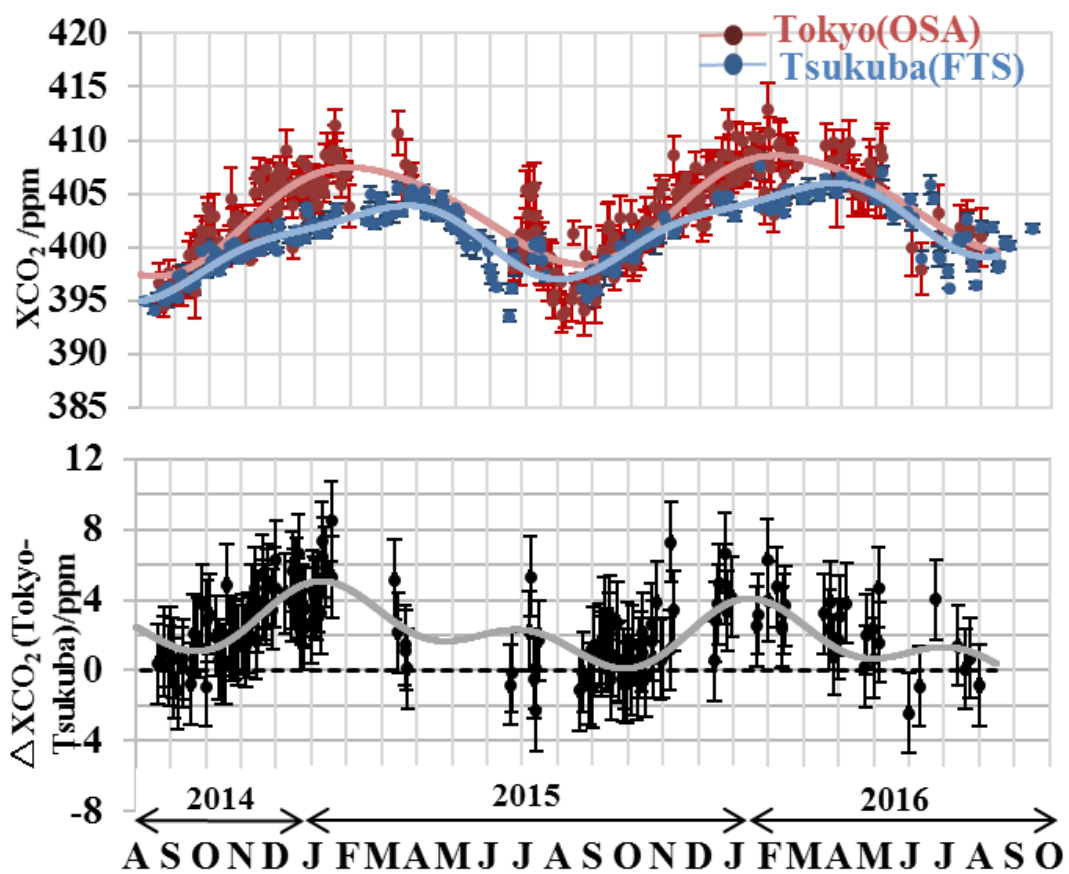
Fig 5.2 (Upper) Daily average of XCO_2 at the Tokyo OSA and Tsukuba TCCON sites. The solid lines are the seasonal variations fitted using Eq. 5.1 (Lower) Differences between the Tokyo and Tsukuba sites. Black circle: differences on the same day base. Solid curve: differences between the fitting curves for the Tokyo and Tsukuba sites.
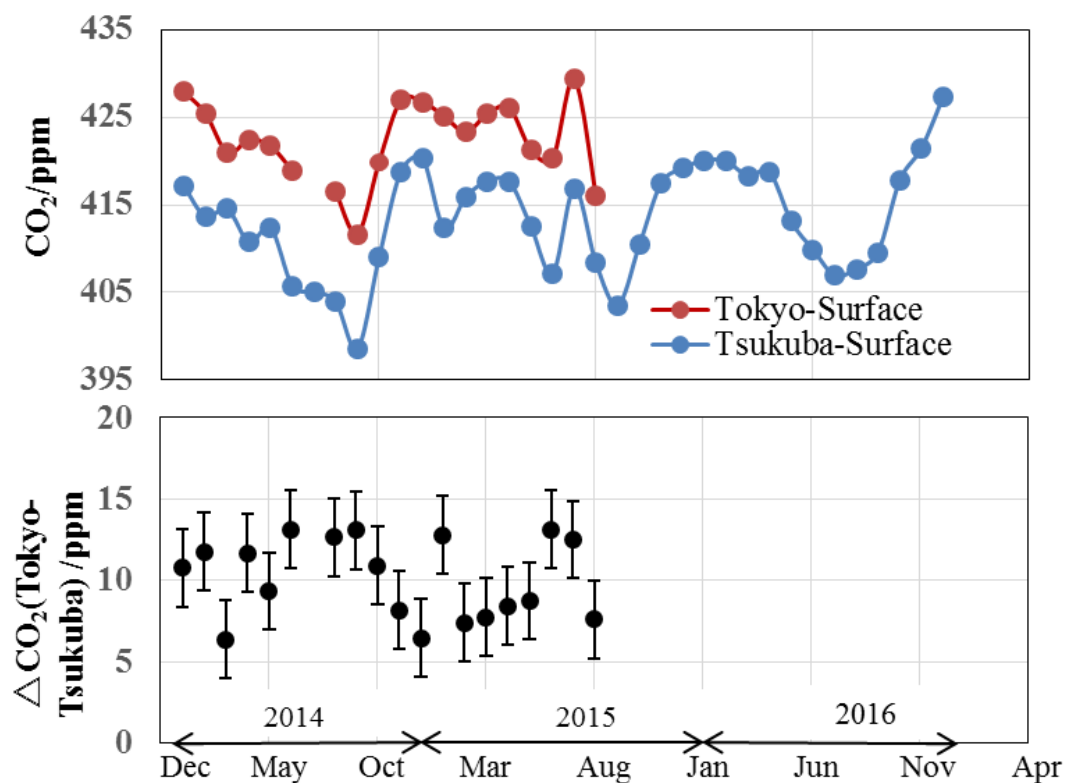
Fig 5.3 Upper: (red) The monthly average surface CO_2 concentrations of Tokyo that were obtained by the Tokyo Metropolitan Research Institute for Environmental Protection; (blue) the monthly average surface CO_2 concentrations of Tsukuba that were obtained by the National Institute of Advanced Industrial Science and Technology. Only the data during daytime (10:00–14:00) are used to perform comparison with the data obtained by the column measurements using the OSA and FTS instruments. Lower: The difference between the Tokyo and Tsukuba data
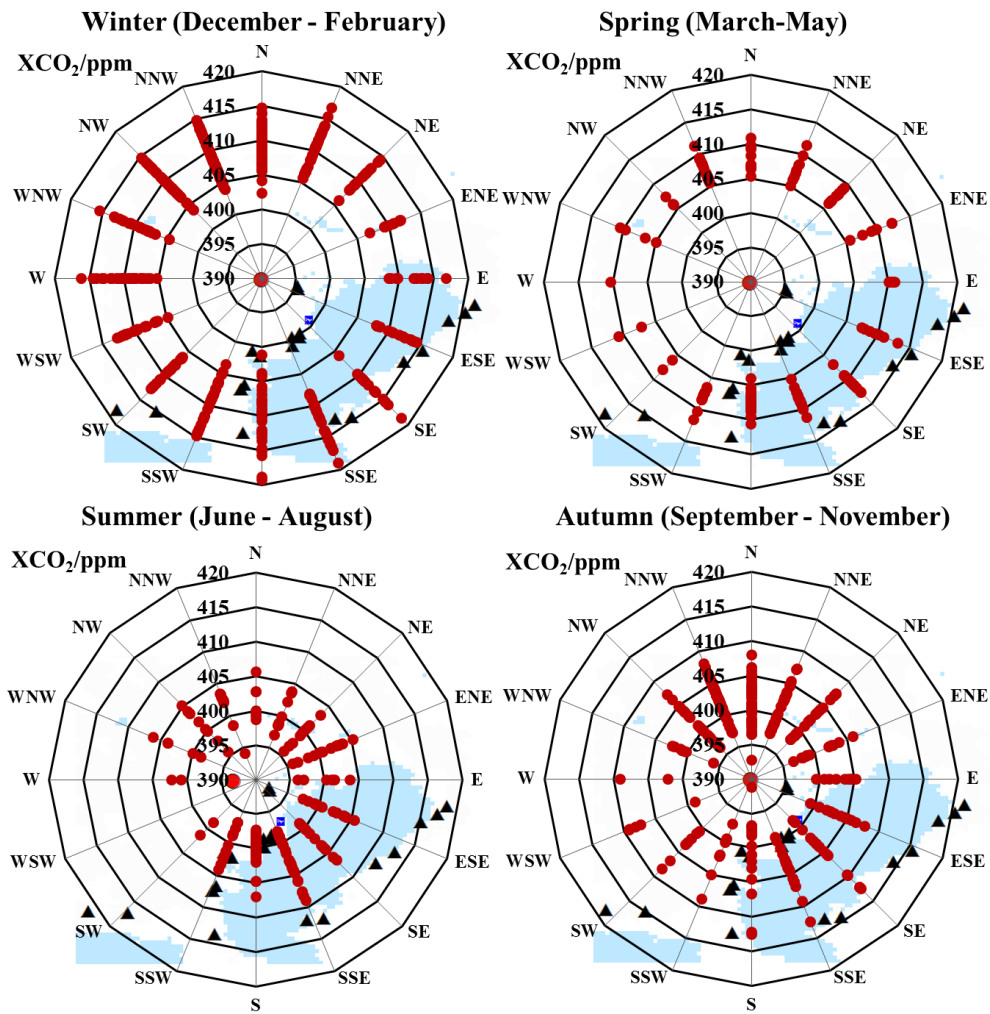
Fig 5.4 The one-hour average concentrations of XCO_2 that were measured at the Tokyo site, and the wind directions during each season. Background maps are the same as Fig. 5.1b, where the positions of power plants are indicated by black triangles.
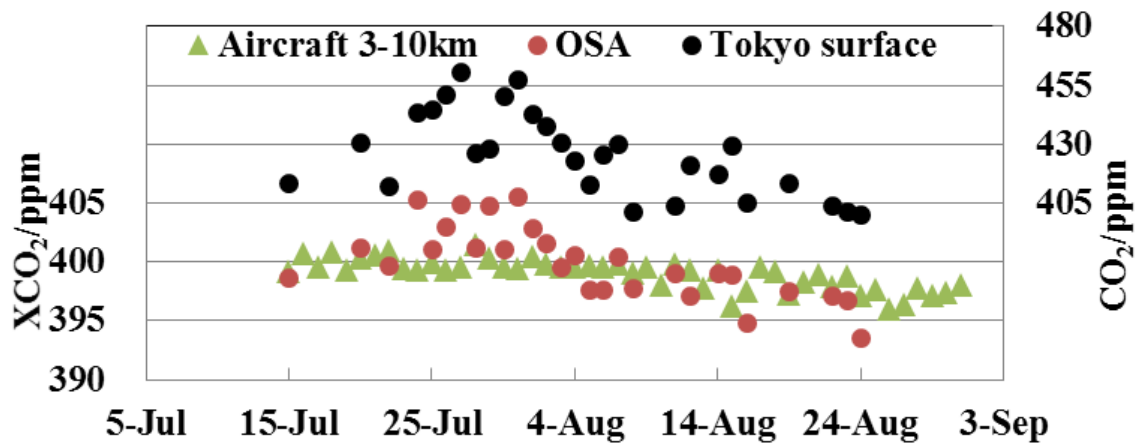
Fig 5.5 Time series of XCO_2 in July–August, 2015 in the Tokyo central area. Red circle: daily average value of XCO_2 measured by the OSA, black circle: surface CO_2 concentration, triangle: partial column-averaged XCO_2 between the heights of 3 and 10 km from the CONTRAIL data.
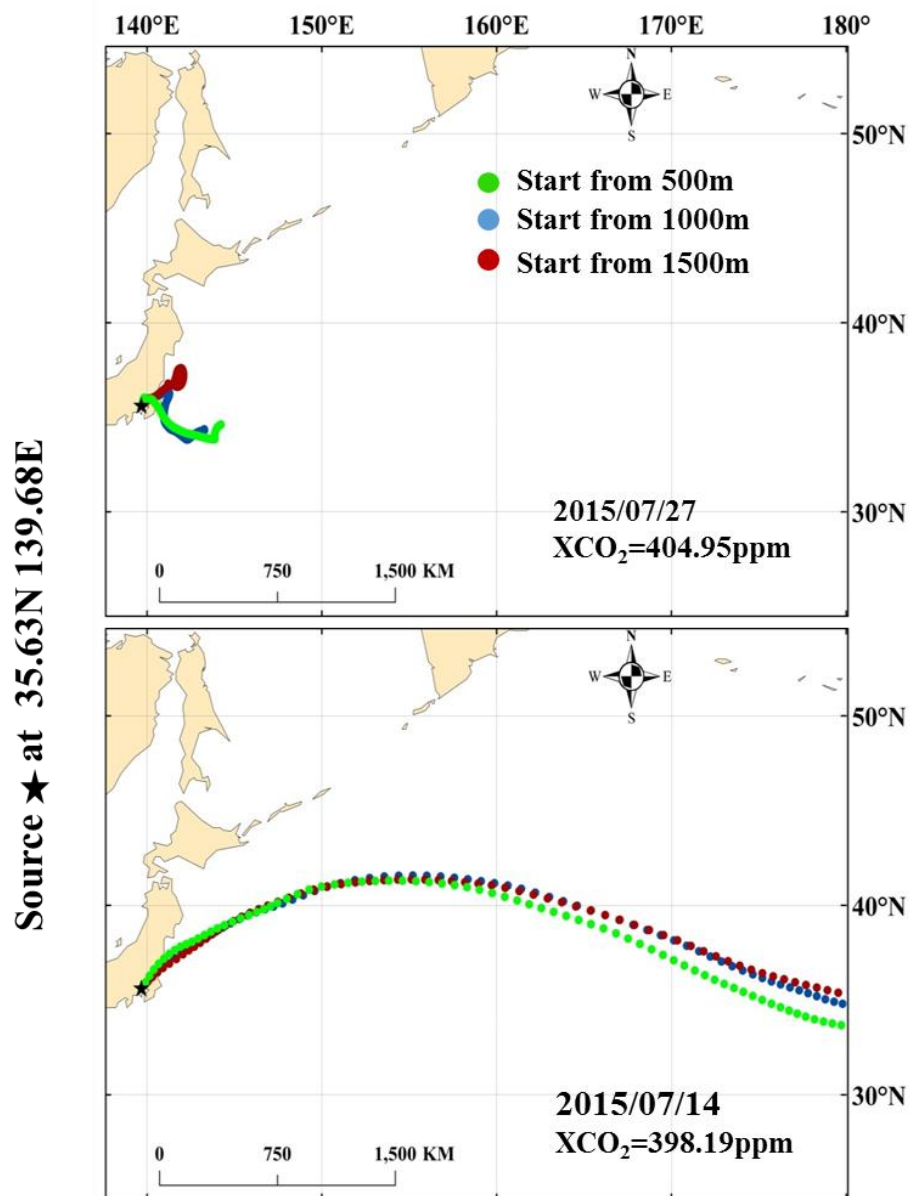
Fig 5.6 Seventy-two hour forward trajectories of air masses from the Tokyo site starting at 12:00 (local time) on July 27, 2015 and July 14, 2015.
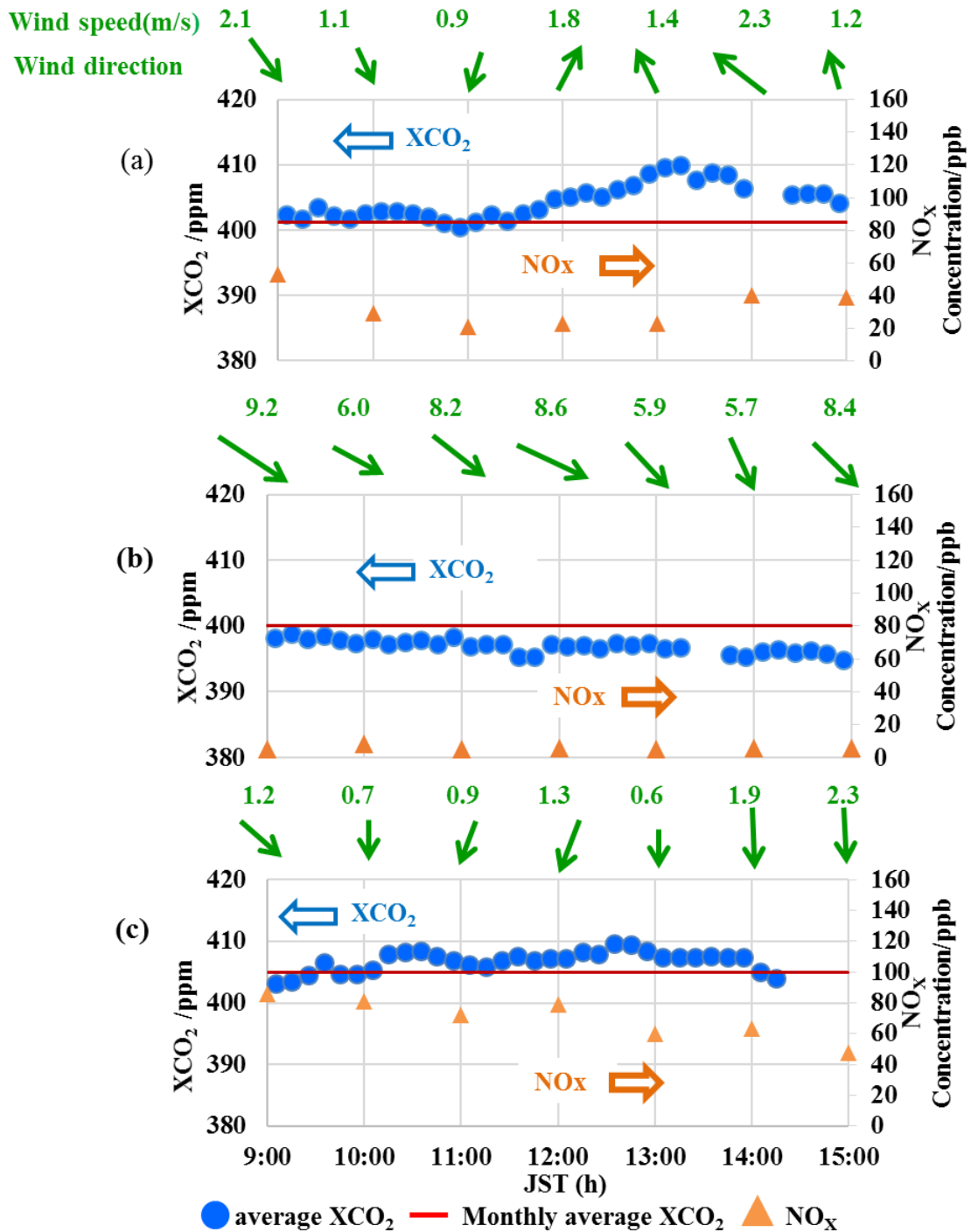
Fig 5.7 Diurnal variations of the XCO_2 concentration, wind direction/speed, and NO_X(= $NO + NO_2$) concentration on (a) November 14, 2015, (b) December 16, 2015, and (c) October 8, 2015. Blue dot: XCO_2 measured at the Tokyo site, red horizontal line: the monthly average of XCO_2. Arrows: wind directions (downward arrow: north wind, leftward: east wind, upward: south wind, and rightward: west wind). The length of the arrow indicates the wind speed.
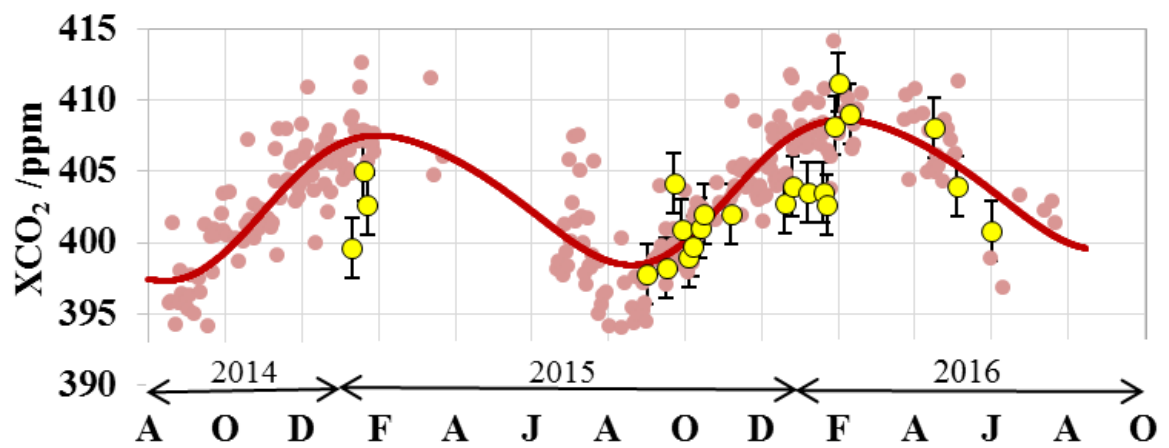
Fig 5.8 Time series of the daily average XCO_2 averaged over 12:30-13:30 solar time obtained by the OSA measurements at the Tokyo site (red circle) with those of the observations by the GOSAT satellite (yellow circle) in the central Tokyo area (see Fig. 5.1 b) at 13:00 (solar time) during the same days from September 2014 to August 2016.

References

[1] Briber, B. M., L, R. Hutyra, A. L. Dunn, S. M. Raciti and J. W. Munger., 2013. Variations in Atmospheric CO_2 Mixing Ratios across a Boston. MA Urban to Rural Gradient, Land, 2, 304-327. http://www.mdpi.com/2073-445X/2/3/304/htm.

[2] Bréon, F. M., Broquet, G., Puygrenier, V., Chevallier, F., Xueref-Remy, I., Ramonet, M., Dieudonné, E., Lopez, M., Schmidt, M., Perrussel, O., and Ciais, P., 2015. An attempt at estimating Paris area CO_2 emissions from atmospheric concentration measurements, Atmos. Chem. Phys., 15, 1707-1724, https://www.atmos-chem-phys.net/15/1707/2015/.

[3] Duren, R. M. and Miller, C. E., 2012. Measuring the carbon emissions of megacities. Nature Climate Change, 2, 560–562. https://www.nature.com/articles/nclimate1629.

[4] Frey, M., Hase, F., Blumenstock, T., Groß, J., Kiel, M., Mengistu Tsidu, G., Schäfer, K., Sha, K. M., and Orphal, J., 2015. Calibration and instrumental line shape characterization of a set of portable FTIR spectrometers for detecting greenhouse gas emissions. Atmos. Meas. Tech., 8, 3047–3057. https://search.proquest.com/docview/1979665746?pq-origsite=gscholar.

[5] Gavrilov,N.M., Koval, A.V., 2013. Parameterization of mesoscale stationary orographic wave impact for usage in numerical models of atmospheric dynamics. Izvestiya Atmos Oceanic Phys, 49,244–251. https://link.springer.com/article/10.1134%2FS0001433813030067.

[6] Hakkarainen, J., Ialongo, I., and Tamminen, J., 2016. Direct space-based observations of anthropogenic CO_2 emission areas from OCO_2. Geophys. Res. Lett., 43, 11,400-11,406. http://doi.org/10.1002/2016GL070885.

[7] Hase, F., Frey, M., Blumenstock, T., Groß, J., Kiel, M., Kohlhepp, R., Mengistu Tsidu, G., Schäfer, K., Sha, M. K., and Orphal, J., 2015. Application of portable FTIR spectrometers for detecting greenhouse gas emissions of the major city Berlin. Atmos. Meas. Tech., 8, 3059-3068. https://www.atmos-meas-tech.net/8/3059/2015/.

[8] IEA, World Energy Outlook 2017. International Energy Agency, Paris, France. http://www.iea.org/weo/.

[9] Inoue, M., et al., 2016. Bias corrections of GOSAT SWIR XCO_2 and XCH_4 with TCCON data and their evaluation using aircraft measurement data. Atmos. Meas. Tech., 9, 3491-3512. https://doi.org/10.5194/amt-9-3491-2016.

[10] Ishidoya, S and Murayama, S., 2014. Development of a new high precision continuous measuring system for atmospheriCO_2/N_2 and Ar/N_2 and its application to the observation in Tsukuba, Japan. Tellus B: Chemical and Physical Meteorology, 66, 1-2. https://doi.org/10.3402/tellusb.v66.22574.

[11] Janardanan, R., Maksyutov, S., Oda, T., Saito, M., Kaiser, J. W., Ganshin, A., Yokota, T., 2016. Comparing GOSAT observations of localized CO_2 enhancements by large emitters with inventory-based estimates. Geophys. Res. Lett., 43, 3486–3493. http://doi.org/10.1002/2016GL067843.

[12] Kawasaki, M., Yoshioka, H., Jones, N. B., Macatangay, R., Griffith, D. W. T., Kawakami, S., Ohyama, H., Tanaka, T., Morino, I., Uchino, O. and Ibuki, T., 2012. Usability of optical spectrum analyzer in measuring atmospheric CO_2 and CH_4 column densities: inspection with FTS and aircraft profiles in situ Atmos. Meas. Tech. 5, 2593-2600. http://dx.doi.org/10.5194/amt-5-2593-2012.

[13] Kobayashi, N., Inoue, G., Kawasaki, M., Yoshioka, H., Minomura, M., Murata, I., Nagahama, T., Matsumi, Y., Tanaka, T., Morino, I., and Ibuki, T., 2010. Remotely operable compact instruments for measuring atmospheric CO_2 and CH_4 column densities at surface monitoring sites. Atmos. Meas. Tech., 3, 1103– 1112. https://www.atmos-meas-tech.net/3/1103/2010/amt-3-1103-2010.html.

[14] Kort, E. A., Frankenberg, C., Miller, C. E., Oda, T., 2013. Space-based observations of megacity carbon dioxide. Geophys. Res. Lett., 39, 1–5. http://doi.org/10.1029/2012GL052738.

[15] Machida, T., Matsueda, H., Sawa, Y., Nakagawa, Y., Hirotani, K., Kondo, N., Goto, K., Nakazawa, T., Ishikawa, K., and Ogawa, T., 2008. Worldwide measurements of atmospheric CO_2 and other trace gas species using commercial airlines. J. Atmos. Ocean. Technol., 25, 1744–1754. https://journals.ametsoc.org/doi/abs/10.1175/2008JTECHA1082.1.

[16] Oda, T., Maksyutov S., Andres, R. J., 2018. The Open-source Data Inventory for Anthropogenic CO_2 version 2016 (ODIAC2016): a global monthly fossil fuel CO_2 gridded emissions data product for tracer transport simulations and surface flux inversions, Earth Syst. Sci. Data, 10, 87–107, 2018, https://doi.org/10.5194/essd-10-87-2018. Data downloaded in Jul. 2017. Available at: http://db.cger.nies.go.jp/dataset/ODIAC.

[17] Parrish, D. D, Singh H. B., Molina L., Madronichd S., 2011. Air quality progress in North American megacities: A review. Atmos. Environ., 45, 7015 – 7025. https://doi.org/10.1016/j.atmosenv.2011.09.039.

[18] Schwandner, F. M. et al., 2017. Spaceborne detection of localized carbon dioxide sources. Science, 358, 3-4. http://science.sciencemag.org/content/358/6360/eaam5782.

[19] Stein, A. et al., 2015. NOAA's HYSPLIT atmospheric transport and dispersion modeling system. Bull. Am. Meteorol. Soc. 96, 2059–2077. https://journals.ametsoc.org/doi/abs/10.1175/BAMS-D-14-00110.1.

[20] UN: World Urbanization Prospects e Revision 2005, Factsheet 7: Mega-cities, 2006, United Nations, Department of Economic and Social Affairs, Population Division. World Urbanization Prospects: The 2005 Revision, Working Paper No. ESA/P/WP/200, Tech. rep., 2006.

[21] Wilson, E. L., Georgieva, E. M., and Heaps, W. S., 2007. Development of a Fabry–Perot interferometer for ultra-precise measurements of column CO_2. Meas. Sci. Technol., 18, 1495–1502. http://iopscience.iop.org/article/10.1088/0957-0233/18/5/040/meta.

[22] Wunch, D. et al., 2011. A method for evaluating bias in global measurements of CO_2 total columns from space, Atmos. Chem. Phys., 11, 12317–12337. https://www.atmos-chem-phys.net/11/12317/2011/acp-11-12317-2011.html.

[23] Wunch, D, P. O. Wennberg, J. Messerschmidt, N. C. Parazoo, G. C. Toon, N. M. Deutscher, G. Keppel-Aleks, C. M. Roehl, J. T. Randerson, T. Warneke, and J. Notholt,, 2013. The covariation of Northern Hemisphere summertime CO_2 with surface temperature in boreal regions. Atmos. Chem. Phys., 13, 9447–9459. https://doi.org/10.5194/acp-13-9447-2013.

[24] Xueref-Remy, I., Dieudonné, E., Vuillemin, C., Lopez, M., Lac, C., Schmidt, M., Delmotte, M., Chevallier, F., Ravetta, F., Perrussel, O., Ciais, P., Bréon, F.-M., Broquet, G., Ramonet, M., Spain, T. G., and Ampe, C., 2018. Diurnal, synoptic and seasonal variability of atmospheric CO_2 in the Paris megacity area, Atmos. Chem. Phys., 18, 3335-3362, https://doi.org/10.5194/acp-18-3335-2018.

[25] Yokota, T., Yoshida, Y., N. Eguchi, Ota, Y., Tanaka, T., Watanabe, H., Maksyutov, S., 2009. Global Concentrations of CO_2 and CH4 Retrieved from GOSAT: First Preliminary Results. Sola 5, 160–163. https://doi.org/10.2151/sola.2009-041.

Chapter 6

Summary of the thesis

6.1 Conclusions

In this study, solar spectrum observations were performed using small ground-based spectrometers in Sichuan, China, and Tokyo, Japan. XCO_2 and XCH_4 were calculated, and the results were compared with satellite observations. Combined with the meteorological data and in-situ data, the reasons for the changes of XCO_2 and XCH_4 were further analyzed. The advantages and practicability of small-ground observation systems in greenhouse gas observation research are proved.

GOSAT-XCH_4 data from January 2010 to December 2013 are used to study the spatio-temporal variation of XCH_4 in China, especially for Sichuan Basin where it presents consistent higher XCH_4 values than other parts of China. We further investigate the driving factors, including the CH_4 emissions and regional atmosphere dynamic transport, to study the variations of CH_4 concentration in the basin, and evaluate the potential role of satellite-observed XCH_4 data in analyzing the regional variation of CH_4. Our results show that the spatial distribution of GOSAT-XCH_4 is generally consistent with that of CH_4 emission, and abnormal high XCH_4 values can be seen in the Sichuan Basin, which is consistent with previous results from SCIAMACHY. The seasonal variation of XCH_4 is highly related to the CH_4 emissions from rice paddy fields during rice growing period from April to October, and presents a difference feature from

background CH_4 variation related to stronger CH_4 lose in summer due to chemical reaction. During the rice harvesting season of August to September, XCH_4 data are higher than that in early stage of rice growing about in April. However, the abnormal high XCH_4 data are shown in the winter when the CH_4 emissions from rice paddy fields are weak and the surface air temperature is low. By implementing the trajectory simulation using HYSPLIT in the basin, we found the typical closed topography of Sichuan Basin, which may leads to CH_4 accumulation and keep it from diffusion, is one possible reason for the extreme high XCH_4 value in winter. The influence of CH_4 emissions from sources other than rice paddies is also discussed and bottom-up emission inventory data show that they are not likely big causes of the observed winter high XCH_4 value in Sichuan Basin. It can be indicated that the regional variations of XCH_4 observed by GOSAT in Sichuan Basin are determined by not only the CH_4 emissions from ground sources but also very likely the regional topography and the related regional air transport.

Our result from studying the CH_4 variations in Sichuan Basin, especially the abnormal higher value during winter, and their driving factors demonstrate a certain potential of using GOSAT-XCH_4 for investigating the regional CH_4 changes. This study presents preliminary results of CH_4 in China, and a further investigation of the CH_4 in the basin is still necessary as more satellite observations of CH_4 with improving accuracy are available in the coming future to further study the CH_4 variations and regional emissions.

We have utilized a portable column concentration observing instrument at the Yanting station in the Sichuan Basin of China for September-November of 2013 because no ground-based column concentration data are available in this remote area. By analyzing

the near-infrared solar spectra measured with the OSA, we obtain the column-averaged dry-air molar mixing ratios of atmospheric methane, XCH_4, and carbon dioxide, XCO_2. The diurnal variations of both species are not conspicuous for local time of 10:00-14:00 during the campaign period. Furthermore, we compare the OSA results with those of GOSAT satellite, which targeted the spots within 300 km range region from the Yanting station in the same observation period. Both data sets are in good agreement. The results are also compared with the TCCON observation at the Lamont station that is located in the latitude zone same to the Yanting station. The OSA, GOSAT and TCCON values of the concentration ratios, XCH_4/XCO_2, are in good agreement except in the middle of September. There is an appreciable difference between the OSA observation in the Sichuan Basin and the TCCON observation at the Lamont station in September. This handy OSA measurement can provide the time-varying data and will be useful for future constructions of a ground-based greenhouse gas observation network.

The column-averaged concentrations of CO_2, XCO_2, at the central area of the Tokyo metropolitan city were measured for two years using a portable OSA instrument. To perform comparison, the data from a TCCON site in Tsukuba, which was located at the northeast edge of the metropolitan, were used. The seasonal trend coincided with the observations of the ground in situ instruments in metropolitan urban areas. The diurnal variation in XCO_2 was correlated with the wind direction. The high XCO_2 values in central Tokyo were attributed to the large local emission sources, e.g., thermal power plants and automobile exhausts. The high XCO_2 concentration during July 2015 may be caused by the local air retention. The OSA instrument was portable and cheap, and it can be easily operated at any place to measure the XCO_2 values and to estimate the local CO_2 emissions and absorption processes. While the satellite passes over a specific study

111

area once every three days at approximately 13:00, the OSA instrument can provide continuous diurnal observations of XCO_2 during daytime. In future, the ground site network with several OSA instruments will provide systematic analyses of the carbon cycles.

6.2 Future prospects

In addition to the OSA observing system, we have also developed a smaller observation system using a fiber spectrometer of a commercially available array type infrared sensor (Ocean Optics, NIR Quest, 1557-1625 nm resolution 1.0 cm^{-1}) and an equatorial mount for amateur astronomy (Kenko Sky Memo S). Since it is sufficient for a budget of 1/50 or less of the large FTS and about 1/10 of the small FTS, this compact apparatus can be arranged in a large number. This instrument had been used to conduct continuous solar spectrum observations at Nagoya University for one month. Much data on solar spectrum had been obtained and analyzed to obtain the XCO_2 column concentration.

In the future, we will to develop a low-cost, compact ground-based CO_2 solar spectrum observation system that can perform observations under unstable weather conditions, and it not only in satellite verification at various places, is also possible to analyze the dynamics of CO_2 in urban areas from multipoint observations. In the future, through international cooperation research, this ground equipment will can be used for observation in various regions to obtain more information about sources and sinks on CO_2 concentration, and to contribute to global CO_2 concentration observation research. And I hope to improve the existing CO_2 concentration inversion algorithm through data analysis, reduce the dependence of the algorithm on external data, and improve the

robustness of the algorithm.

Acknowledgments